DOCTORAL COURSE IN PHYSICS

CYCLE XXXIV

PhD Coordinator: Prof.ssa Eleonora Luppi

Lattice Kinetic Algorithms for Relativistic Flows: a Unified Treatment

Scientific/Disciplinary (SDS) FIS/02

Candidate

Daniele Simeoni

Supervisor:

Prof. Raffaele Tripiccione

Supervisor:

Prof. Matthias Ehrhardt

Supervisor:

Prof. Constantia Alexandrou

Co-Supervisor:

Prof. Sebastiano Fabio Schifano

Years 2018-2021

Lattice Kinetic Algorithms
for Relativistic Flows:
a Unified Treatment

Scientific/Disciplinary (SDS) FIS/02

Candidate

Daniele Simeoni

Supervisor:

Prof. Raffaele Tripiccione

Supervisor:

Prof. Matthias Ehrhardt

Supervisor:

Prof. Constantia Alexandrou

Co-Supervisor:

Prof. Sebastiano Fabio Schifano

Years 2018-2021

A Raffaele.

Abstract

In this thesis, I present the results obtained during the course of the Ph.D. project Algorithms for Relativistic Lattice Boltzmann, one of the projects created in the framework of the European network of Joint Doctorates STIMULATE.

The main focus of the project has been the algorithmic refinement and extension of existent lattice kinetic solvers for the simulation of relativistic hydrodynamics and their applications in the fields of astrophysics, condensed matter, nuclear physics.

The first achievement reported in the thesis is the generalization of the method to a generic number of spatial dimensions, particularly instrumental to the correct simulation of condensed matter systems, which are typically laid out in bidimensional fashion.

This process involves the proper calibration of transport coefficients indipendently of the spatial dimension, as this is a crucial aspect when trying to reproduce relativistic fluids with the desired dissipative properties.

Next, I present the benchmarking results obtained by the method in the simulation of two popular systems in relativistic hydrodynamics, namely the Bjorken flow and the relativistic Riemann problem, showing that the numerical results are compatible with both analytic solutions and data from other numerical solvers.

A technique for the extension of the numerical scheme to ballistic regimes is then discussed. The extension is performed by adopting of product quadrature rules in the discretization of the radial and angular variables in the momentum space. Results of improvements in the solution of the Riemann problem in the ballistic regime are shown.

Lastly, I present a new Lattice Boltzmann inspired kinetic scheme for the simulation of radiative transfer. This scheme draws from the structural similarities

of the main equation of Radiative Transfer with the Boltzmann equation, and is able to correctly reproduce radiation dynamics both in the optically thin and optically thick limit.

In questa tesi presento i risultati ottenuti durante il corso del Dottorato 'Algoritmi per Metodi Relativistici di Boltzmann su Reticolo', uno dei progetti realizzati nell'ambito del Progetto Europeo Joint Dottorates STIMULATE.

L'obiettivo principale del progetto è stato il perfezionamento algoritmico e l'estensione degli schemi numerici pre-esistenti su reticolo per la simulazione dell' idrodinamica relativistica e la loro applicazione nei campi dell'astrofisica, della Fiica della Materia Condensata, e della Fisica Nucleare.

Il primo risultato riportato nella tesi è la generalizzazione del metodo ad un numero generico di dimensioni spaziali, cosa che è strumentale per la corretta simulazione dei sistemi di materia condensata, che sono tipicamente bidimensionali.

Questo processo comporta la corretta calibrazione dei coefficienti di trasporto indipendentemente dalla dimensione spaziale, dal momento che questo è un aspetto cruciale quando si tenta di riprodurre flussi relativistici con le desiderate proprietà dissipative.

In seguito presento i risultati ottenuti nel benchmarking di due sistemi popolari in idrodinamica relativistica, vale a dire il flusso di Bjorken e l'iterazione relativistica del problema di Riemann. In entrambi i casi si mostra che i risultati dello schema numerico sono compatibili sia con le soluzioni analitiche che con i dati di altri solver numerici.

Poi, viene discussa una tecnica per l'estensione dello schema numerico ai regimi balistici. L'estensione si effettua adottando regole di quadratura prodotto tra le discretizzazioni radiali e angolari nello spazio dei momenti. Viene mostrato un miglioramento della soluzione del problema di Riemann nel regime balistico.

Infine, presento un nuovo schema cinetico ispirato al metodo Lattice Boltzmann per la simulazione del trasporto radiativo. Questo schema attinge dalle somiglianze strutturali dell'equazione principale del trasporto radiativo con l'equazione di Boltzmann, ed è capace di riprodurre la dinamica radiativa sia nel regime ottico sottile che spesso.

Contents

Introduction

Relativistic hydrodynamics is concerned with the study of fluids which move at velocities close to the speed of light, and as such it has been historically developed to be applied to astrophysical and cosmological contexts [1].

In these frameworks, a non dissipative theory is formulated as the zeroth-order expansion of relativistic kinetic theory (a treatment of classical kinetic theory of gases within the language of special relativity), that leads to the development of the so called Relativistic Euler equations.

In the last years, new applications in fields other than astrophysics and cosmology (look for example at the dynamic of Quark Gluon Plasma for high energy nuclear physics [2] and the study of electron flows in graphene for condensed matter [3]) have made clear the necessity for a solid and structured theory of dissipative relativistic hydrodynamics, *i.e.* for a relativistic equivalent of the Navier-Stokes Equations, on which to build upon for reliable numerical simulations.

In fact, Relativistic Navier-Stokes equations have historically been plagued by theoretical shortcomings (the presence of second order space derivatives and first order time derivative implies super-luminal propagation) and show numerical instabilities in simulations. Although multiple steps have been made to overcome these shortcomings [4–6], a definitive flawless theory has yet to be formulated.

An alternative approach to the problem consists in exploiting the dynamic at the kinetic scale to resolve the evolution at the hydrodynamic scale. The relativistic Boltzmann equation in fact does not suffer from the same theoretical shortcomings of the relativistic Navier-Stokes equations, since due to the hyperbolic structure of kinetic equations the emergence of viscous effects does not break causality.

In the non relativistic scenario, this bottom-up approach can be numerically

achieved via the so called Lattice Boltzmann Methods, that evolve a seminal version of the Boltzmann equation to get the solution of the Navier-Stokes equations. So the extension of Lattice Boltzmann Methods to the relativistic regime (from now on called Relativistic Lattice Boltzmann Methods, RLBM) appears only natural.

In the past years, there have been several attempts in this direction. In [7,8] Mendoza et al. developed a scheme using Grad's moment matching technique, while in [9] Romatschke et al. established a scheme for an ultra-relativistic gas of particles via Laguerre polynomials expansion of the Maxwell-Jüttner distribution, at the expense of the loss of perfect streaming and therefore the need for an interpolation scheme.

An attempt at multi-time relaxation schemes has been done in [10], with the implicit goal of the independent tuning of shear viscosity and bulk viscosity, and with the additional positive effect of retaining perfect streaming on a Cartesian lattice. In [11] it has been shown that it is possible to avoid multi-time relaxation schemes, still using a Cartesian lattice and properly tuning the bulk viscosity for ultra-relativistic flows, so as to recover only the conservation of the momentum energy tensor, but still lacking the capability of recovering higher order moments. A further improvement has been obtained in [12], where an ultra relativistic scheme is developed with perfect streaming on a Cartesian grid, and with the ability to recover, in principle, higher order moments of the Maxwell-Jüttner distribution. In practice, such an improvement would require velocity stencils too big to be be practical.

Blaga and Ambruş [13,14] have developed a class of off-lattice quadrature based models capable of including arbitrarily high order moments, thus supporting simulations well beyond the hydrodynamic regime, spanning in principle between the inviscid regime all the way to the ballistic regime. Most of these previous schemes are focused on the simulation of $(3 + 1)$ dimensional ultra-relativistic systems. Through the years several attempts at $(2 + 1)$ dimensional schemes for the study of condensed matter systems have been realized [15–19], and attempts at bridging the gap between ultra-relativistic and non relativistic schemes were made as well [20].

This Ph.D program has been focused on the extension and generalization of [20] to a unified, dimension independent, kinematically wide Relativistic Lattice Boltzmann Method capable of simulating the whole mass spectrum, (from the ultra-relativistic to non-relativistic regime), the whole rarefaction spectrum, (from ideal flows to free streaming flows), and systems in every number of spatial dimensions, with particular focus on the most common cases ($d = 2$ and $d = 3$).

In the last part of the program the new techniques applied to extend the validity of RLBM to rarefied regimes have also been employed to describe radiation dynamics, a problem with relevant applications in astrophysical contexts [21–23]. A new special relativistic numerical scheme, capable of bridging the gap between optically thin regimes (when radiation weakly interacts with matter) to optically thick regimes (strong radiation-matter interaction) has been realized.

This thesis is organized as follows, with chapters from 2 to 6 representing original work:

- In Ch. 1 an account on the theory of Relativistic Kinetic Theory and Relativistic Hydrodynamics is given, starting from a brief derivation of Relativistic Boltzmann's Equation, with an introduction on two popular models for the approximation of the Collision Integral. Next, a dimension-independent treatment of Ideal Relativistic Hydrodynamics is provided, together with a description of the equilibrium distribution function and an ideal Equation of State. Lastly, dissipative effects are taken into account with the two most popular decompositions for the dissipative contributions to particle flow and energy momentum tensor.

  The content of this Chapter closely follows [24] generalizing the discussion to (d+1) dimensions, giving in particular d-dimensional expressions for the Ideal Equation of State, the equilibrium distribution function, and non equilibrium components of the energy-momentum tensor.

- In Ch. 2, after a quick introduction on non-relativistic Lattice Boltzmann Methods, the derivation of the Relativistic Lattice Boltzmann Method (RLBM), a numerical scheme capable of exploring all relativistic regimes and expressed in a (d+1) dimensional language, is provided. Particular focus is given to the truncated expansion of the equilibrium distribution function, to momentum discretization, and to the conversion from Physical to Lattice units. Lastly, a step by step description of the algorithm is provided.

  An extensive discussion of the method can be found in [25], where a detailed explanation of the velocity discretization procedure, together with additional benchmarks of the method and an application to (2+1) electron dynamics is given.

- In Ch. 3 the link between kinetic and macroscopic layer is established, by means of the Chapman-Enskog expansion and Grad's method of moments. Next, RLBM is used to discern which of the two methods provides the

correct link to relativistic hydrodynamics, and three different test flows are considered in order to provide a calibration for the transport coeficients of the fluid.

Further details on the (2+1) picture and on Bulk viscosity can be found respectively in [26] and [27], and again a general discussion is present in [25].

- In Ch. 4 two benchmarks for the RLBM scheme are presented: the Bjorken flow, a toy model used in Particle Physics to mimic the hydrodynamic behavior of Quark Gluon Plasma, and the Relativistic Sod Shock Tube, a benchmark commonly used in hydrodynamics to evaluate the quality of a numerical scheme in the presence of strong velocity gradients. In particular, it is evidenced how the previously exposed RLBM struggles in correctly reproducing the dynamic in the presence of weakly interacting fluids.

  An in depth discussion of the RLBM testing in the presence of Shock Waves can also be found in [28].

- In Ch. 5 I present an extension of RLBM that enables the simulation of flows at high Knudsen number (characterizing the level of interaction bewteen particles in the fluid), correcting the issues of the previous scheme by means of a new momentum space discretization. In this new procedure, the perfect streaming nature of the earlier iteration is sacrificed for more capillary and isotropic velocity stencils, that cure the issues previously evidenced in the Relativistic Sod Shock Tube benchmark.

  Further details on the new momentum discretization can be found for the (2+1) ultra-relativistic case in [29]. An article extending the method to (3+1) dimensions is in preparation.

- In Ch. 6, a brief introduction on a new lattice kinetic scheme, based on the improved stencil discretization exposed in Ch. 5, is exposed. The method is tasked with the reproduction of radiation dynamics in both the optically thick and thin regime.

  As in this thesis work only few details on the algorithmic development are presented, the interested reader will find an in depth description of the method in [30].

  Additionally, I present an application of the method to relativistic jets, systems that are encountered in astrophysics contexts [31–33].

A list of the publications produced through the years by the author is given below:

1. A. Gabbana, D. Simeoni, S. Succi, R. Tripiccione
   Relativistic dissipation obeys Chapman-Enskog asymptotics: Analytical
   and numerical evidence as a basis for accurate kinetic simulations
   [26] *Physical Review E, 99:052126, May 2019*

2. A. Gabbana, D. Simeoni, S. Succi, R. Tripiccione
   Probing bulk viscosity in relativistic flows
   [27] *Philosophical Transactions of the Royal Society A: Mathematical, Physical and Engineering Sciences, 378(2175):20190409, 2020*

3. A. Gabbana, S. Plumari, G. Galesi, V. Greco, D. Simeoni, S. Succi, R. Tripiccione
   Dissipative hydrodynamics of relativistic shock waves in a quark gluon
   plasma: Comparing and benchmarking alternate numerical methods
   [28] *Physical Reviews C, 101:064904, Jun 2020*

4. A. Gabbana, D. Simeoni, S. Succi, R. Tripiccione
   Relativistic lattice boltzmann methods: Theory and applications
   [25] *Physics Reports, 863:1–63, 2020*

5. L.R. Weih, A. Gabbana, D. Simeoni, L. Rezzolla, S. Succi, and R. Tripiccione
   Beyond moments: relativistic lattice Boltzmann methods for radiative
   transport in computational astrophysics
   [30] *Monthly Notices of the Royal Astronomical Society, 498(3):3374–3394, 08 2020*

6. L. Bazzanini, A. Gabbana, D. Simeoni, S. Succi, R. Tripiccione
   A Lattice Boltzmann Method for Relativistic Rarefied Flows in $(2 + 1)$
   Dimensions
   [29] *Journal of Computational Sciences, 51:101320, 2021*

7. L. Bazzanini, A. Gabbana, D. Simeoni, S. Succi, R. Tripiccione
   Quadrature rules for relativistic Lattice Kinetic Schemes: from hydrodynamics to rarefied flows
   (In preparation)

1

Relativistic Hydrodynamics

Here I give a brief description on the main principles of the theory behind Relativistic Kinetic Theory and Hydrodynamics, since the numerical method at the base of this thesis work is based on the first and resolves the second. The derivations included in these chapter closely follow [24], but are often enriched with additional original considerations that are meant to generalize the theory to (d+1)-dimensional systems, whereas [24] often focuses on the (3+1)-dimensional case.

This chapter is divided as follows: In Sec: *1.1* I give a review on Relativistic Kinetic Theory, a special relativistic extension of Boltzmann's kinetic theory of gases. Then in Sec: *1.2* and Sec: *1.3* the main theoretical concepts of relativistic hydrodynamics are given, respectively for fluids at equilibrium and outside equilibrium.

In this thesis I consider a gas of particles with mass m in a (d+1)-dimensional Flat space-time. The metric tensor is given by $\eta^{\alpha\beta} = \mathrm{diag}(+, -)$. Einstein's summation convention is in place, with Greek indexes running from 0 to d, and latin indexes running from 1 to d (d-dimensional vectors are represented in bold). In the next sections the projector on the orthogonal velocity space $\Delta^{\alpha\beta}$ will be largely used. Its definition and properties are summed up in Appendix. A.

1.1   Relativistic Kinetic Theory

The starting point in the development of a relativistic kinetic theory is the single-particle distribution function $f(x^\alpha, p^\alpha)$, where $x^\alpha = (ct, \boldsymbol{x})$ are space-time coordinates, and $p^\alpha = (p^0, \boldsymbol{p})$ is relativistic momentum, that accounts for the

number of particles contained at time t in the $2d$-dimensional phase space of initesimal volume $\mathrm{d}\mu(t) = \mathrm{d}\boldsymbol{x}\mathrm{d}\boldsymbol{p}$,

$$N(t) = f(x^\alpha, p^\alpha)\mathrm{d}\mu(t) . \tag{1.1}$$

It can be shown that the distribution function is invariant with respect to Lorentz transformations, since the number of particles is obviously invariant, and $\mathrm{d}\mu(t)$ can be proved to be invariant as well [24].

It can be verified [24] that the invariant equation that determines the change in the number of particles with respect to proper time is

$$m\frac{\Delta N(t)}{\Delta \tau} = \left[p^\alpha \frac{\partial f}{\partial x^\alpha} + mK^\alpha \frac{\partial f}{\partial p^\alpha} \right] d\mu(t) \tag{1.2}$$

with $K^\alpha = \frac{\mathrm{d}p^\alpha}{\mathrm{d}t}$ the so called Minkowsky Force, here supposed to not directly depend on momentum.

The term at first member accounts for the change in the number of particles due to collisions, and can be derived pretty much by following the rules of non-relativistic Boltzmann Theory, provided that the language of special relativity is used to describe collisions, and that the following assumptions (the same taken in classical kinetic theory) are taken:

- The gas is dilute enough that only binary elastic collisions are considered, and collisions involving more than two particles are ignored.

- *Molecular Chaos Hypothesis*: The momenta of the particles involved in the collisions are not correlated among each other.

- The time scales over which f changes significantly are bigger with respect to collision times, but smaller than times between two collisions. Same apply for length scales.

Following these hypothesis, and considering the binary collision depicted in Fig. 1.1, one derives this form for the LHS of Eq. 1.2:

$$m\frac{\Delta N(t)}{\Delta \tau} = \frac{p^0}{c} \left[\int (f'_* f' - f_* f) g_\emptyset \sigma \mathrm{d}\Omega \mathrm{d}\boldsymbol{p}_* \right] \mathrm{d}\mu(t) , \tag{1.3}$$
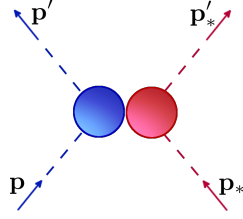
Figure 1.1: *Representation of an elastic collision between two particles of the fluid. The momenta of the particles before collision are denoted by $(\boldsymbol{p}, \boldsymbol{p_*})$, while the momenta after collision are denoted by $(\boldsymbol{p'}, \boldsymbol{p'_*})$. Consequently denote $f = f(\boldsymbol{x}, \boldsymbol{p}, t)$, $f_* = f(\boldsymbol{x}, \boldsymbol{p_*}, t)$, $f' = f(\boldsymbol{x}, \boldsymbol{p'}, t)$, $f'_* = f(\boldsymbol{x}, \boldsymbol{p'_*}, t)$*

with $g_\emptyset$ the so called Møller speed, a measure of the relative speed between the particles, σ the differential cross section of the scattering process. By defining the invariant flux

$$F = \frac{p^0 p_*^0}{c} g_\emptyset = \sqrt{(p^\alpha p_*^\alpha)^2 - m^4 c^2} \tag{1.4}$$

one can finally write down the final form of the *Relativistic Boltzmann Equation* for non degenerate relativistic gases

$$p^\alpha \frac{\partial f}{\partial x^\alpha} + m K^\alpha \frac{\partial f}{\partial p^\alpha} = \int (f'_* f' - f_* f) F \sigma \mathrm{d}\Omega \frac{\mathrm{d}\boldsymbol{p_*}}{\mathrm{p}_*^0} \ . \tag{1.5}$$

Note here that this equation is invariant with respect to Lorentz transformations, as in its derivation only invariant quantities have been used. Further, note that although particle mass is present into Eq. 1.5, equivalent formulations can be proposed that are perfectly well defined also for mass-less particles (dividing everything by p^0 does in fact get rid of the mass, but also doesn't manifestly show the coordinate invariance of the equation).

1.1.1 Model Equations

Eq. 1.5 is a complicated integro-differential equation, and its complications derive mainly from the quadratic nature of its collision integral, on the RHS of the equation (from now on said term will be denoted as Ω)

$$\Omega = \int (f'_* f' - f_* f) F \sigma \mathrm{d}\Omega \frac{\mathrm{d}\boldsymbol{p}_*}{\mathrm{p}^0_*} \ . \tag{1.6}$$

In the next sections, (specifically Sec. *1.2*) it will be shown that Ω satisfies among the others two main properties:

- For any collisional invariant ψ (introduced in the next section) the following equality must hold:

$$\int \Omega \psi \frac{\mathrm{d}\boldsymbol{p}}{p^0} = 0 \ . \tag{1.7}$$

- The H-theorem holds, meaning that the one particle distribution function f tends in time toward an equilibrium value f^{eq} (its description is given in Sec. *1.2.2*), or equivalently that

$$\int \Omega \log f \frac{\mathrm{d}\boldsymbol{p}}{p^0} \leq 0 \ : \tag{1.8}$$

the entropy production rate (introduced later on in this chapter) is bigger than zero and equals zero only when it is computed at equilibrium ($f = f^{\mathrm{eq}}$). More on this at the end of Sec. *1.2*

In order to simplify Eq. 1.5, approximated and simplified collision models are often introduced in place of Ω, especially when one develops Lattice Kinetic schemes or approaches analytical solutions of the Boltzmann equation. A sufficient conditions for the validity of said models is that they satisfy the conditions mentioned above (Eq. 1.7 and Eq. 1.8).

The most common Collision model for the classical non-relativistic case is given by the widely known Bhatnagar-Gross-Krook relaxation time approximation [34] (which is in fact at the base of the development of the classical Lattice Boltzmann scheme, see Sec. *2.1*), but other collision models have been used in the past [35].

As for relativistic theories, two main models have been used in the literature, both extensions of the BGK model to special relativity: Marle's model [36–38] and Anderson-Witting's model [39].

Marle's model is introduced by the following approximation:

$$\Omega \sim -\frac{m}{\tau}\left(f - f^{\mathrm{eq}}\right) \ , \tag{1.9}$$

with τ a typical relaxation time, *i.e.* the typical time needed to f to approach its equilibrium value f^{eq}. This model exhibits problems for mass-less particles, since in this case space homogeneous solutions of the relativistic Boltzmann equation relax to equilibrium in infinite time.

This argument was the reason why Anderson and Witting proposed their collision model:

$$\Omega \sim -\frac{p^{\alpha}U_{\alpha}}{c^2\tau}\big(f - f^{\text{eq}}\big) \, , \tag{1.10}$$

where U^{α} is the macroscopic velocity of the fluid in the Landau-Lifshitz decomposition (see Sec. *1.3.2* for more details). This collision model does not exhibit the problems highlighted in Marle's model, therefore it has been selected for the development of the Relativistic Lattice Boltzmann Method presented in Chapter *2*.

1.2   Ideal Relativistic Hydrodynamics

Eq. *1.5* is the base to work out the whole theory of relativistic hydrodynamics. As a starter, one can use it to obtain balance equations for macroscopic thermodynamic quantities, obtained as moments of the distribution function.

Consider a generic function $\psi(x^{\alpha}, p^{\alpha})$ of space, time and momentum, and multiply Eq. *1.5* by it. Then integrate over the invariant momentum space $\frac{d\boldsymbol{p}}{p^0}$

$$\int \psi \left[p^{\alpha}\frac{\partial f}{\partial x^{\alpha}} + mK^{\alpha}\frac{\partial f}{\partial p^{\alpha}} \right] \frac{\mathrm{d}\boldsymbol{p}}{p^0} = \int \psi(f'_* f' - f_* f)F\sigma\mathrm{d}\Omega\frac{\mathrm{d}\boldsymbol{p_*}}{\mathrm{p}^0_*}\frac{\mathrm{d}\boldsymbol{p}}{\mathrm{p}^0} \, . \tag{1.11}$$

Further manipulations of Eq. *1.11* lead to the so called *Generalized Transfer Equation*

$$\frac{\partial}{\partial x^{\alpha}}\int \psi p^{\alpha}f\frac{\mathrm{d}\boldsymbol{p}}{p^0} - \int f\left[p^{\alpha}\frac{\partial\psi}{\partial x^{\alpha}} + mK^{\alpha}\frac{\partial\psi}{\partial p^{\alpha}} \right]\frac{\mathrm{d}\boldsymbol{p}}{p^0} \tag{1.12}$$

$$= \frac{1}{4}\int (\psi + \psi_* - \psi' - \psi'_*)(f'_* f' - f_* f)F\sigma\mathrm{d}\Omega\frac{\mathrm{d}\boldsymbol{p_*}}{\mathrm{p}^0_*}\frac{\mathrm{d}\boldsymbol{p}}{\mathrm{p}^0} \, ,$$

that is basically a balance equation for the macroscopic quantity $\int \psi p^{\alpha}f\frac{\mathrm{d}\boldsymbol{p}}{p^0}$,

with production term due to collisions given by the RHS, and diffusive term given by the second bit in the LHS. The primed/star notation on the ψ is self explanatory, and it is immediately evident that quantities such that

$$\psi + \psi_* - \psi' - \psi'_* = 0 \tag{1.13}$$

identify a particular class of functions, that are called *Summational Invariants* or also *Collision Invariants*. For such quantities it is possible to verify the following theorem (proofs can be found in [24, 40, 41]):

Theorem:. *Any continuous and differentiable (at least $\in C^2$) function of momentum $\psi(p^\alpha)$ is a summational invariant if and only if it has the following form:*

$$\psi(p^\alpha) = a + b_\alpha p^\alpha \ , \tag{1.14}$$

with a/b_α any scalar/vector quantity that does not depend on p^α.

Choosing $\psi = c, cp^\beta$ one obtains balance equations for the most important quantities in relativistic fluid dynamics (in the second case assume for the moment external forces to be zero):

$$0 = \frac{\partial}{\partial x^\alpha} \left[c \int p^\alpha f \frac{\mathrm{d}\boldsymbol{p}}{p^0} \right] \ , \tag{1.15}$$

$$0 = \frac{\partial}{\partial x^\alpha} \left[c \int p^\alpha p^\beta f \frac{\mathrm{d}\boldsymbol{p}}{p^0} \right] \ , \tag{1.16}$$

where we define the *Particle Flow N^α* and the *Energy Momentum-Tensor $T^{\alpha\beta}$* as respectively the first and second moment of the one-particle distribution:

$$N^\alpha = c \int p^\alpha f \frac{\mathrm{d}\boldsymbol{p}}{p^0} \ , \tag{1.17}$$

$$T^{\alpha\beta} = c \int p^\alpha p^\beta f \frac{\mathrm{d}\boldsymbol{p}}{p^0} \ . \tag{1.18}$$

so that Eq. 1.15 and Eq. 1.16 become

$$\partial_\alpha N^\alpha = 0 \quad , \quad \partial_\alpha T^{\alpha\beta} = 0 \ . \tag{1.19}$$

Another interesting macroscopic quantity that can be introduced by setting $\psi = -k_{\mathrm{B}} c f \log f$ (not a summational invariant!) is the Entropy flow S^α.

$$S^\alpha = -k_{\mathrm{B}} c \int p^\alpha f \log f \frac{\mathrm{d}\boldsymbol{p}}{p^0} \, , \tag{1.20}$$

$$\varsigma = -\frac{k_{\mathrm{B}} c}{4} \int (f'_* f' - f_* f) \log \left(\frac{f' f'_*}{f f_*} \right) F \sigma \mathrm{d}\Omega \frac{\mathrm{d}\boldsymbol{p}_*}{\mathrm{p}^0_*} \frac{\mathrm{d}\boldsymbol{p}}{\mathrm{p}^0} \, , \tag{1.21}$$

so that Eq. 1.12 becomes in this case the balance equation

$$\partial_\alpha S^\alpha = \varsigma \, . \tag{1.22}$$

The entropy production rate ς here gives the rate at which entropy rises due to collisions. By introducing

$$H^\alpha = -\frac{S^\alpha}{k_{\mathrm{B}}} = c \int p^\alpha f \log f \frac{\partial \boldsymbol{p}}{p^0} \, , \tag{1.23}$$

$$S = -\frac{\varsigma}{k_{\mathrm{B}}} = \frac{c}{4} \int (f'_* f' - f_* f) \log \left(\frac{f' f'_*}{f f_*} \right) F \sigma \mathrm{d}\Omega \frac{\mathrm{d}\boldsymbol{p}_*}{\mathrm{p}^0_*} \frac{\mathrm{d}\boldsymbol{p}}{\mathrm{p}^0} \, , \tag{1.24}$$

Eq. 1.22 becomes

$$\partial_\alpha H^\alpha = S \, . \tag{1.25}$$

The following two important theorems can be proven [42] and the result goes under the name of H-theorem:

Theorem:. *If $H(t) = \frac{1}{c^2} H^\alpha U_\alpha$ is a continuous and differentiable function of time, and satisfies the following:*

$$\frac{\partial H}{\partial t} \leq 0 \qquad H \geq H_E = H(f^{eq})$$

and if both f and $\int p_0^{\eta+1} f \mathrm{d}\boldsymbol{p}$ are uniformly bounded [43] (f being also equicontinuous [44]) then

$$\lim_{t \to \infty} H(t) = H_E$$

Theorem:. *If one has* $\left[\lim\limits_{t\to\infty} H(t) = H_E\right]$ *then* $\left[\lim\limits_{t\to\infty} f(t) = f^{eq}\right]$

1.2.1 Fields at Equilibrium

Goal of this section will be to describe in more detail the particle flow N^α defined in Eq. 1.17 and the energy-momentum tensor $T^{\alpha\beta}$ defined in Eq. 1.18, when considering a fluid at equilibrium. It is useful to consider these quantities in a local Lorentz rest frame, *i.e.* the frame of an observer which is moving with the fluid and thus measures its macroscopic velocity U^α at rest:

$$U_R^\alpha = (c, \mathbf{0}) \tag{1.26}$$

Since one has the following physical understanding of the various components of the particle flow and energy momentum tensor

$$\begin{cases} \frac{1}{c}N^0 & = \text{particle number density} \\ N^i & = \text{particle flux density} \end{cases} , \qquad \begin{cases} T^{00} & = \text{internal energy density} \\ cT^{0i} & = \text{energy flux density} \\ \frac{1}{c}T^{i0} & = \text{momentum density} \\ T^{ij} & = \text{momentum flux density} \end{cases}$$

once the following quantities are introduced,

- n: particle number density

- P: isotropic pressure

- ϵ: internal energy density

- T: temperature

- s: entropy per particle

it is possible to specify N_R^α and $T_R^{\alpha\beta}$, since in a fluid at rest there is no particle/energy flux going on, and the only momentum contribution is given by hydrostatic pressure:

$$\begin{cases} N_R^0 & = cn \\ N_R^i & = 0 \end{cases} \quad , \quad \begin{cases} T^{00} & = \epsilon \\ T^{0i} & = 0 \\ T^{i0} & = 0 \\ T^{ij} & = P\delta^{ij} \end{cases}$$

At this point, the equilibrium versions in a generic reference frame can be identified just by considering an inverse Lorentz boost from the rest frame to the frame where the fluid has velocity U^α:

$$U^\alpha = \Lambda^\alpha{}_\beta U_R^\beta \rightarrow \begin{cases} N_E^\alpha & = \Lambda^\alpha{}_\beta N_R^\beta \\ T_E^{\alpha\beta} & = \Lambda^\alpha{}_\mu \Lambda^\beta{}_\nu T_R^{\mu\nu} \end{cases} ; \qquad (1.27)$$

therefore

$$N_E^\alpha = nU^\alpha \ , \qquad (1.28)$$

$$T_E^{\alpha\beta} = (P + \epsilon)\frac{U^\alpha U^\beta}{c^2} - P\eta^{\alpha\beta} \ . \qquad (1.29)$$

Once the equilibrium distribution moments are defined, it is possible to derive the *Constitutive Equations of an Ideal Fluid*, which are the relativistic version of Euler equations. By imposing Eq. 1.19 on the equilibrium quantities N_E^α and $T_E^{\alpha\beta}$, one gets:

$$\begin{cases} 0 & = \partial_\alpha N_E^\alpha & \textbf{Mass Conservation} \\ 0 & = U_\beta \partial_\alpha T_E^{\alpha\beta} & \textbf{Energy Conservation} \\ 0 & = \Delta_\beta \partial_\alpha T_E^{\alpha\beta} & \textbf{Momentum Conservation} \end{cases} , \qquad (1.30)$$

Then, taking Eq. 1.28 and Eq. 1.29, and by employing the decomposition of the gradient ∂_α into U^α parallel-orthogonal components (more on this decomposition in Appendix A) one can recover the conservation equations in a form similar to their non relativistic equivalents:

$$\begin{cases} 0 & = Dn + n\Delta^\alpha U_\alpha \\ 0 & = D\epsilon + (P+\epsilon)\nabla_\alpha U^\alpha \\ 0 & = DU^\alpha + \frac{c^2}{P+\epsilon}\nabla^\alpha P \end{cases} . \qquad (1.31)$$

1.2.2 Equilibrium distribution function

Having derived the equilibrium thermodynamic quantities, it is also possible to derive a functional form for the equilibrium distribution function f^{eq} that leads to said quantities. The first to derive such a functional form was Jüttner in [45], and therefore the relativistic counterpart of Maxwell-Boltzmann equilibrium distribution is called Maxwell- Jüttner distribution. It is easy to see that taking the non relativistic limit one recovers the usual Maxwell-Boltzmann statistics.

At equilibrium, the entropy production rate ς has to vanish, meaning that the distribution function f^{eq} has to satisfy (look at Eq. 1.20)

$$f_*^{\text{eq}\prime} f^{\text{eq}\prime} - f_*^{\text{eq}} f^{\text{eq}} = 0 , \qquad (1.32)$$

or, taking logarithms,

$$\log f_*^{\text{eq}\prime} + \log f^{\text{eq}\prime} = \log f_*^{\text{eq}} + \log f^{\text{eq}} , \qquad (1.33)$$

meaning that $\psi = \log f^{\text{eq}}$ is a summational invariant, and therefore according to Eq. 1.14 has to be written as

$$\log f^{\text{eq}} = a + b_\alpha p^\alpha \Rightarrow f^{\text{eq}} = exp(a + b_\alpha p^\alpha) . \qquad (1.34)$$

By resorting at the equilibrium quantities defined in Eq. 1.28 and Eq. 1.29, one can work out the values for a and b_α, and therefore write down explicitly Eq. 1.34:

$$f^{\text{eq}} = B(n,T)exp\left(-\frac{p^\alpha U_\alpha}{k_\text{B}T}\right) , \qquad (1.35)$$

with $B(n,T)$ a normalization coefficient that can be determined by using

Eq. 1.35 into Eq. 1.17 and setting B in order to satisfy the definition Eq. 1.28:

$$N_E^\alpha = c \int f^{\text{eq}} p^\alpha \frac{\mathrm{d}\boldsymbol{p}}{p_0} = cB \int e^{-\frac{p_\mu U^\mu}{k_{\text{B}} T}} p^\alpha \frac{\mathrm{d}\boldsymbol{p}}{p_0} = c \; B \; Z^\alpha = nU^\alpha \; , \qquad (1.36)$$

so that together with the analytical expression for the integral Z^α (see Appendix B for details), the correct normalization factor for the equilibrium distribution function can be determined:

$$B(n,T) = \left(\frac{c}{k_{\text{B}} T} \right)^d \frac{n}{2^{\frac{d+1}{2}} \pi^{\frac{d-1}{2}} \zeta^{\frac{d+1}{2}} K_{\frac{d+1}{2}}(\zeta)} \; , \qquad (1.37)$$

where $K_i(\zeta)$ is the modified Bessel function of the second kind of index i.

The relativistic parameter $\zeta = \frac{mc^2}{k_{\text{B}} T}$, named *Relativistic Coldness*, is the ratio between the rest energy of a particle mc^2 and $k_{\text{B}} T$, which gives the order of magnitude of the thermal energy in the gas. This is the parameter that quantifies the level of 'relativity' of the gas:

$$\zeta << 1 \quad \Rightarrow \text{ ultra-relativistic regime (mass-less particles)}$$
$$\zeta \sim 1 \quad \Rightarrow \text{ mildly-relativistic regime}$$
$$\zeta >> 1 \quad \Rightarrow \text{ classical (non-relativistic) regime}$$

1.2.3 Ideal Equation of State

The closure for the conservation equations is given by an appropriate Equation of State (EOS). In order to derive the EOS for a perfect gas in (d + 1) space-time coordinates in a relativistic regime, one can compute Eq. 1.18 using the definition in Eq. 1.35, together with the analytical expression for $Z^{\alpha\beta}$ (see again Appendix B):

$$T_E^{\alpha\beta} = c \int f^{\text{eq}} p^\alpha p^\beta \frac{\mathrm{d}\boldsymbol{p}}{p_0} = c \; B \; Z^{\alpha\beta} = PG_d \frac{U^\alpha U^\beta}{c^2} - nk_{\text{B}} T\eta^{\alpha\beta} \; , \qquad (1.38)$$

where the dimensionless parameter G_d has been introduced:

$$G_d = \frac{\epsilon + P}{P} = \zeta \frac{K_{\frac{d+3}{2}}(\zeta)}{K_{\frac{d+1}{2}}(\zeta)} \; . \qquad (1.39)$$

In order to identify the EOS it is then sufficient to match the terms with the same tensor structure in Eq. 1.38 and Eq. 1.29; one finally obtains:

$$\begin{aligned} \epsilon &= P\left(G_d - 1\right) , \\ P &= nk_{\mathrm{B}}T . \end{aligned} \tag{1.40}$$

It is interesting to check whether the formulation appearing in Eq. 1.40 is compatible to the known ideal EOSs of the ultra-relativistic and non-relativistic cases. First, it is easy to verify that for $\zeta \to 0$ one gets the expected result:

$$\epsilon_{\mathrm{ur}} = dP . \tag{1.41}$$

For the classical case one has instead to first define a kinetic energy density $\epsilon_{\mathrm{c}} = \epsilon - nmc^2$ by subtracting the rest energy density to ϵ. Then the limit $\zeta \to \infty$ provides the known result:

$$\lim_{\zeta \to \infty} \epsilon_{\mathrm{c}} = \lim_{\zeta \to \infty} P(G_d - 1 - \zeta) = \frac{d}{2}P . \tag{1.42}$$

In Fig. 1.2 the ratio $\frac{\epsilon_{\mathrm{c}}}{\epsilon_{\mathrm{ur}}}$ shows the behavior of the EOS for different spatial dimensions, and provides also the results for the two limiting cases.

From the EOS one can obtain a few more thermodynamic quantities which will be useful in the coming sections, such as the heat capacity at constant volume c_v:

$$c_v = \frac{\partial(\epsilon/n)}{\partial T} = k_{\mathrm{B}} \left[(2 + d)G_d + \zeta^2 - G_d^2 - 1\right] , \tag{1.43}$$

the heat capacity at constant pressure c_P ($h_e = (\epsilon + P)/n$ is the relativistic enthalpy per particle) :

$$c_P = \frac{\partial h_e}{\partial T} = k_{\mathrm{B}} \left[(2 + d)G_d + \zeta^2 - G_d^2\right] , \tag{1.44}$$

and the adiabatic sound speed c_s:
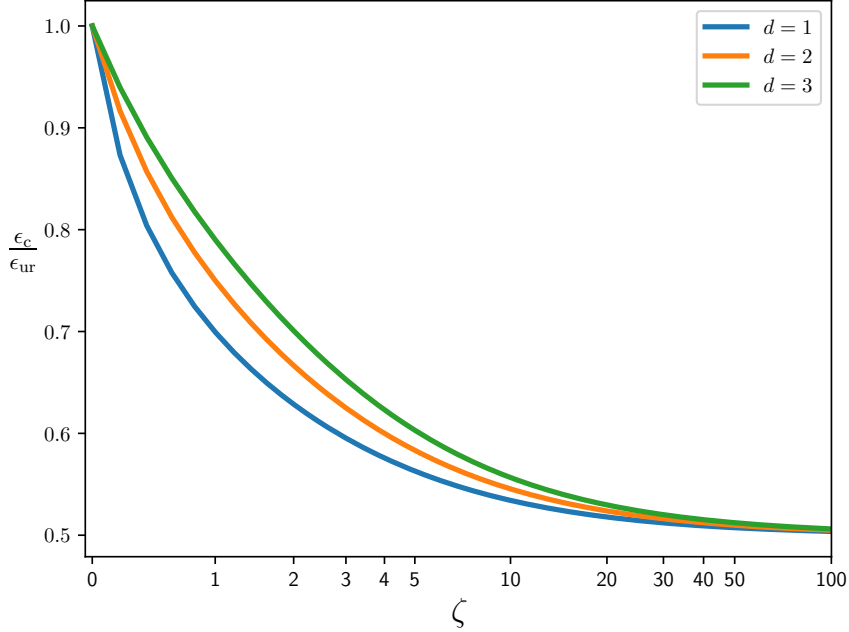
Figure 1.2: *Ratio of kinetic energy density to ultra-relativistic energy density for a gas obeying an ideal gas law, for different values of the spatial dimension d. One can appreciate that the limiting cases are well recovered.*

$$c_s = c\sqrt{\frac{P}{\epsilon + P}\frac{c_p}{c_v}} = c\sqrt{\frac{(2+d)G_d + \zeta^2 - G_d^2 - 1}{G_d\left((2+d)G_d + \zeta^2 - G_d^2\right)}}\;. \tag{1.45}$$

1.3 Dissipative Effects

The following explanation is a summary and d-dimensional generalization of the contributions that can be found in [1, 24, 46].

When considering non ideal fluids, dissipative effects have to be taken into account. Energy and momentum are transferred between infinitesimal parcels of fluid, and additional non equilibrium components enter in the definitions of N^α and $T^{\alpha\beta}$.

In order to identify these values, it is necessary to understand that N^α and $T^{\alpha\beta}$ have respectively $(d+1)$ and $\frac{1}{2}(d+1)(d+2)$ idependent terms (from Eq. 1.18 it is possible to see in fact that $T^{\alpha\beta}$ is symmetric)

$$\frac{1}{2}(d+1)(d+4) = \begin{cases} (d+1) & N^\mu \\ \frac{1}{2}(d+1)(d+2) & T^{\mu\nu} \end{cases} . \tag{1.46}$$

These fields have to be indentified with corresponding physical quantities, with some of them already defined in Sec. *1.2.1*. With the help of the decompositions Eq. A.8, Eq. A.9 and Eq. A.14 defined in Appendix A, one has

$$N^\alpha = nU^\alpha + q_N^\alpha , \tag{1.47}$$

$$T^{\alpha\beta} = \epsilon\frac{U^\alpha U^\beta}{c^2} + \frac{1}{c^2}\left(q_T^\alpha U^\beta + q_T^\beta U^\alpha\right) + \pi^{<\alpha\beta>} - (P+\varpi)\Delta^{\alpha\beta} . \tag{1.48}$$

The physical quantities appearing above are summed up in the following table

field	*nr. of terms*	*eq/neq*	*formula*
Fluid Velocity U^α	$(d+1)$	eq.	-
Particle density n	1	eq.	$n = \frac{1}{c^2}N_\alpha U^\alpha$
Energy density ϵ	1	eq.	$\epsilon = \frac{1}{c^2}U_\alpha U_\beta T^{\alpha\beta}$
Temperature T	1	eq.	EOS
hydrostatic pressure P	1	eq.	EOS
dynamic pressure ϖ	1	neq.	$\varpi = -P - \frac{1}{d}\Delta_{\alpha\beta}T^{\alpha\beta}$
Pressure deviator $\pi^{\alpha\beta}$	$\frac{d}{2}(d+3)$	neq.	$\pi^{<\alpha\beta>} = \left(\Delta_\gamma^\alpha\Delta_\delta^\beta - \frac{1}{d}\Delta^{\alpha\beta}\Delta_{\gamma\delta}\right)T^{\gamma\delta}$
Heat flow $q^\alpha = q_T^\alpha - q_N^\alpha$	$(d+1)$	neq.	$q_N^\alpha = \frac{P+\epsilon}{n}\Delta_{\alpha\beta}N^\beta$ $q_T^\alpha = \Delta_\mu^\alpha U_\nu T^{\mu\nu}$

and count a total of $\frac{1}{2}(14 + 7d + d^2)$ indipendent elements, that are reduced to the expected value Eq. 1.46 once the conditions

$$d+5 = \begin{cases} 1 & P = nk_\text{B}T \\ 1 & \epsilon = P(G_d - 1) \\ 1 & U_\mu U^\mu = c^2 \\ 1 & \partial_\mu N^\mu \\ d+1 & \partial_\mu T^{\mu\nu} \end{cases} \tag{1.49}$$

are taken into account.

Unfortunately, it is evident from the table *1.3* that all the non equilibrium components appearing in dissipative hydrodynamics depend on the definition of the macroscopic velocity U^μ, and therefore are not uniquely defined.

Two main definitions have been identified in the theory:

- **Eckart Decomposition** [47] In this frame, the macroscopic velocity is directly connected to the particle flux, meaning that the particle flow N^α is formally defined as its equilibrium counterpart N^α_E. This frame is also called *Particle frame*.

- **Landau-Lifshitz Decomposition** [48] In this frame, the macroscopic velocity is directly connected to the energy flux, meaning that the energy momentum tensor has only additional components that are Minkowsky-orthogonal to U^α. This frame is also called *Energy frame*.

1.3.1 Eckart Decomposition

In the Eckart decomposition (every quantity in this frame will be denoted using a subscript $_e$) the macroscopic velocity is chosen to be parallel to the particle flow:

$$U_e^\alpha = \frac{n_e c^2}{N^\mu N_\mu} N^\alpha \ . \tag{1.50}$$

With this prescription, it is easy to show that

$$q_N^\alpha = 0 \rightarrow q^\alpha = q_T^\alpha \equiv q_e^\alpha \tag{1.51}$$

Therefore N^α and $T^{\alpha\beta}$ are defined as follows:

$$N^\alpha = n_e U_e^\alpha \ , \tag{1.52}$$

$$T^{\alpha\beta} = \epsilon_e \frac{U_e^\alpha U_e^\beta}{c^2} - (P_e + \varpi_e)\Delta_e^{\alpha\beta} + \pi_e^{<\alpha\beta>} + \frac{1}{c^2}\left(U_e^\alpha q_e^\beta + U_e^\beta q_e^\alpha\right) \ . \tag{1.53}$$

Another quantity that can be decomposed is the entropy flow $S^\alpha = s_e U_e^\alpha + \phi_e^\alpha$,

- **entropy density:** $s_e = \frac{1}{c^2} S_\alpha U_e^\alpha$

- **entropy flux:** $\phi_e^\alpha = \Delta_{e\beta}^\alpha S^\beta$

1.3.2 *Landau-Lifshitz Decomposition*

The Landau decomposition (denoted by the subscript ℓ) proposes instead the following implicit definition of U_ℓ^α:

$$U_\ell^\alpha = \frac{c^2 U_{\ell\beta} T^{\alpha\beta}}{U_{\ell\mu} U_{\ell\nu} T^{\mu\nu}} \tag{1.54}$$

which implies

$$q_T^\alpha = 0 \rightarrow q^\alpha = -q_N^\alpha \equiv q_\ell^\alpha \tag{1.55}$$

and the following decomposition for the particle flow and the energy-momentum tensor:

$$N^\alpha = n_\ell U_\ell^\alpha + A^\alpha \ , \tag{1.56}$$

$$T^{\alpha\beta} = \epsilon_\ell \frac{U_\ell^\alpha U_\ell^\beta}{c^2} - (P_\ell + \varpi_\ell)\Delta_\ell^{\alpha\beta} + \pi_\ell^{<\alpha\beta>} \ , \tag{1.57}$$

where A^α is an additional, U^α-orthogonal term to be determined. In order to do so, one defines as V^α the difference between the macroscopic velocities in the two decompositions:

$$U_\ell^\alpha = U_e^\alpha + V^\alpha \ . \tag{1.58}$$

Obviously, at equilibrium both descriptions are equivalent, so V^α represents a non-equilibrium quantity. Assuming to be close to equilibrium, so that quadratic terms can be ignored, one can determine some useful properties by imposing $U_\ell^\alpha U_{\ell\alpha} = U_e^\alpha U_{e\alpha} = c^2$:

$$V_\alpha U_\ell^\alpha = U_\ell^\alpha U_{e\alpha} = 0 \ . \tag{1.59}$$

Then, by imposing the equality of N^α among the two decompositions,

$$N^\alpha = n_e U_e^\alpha = n_\ell U_\ell^\alpha + A^\alpha \ , \tag{1.60}$$

one can determine (by taking the scalar product by U_ℓ^α) that $n_{\rm e} = n_\ell \equiv n$. Further, it is easy to then verify that

$$V^\alpha = -\frac{A^\alpha}{n} \; , \tag{1.61}$$

and by applying the same procedure to the energy momentum tensor, (equate Eq. 1.53 to Eq. 1.57, use Eq. 1.61, and ignore all non linear terms) and entropy density, it is possible to verify that

$$
\begin{aligned}
\pi_{\rm e}^{<\alpha\beta>} &= \pi_\ell^{<\alpha\beta>} \equiv \pi^{<\alpha\beta>}, \\
P_{\rm e} &= P_\ell \equiv P, \\
\varpi_{\rm e} &= \varpi_\ell \equiv \varpi, \\
\epsilon_{\rm e} &= \epsilon_\ell \equiv \epsilon, \\
s_{\rm e} &= s_\ell \equiv s
\end{aligned}
\tag{1.62}
$$

and all these relationships hold as long as one stays close to equilibrium. In the end, the Landau-Lifshitz decomposition for N^α and $T^{\alpha\beta}$ reads as

$$N^\alpha = nU_\ell^\alpha - \frac{n}{P+\epsilon}q^\alpha \; , \tag{1.63}$$

$$T^{\alpha\beta} = \epsilon\frac{U_\ell^\alpha U_\ell^\beta}{c^2} - (P+\varpi)\Delta_\ell^{\alpha\beta} + \pi^{<\alpha\beta>} \; , \tag{1.64}$$

and the relationship between the two decompositions is given by

$$U_\ell^\alpha = U_{\rm e}^\alpha + \frac{n}{P+\epsilon}q^\alpha \; . \tag{1.65}$$

In the following, unless explicitly stated, the Landau-Lifshitz decomposition will be used, so the subscript ℓ will be from now on omitted. All formulas defined in Tab. 1.3 are used.

1.3.3 Transport Equations

Once a decomposition among the ones previously presented is chosen, one can work out the conservation equations for a dissipative fluid just like it was previously

done for an ideal fluid at the end of Sec. *1.2.1* (Eq. 1.31). For Landau-Lifshitz, for example, one can take Eq. 1.63 and Eq. 1.64 and insert them into Eq. 1.19.

In this way one would get the relativistic versions of Navier-Stokes and Fourier equations. The problem is that, just like in the classical case one has to specify a form for the shear stress tensor, here the obtained conservation equations would not be of relevant use if one does not specify a functional form for ϖ, $\pi^{<\alpha\beta>}$, and q^α.

Traditionally, the most straight forward way of building such constitutive equations is the thermodynamic theory of irreversible processes, that assumes a linear relationships between the thermodynamic forces and fluxes:

$$\varpi = -\mu\nabla_\alpha U^\alpha \ , \tag{1.66}$$

$$\pi^{<\alpha\beta>} = 2\eta\nabla^{<\alpha}U^{\beta>} \ , \tag{1.67}$$

$$q^\alpha = \lambda\left(\nabla^\alpha T - \frac{T}{c^2}DU^\alpha\right) \ . \tag{1.68}$$

μ, η, and λ are respectively known as *Bulk Viscosity*, *Shear Viscosity*, and *Thermal Conductivity*. The three quantities are collectively called *Transport Coefficients*, and Eq. 1.66, Eq. 1.67 and Eq. 1.68 are known as *First Order Transport Equations*.

When considering non relativistic velocities, these equations assume the classical non-relativistic forms (since $U^\alpha = \gamma(c, \boldsymbol{u})$, with γ the Lorentz Factor, the non relativistic limit is represented by $\gamma \sim 1 + O((\boldsymbol{u}/c)^2)$):

$$\begin{cases} \varpi & = \mu\partial_k u_k \\ \pi^{<ij>} & = \eta(\partial_i u_j + \partial_j u_i - \frac{2}{d}\delta_{ij}\partial_k u_k) \\ q^i & = -\lambda\partial_i T \end{cases} \tag{1.69}$$
$$0 = \pi^{<00>} = \pi^{<0i>} = \pi^{<i0>} = q^0 \ .$$

By comparing Eq. 1.68 with the last of Eq. 1.69, one notes that a completely relativistic effect occurs: even when considering isothermal flows, there is a heat flux due to pressure gradient (as it can be seen by transforming the second term of Eq. 1.68 with the help of Eq. 1.31).

Also, a problematic property of the first order transport equations is that they are not causal, meaning that if one inserts them into balance equations Eq. 1.19, the second order derivatives would make them parabolic equations and

therefore would imply that information travels faster than light [49] (see [1] for a detailed explanation).

First order theories are not compatible with special relativity, therefore *second order theories* have been proposed through the years [50, 51] that try to restore causality: the most successful among those, known as Israel-Stewart theory (IS), encapsulates Maxwell-Cattaneo's relaxation formulation [52] into a theory of dissipative hydrodynamics [4, 5, 53]. Reviews on second order theories are available in [54, 55].

$$\tau_0 D\varpi + \varpi = -\mu \nabla_\alpha U^\alpha \ , \tag{1.70}$$

$$\tau_1 \Delta^\alpha_\nu \Delta^\beta_\mu D\pi^{<\mu\nu>} + \pi^{<\alpha\beta>} = 2\eta \nabla^{<\alpha} U^{\beta>} \ , \tag{1.71}$$

$$\tau_2 \Delta^\alpha_\mu Dq^\mu + q^\alpha = \lambda \left(\nabla^\alpha T - \frac{T}{c^2} DU^\alpha \right) \ . \tag{1.72}$$

However, in recent years it has been shown that IS formulation exhibits some theoretical shortcomings [6] as well as poor agreement with numerical solutions of the Boltzmann equation [56,57]. In practice, there is still some work to do in order to obtain an efficient, stable and causal theory of dissipative hydrodynamics.

For this reason resorting to a kinetic description to detail relativistic hydrodynamics sounds appealing. In fact the basic equation of relativistic kinetic theory, Eq. 1.5, does not present second order derivatives and is thus hyperbolic: it does not show causality problems. This is in fact one of the main advantages of relativistic lattice kinetic schemes: dissipation arises naturally from the dynamics, without posing theoretical shortcomings.

2

Lattice Kinetic Schemes

In this chapter I will describe in detail all the algorithmic steps that have to be taken in order to derive a Relativistic Lattice Boltzmann Method (RLBM), *i.e.* a Lattice Boltzmann Method (LBM) compatible with the special relativistic formulation of kinetic theory and hydrodynamics detailed in Ch. 1.

What will be obtained is a fully fledged numerical scheme capable to simulate fluids ranging from the ultra-relativistic regime to the non-relativistic one, with a firm control on the transport coefficients, and within $d = 1, 2, 3$ spatial dimensions. More detail on the derivation of the method presented in this chapter can be found in [25].

The first RLBM has been derived at the start of the past decade [7,8] as a natural extension of the classical LBM. It focused on the description of gases made up of mass-less relativistic particles, and described (3+1) dimensional fluids. The first model developed using an expansion of the Maxwell-Jüttner distribution, like traditional LBMs, was derived in [9]. The model sacrifices perfect streaming for a more straightforward discretization procedure, but can be formulated using coordinates different than Cartesian ones and can be extended to work with non ideal EOS [58] (an ideal continuation of this work can be represented by [13], that extends the off-lattice approach to also work with beyond hydrodynamic regimes).

Subsequent development to [7,8] (that is based on the use of classical LBM stencils) are represented by [10], that implemented a multi-relaxation time scheme, but was not extensible to higher order moments, and by [11], that cured some difficulties of the original model in the energy-momentum tensor by opportunely tuning the transport coefficients.

All of these improvements were finalized into [12], a (3+1) lattice kinetic scheme for ultra-relativistic flows capable of correctly reproducing the hydrody-

namic moments and with perfect streaming implemented.

All the models mentioned so far only tackle ultra-relativistic flows, and a scheme that bridges the gap between these flows and non-relativistic flows has been presented in [20]. The RLBM presented in this thesis is an algorithmic refinement of this last scheme, that generalizes the method to a generic number of spatial dimensions, and is also equipped with tunable macroscopic transport coefficients. Said scheme has been presented in detail in [25].

The chapter is divided as follows: in Sec: *2.1* I give a review of the algorithmic steps needed to derive a classical (non relativistic) LBM. In Sec: *2.2* the RLBM in its generic (d+1) dimensional formulation is presented.

2.1   *Non relativistic Lattice Boltzmann Methods*

The Relativistic Lattice Boltzmann Method presented in the next sections will naturally build on classical (non-relativistic) Lattice Boltzmann Method (LBM) for its development, therefore a basic knowledge of classical lattice kinetic schemes is advised. In this section I will therefore provide a brief summary on the main features of LBM, in order to ease the understanding of the next sections. The interested reader will be able to find a detailed description of the method in the literature [59, 60].

LBM is a computational scheme that was realized in the past decades to tackle the simulation of classical hydrodynamics. It is powerful, highly parallelizable, and an alternative to the more traditional Computational Fluid Dynamic solvers, that directly solve the macroscopic conservation equations of the fluid flow. LBM relies instead on a statistical description at the mesoscopic scale (which is an intermediate step between the molecular scale, of the order of the nm, and the macroscopic scale, beyond the mm), and is therefore strongly bonded to the kinetic theory of gases [35].

The origins of the method date back to the pioneering work made in the 80s on Lattice Gas Cellular Automata [61–63]. Subsequent developments established a background for LBM as a self contained theory [64–67] to the point of its complete formulation with mathematical foundations grounded in the Hermite Quadrature [68, 69].

As already stated, LBM is theoretically based on the kinetic theory, and therefore has at its core the so called Boltzmann Equation

$$\left(\frac{\partial}{\partial t} + \boldsymbol{v} \cdot \boldsymbol{\nabla}_x + \frac{\boldsymbol{F}}{m} \cdot \boldsymbol{\nabla}_v \right) f(\boldsymbol{x}, \boldsymbol{v}, t) = \Omega , \tag{2.1}$$

where the distribution function $f(\boldsymbol{x}, \boldsymbol{v}, t)$ is the phase space number density of mass m particles with velocity $\boldsymbol{v}$, position $\boldsymbol{x}$, at time t, that are subject to the volume body force $\boldsymbol{F}$.

The right hand side of Eq. 2.1, that accounts for inter-particle collisions, is a complicated integral in the velocity space, that makes Eq. 2.1 an integro-differential Partial Differential Equation. Therefore this term is replaced with the customary Bhatnagar-Gross-Krook (BGK) relaxation time approximation [34]:

$$\Omega \sim -\frac{1}{\tau} \Big[f(\boldsymbol{x}, \boldsymbol{v}, t) - f^{\text{eq}}(\boldsymbol{x}, \boldsymbol{v}, t) \Big] . \tag{2.2}$$

This approximation is physically motivated by the natural tendency of f to reach, in a typical time τ, the equilibrium distribution f^{eq} represented for classical fluids by the Maxwell-Boltzmann distribution

$$f^{\text{eq}}(\boldsymbol{x}, \boldsymbol{v}, t) = \rho(\boldsymbol{x}, t) \left(\frac{m}{2\pi k_{\text{B}} T(\boldsymbol{x}, t)} \right)^{\frac{d}{2}} \exp\left[-\frac{m(\boldsymbol{v} - \boldsymbol{u}(\boldsymbol{x}, t))^2}{k_{\text{B}} T(\boldsymbol{x}, t)} \right] , \tag{2.3}$$

with d the dimensionality of the system, k_{B} the Boltzmann constant and ρ, T, and $\boldsymbol{u}$ respectively the mass density, the temperature, and the macroscopic velocity fields of the fluid (note that f^{eq} depends on space and time trhough these quantities). These fields can be computed as the first moments of the distribution function (T is computed with the aid of an equation of state, and here we use an ideal EOS):

$$\rho(\boldsymbol{x}, t) = \int f(\boldsymbol{x}, \boldsymbol{v}, t) \mathrm{d}\boldsymbol{v} , \tag{2.4}$$

$$\boldsymbol{u}(\boldsymbol{x}, t) = \frac{1}{\rho(\boldsymbol{x}, t)} \int f(\boldsymbol{x}, \boldsymbol{v}, t) \mathrm{d}\boldsymbol{v} , \tag{2.5}$$

$$T(\boldsymbol{x}, t) = \frac{1}{d k_{\text{B}} \rho(\boldsymbol{x}, t)} \int |\boldsymbol{v} - \boldsymbol{u}(\boldsymbol{x}, t)|^2 f(\boldsymbol{x}, \boldsymbol{v}, t) \mathrm{d}\boldsymbol{v} ; \tag{2.6}$$

The algorithmic development of LBM starts, after the variables are made dimensionless, from realizing that both f and f^{eq} can be expanded as a series of

orthonormal polynomials, and specifically the rank n tensors Hermite polynomials $\boldsymbol{H}^{(n)}(\boldsymbol{v})$ (the reason for the choice of such orthonormal basis will become clear afterwards)

$$f(\boldsymbol{x}, \boldsymbol{v}, t) = \omega(\boldsymbol{v}) \sum_n^\infty \frac{1}{n!} \boldsymbol{a}^{(n)}(\boldsymbol{x}, t) \cdot \boldsymbol{H}^{(n)}(\boldsymbol{v}) , \tag{2.7}$$

$$f^{\text{eq}}(\boldsymbol{x}, \boldsymbol{v}, t) = \omega(\boldsymbol{v}) \sum_n^\infty \frac{1}{n!} \boldsymbol{a}_{\text{eq}}^{(n)}(\boldsymbol{x}, t) \cdot \boldsymbol{H}^{(n)}(\boldsymbol{v}) , \tag{2.8}$$

with the expansion coefficients given by

$$\boldsymbol{a}^{(n)}(\boldsymbol{x}, t) = \int f(\boldsymbol{x}, \boldsymbol{v}, t) \boldsymbol{H}^{(n)}(\boldsymbol{v}) \mathrm{d}\boldsymbol{v} , \tag{2.9}$$

$$\boldsymbol{a}_{\text{eq}}^{(n)}(\boldsymbol{x}, t) = \int f^{\text{eq}}(\boldsymbol{x}, \boldsymbol{v}, t) \boldsymbol{H}^{(n)}(\boldsymbol{v}) \mathrm{d}\boldsymbol{v} , \tag{2.10}$$

and the weight function $\omega(\boldsymbol{v})$ given by

$$\omega(\boldsymbol{v}) = \frac{1}{(2\pi)^{d/2}} e^{-\frac{\boldsymbol{v}^2}{2}} . \tag{2.11}$$

Note that a key aspect of the whole procedure is the following equality

$$f^{\text{eq}} = \frac{\rho}{T^{d/2}} \omega \left(\frac{\boldsymbol{v} - \boldsymbol{u}}{\sqrt{T}} \right) , \tag{2.12}$$

since it gives a way to directly compute Eq. 2.10 and provides a direct link between the coefficients $\boldsymbol{a}_{\text{eq}}^{(n)}$ and the hydrodynamic quantities of interest :

$$\boldsymbol{a}_{\text{eq}}^{(0)} = \rho \tag{2.13}$$

$$\boldsymbol{a}_{\text{eq}}^{(1)} = \rho \boldsymbol{u} \tag{2.14}$$

$$\boldsymbol{a}_{\text{eq}}^{(2)} = \rho \left(\boldsymbol{u} \otimes \boldsymbol{u} + (T-1)\mathbb{I} \right) \tag{2.15}$$

This, together with the property of the collision invariants ($\int \psi \Omega \mathrm{d}\boldsymbol{v} = 0$ for $\psi = 1, \boldsymbol{v}, \boldsymbol{v}^2, |\boldsymbol{v} - \boldsymbol{u}|^2$), guarantees the following

$$\boldsymbol{a}_{\text{eq}}^{(0)} = \int f^{\text{eq}} \mathrm{d}\boldsymbol{v} = \rho = \int f \mathrm{d}\boldsymbol{v} = \boldsymbol{a}^{(0)} \tag{2.16}$$

$$\boldsymbol{a}_{\text{eq}}^{(1)} = \int \boldsymbol{v} f^{\text{eq}} \mathrm{d}\boldsymbol{v} = \rho \boldsymbol{u} = \int \boldsymbol{v} f \mathrm{d}\boldsymbol{v} = \boldsymbol{a}^{(1)} \tag{2.17}$$

$$\mathrm{Tr}\left[\boldsymbol{a}_{\text{eq}}^{(2)}\right] + \rho(d - \boldsymbol{u}^2) = \int |\boldsymbol{v} - \boldsymbol{u}|^2 f^{\text{eq}} \mathrm{d}\boldsymbol{v} = \rho dT = \int |\boldsymbol{v} - \boldsymbol{u}|^2 f \mathrm{d}\boldsymbol{v} = \mathrm{Tr}\left[\boldsymbol{a}^{(2)}\right] + \rho(\mathrm{d} - \boldsymbol{u}^2)$$

This has two main consequences: 1), since one is interested only in the first conserved N moments of f, Eq. 2.7 can be truncated up to N, with no fear of losing information on the quantities of interest

$$f = \omega \sum_n^N \frac{1}{n!} \boldsymbol{a}^{(n)} \cdot \boldsymbol{H}^{(n)} \;, \quad f^{\text{eq}} = \omega \sum_n^N \frac{1}{n!} \boldsymbol{a}_{\text{eq}}^{(n)} \cdot \boldsymbol{H}^{(n)} \;, \tag{2.18}$$

and 2), Gauss quadrature rules can be employed for the discretization of the velocity space.

In fact since Eq. 2.18 guarantees that f/ω is at most a polynomial of order N, from Eq. 2.10 one sees that in order to correctly compute the expansion coefficients up to the desired order quadrature rules that exactly integrate $2N$ order polynomials are needed. This means that one needs a rule to choose a set of N_{pop} discrete velocities $\boldsymbol{c}_i$ and related weights w_i, so that the integrals of Eq. 2.10 can be exactly turned into discrete sums without loss of information:

$$\boldsymbol{a}^{(n)}(\boldsymbol{x}, t) = \int f(\boldsymbol{x}, \boldsymbol{v}, t) \boldsymbol{H}^{(n)}(\boldsymbol{v}) \mathrm{d}\boldsymbol{v}$$

$$= \sum_i^{N_{\text{pop}}} \frac{w_i f(\boldsymbol{x}, \boldsymbol{c}_i, t)}{\omega(\boldsymbol{c}_i)} \boldsymbol{H}^{(n)}(\boldsymbol{c}_i) \quad, \tag{2.19}$$

Obviously, Eq. 2.13 and Eq. 2.16 guarantee that quadratures working for the expansion coefficients are also preserving the thermodynamic quantities ρ, $\boldsymbol{u}$ and T, which in the end are exactly the quantities one wants to obtain:

$$\rho = \sum_{i}^{N_{\mathrm{pop}}} w_i \frac{f(\boldsymbol{x}, \boldsymbol{c}_i, t)}{\omega(\boldsymbol{c}_i)} \tag{2.20}$$

$$\rho \boldsymbol{u} = \sum_{i}^{N_{\mathrm{pop}}} w_i \frac{f(\boldsymbol{x}, \boldsymbol{c}_i, t)}{\omega(\boldsymbol{c}_i)} \boldsymbol{c}_i \tag{2.21}$$

$$\rho dT = \sum_{i}^{N_{\mathrm{pop}}} w_i \frac{f(\boldsymbol{x}, \boldsymbol{c}_i, t)}{\omega(\boldsymbol{c}_i)} |\boldsymbol{c}_i - \boldsymbol{u}|^2 \tag{2.22}$$

The determination of minimal sets $\begin{bmatrix} w_i, c_i \end{bmatrix}$ has been studied in the past, and to this day the sets for $d = 1, 2, 3$ and the first values of N are well established in the literature [70] (while the case $d = 1$ can be solved analytically by employing the classical formulas for the Gauss-Hermite quadrature rule [71], the higher dimensional cases have to be solved numerically, by resorting to the so called method of *prescribed abscissae* [72]).

Once discretization in the velocity space is done, one is left with a group of N_{pop} values $f_i(\boldsymbol{x}, t) = f(\boldsymbol{x}, \boldsymbol{c}_i, t)$, which are commonly called *populations*.

By integrating Eq. 2.1 through characteristics, and with the help of a second order explicit Euler forward scheme for the approximation of the subsequent integral (more details on this are available in [60], Ch. 3.5), one can derive the *Lattice Boltzmann Equation*, that dictates how populations f_i evolve in time:

$$f_i(\boldsymbol{x} + \boldsymbol{c}_i \Delta t, t + \Delta t) = f_i(\boldsymbol{x}, t) - \frac{\Delta t}{\tau} \big(f_i(\boldsymbol{x}, t) - f_i^{\mathrm{eq}}(\boldsymbol{x}, t) \big) \tag{2.23}$$

2.2 Relativistic Lattice Boltzmann Methods

In this section a review on the main logical steps needed to develop a Relativistic Lattice Boltzmann Method will be given. It will be immediately evident that although the procedure to define a RLBM stems directly from the one presented in the previous section for LBM, there are complications in the development of the method caused by the request of Lorentz invariance. In particular, the different functional dependency of the equilibrium distribution function (Maxwell-Jüttner versus Maxwell-Boltzmann) on particle's velocities makes it impossible to adopt Hermite polynomials for the truncated expansion of the equilibrium, and to use

Gauss-Hermite quadratures for the velocity space discretization.

The procedure used to define this RLBM has its roots in the schemes used for ultra-relativistic gases in [12, 58], and has been developed though the years by the author's research group [19, 20]. Then a final, comprehensive generalization of the method to (d+1) dimensions has been presented in [25]. This is exactly the RLBM that will be described in this section.

The starting equation for the algorithmic development is the relativistic Boltzmann equation in the Anderson-Witting approximation

$$p^\alpha \frac{\partial f}{\partial x^\alpha} + m K^\alpha \frac{\partial f}{\partial p^\alpha} = -\frac{p^\alpha U_\alpha}{c^2 \tau} \left(f - f^{\text{eq}} \right) . \tag{2.24}$$

As already stated, the derivation is similar to that of a LBM and can be summarized in the following steps (from now on, unless explicitly stated, natural units will be used: $c = k_{\text{B}} = 1$)

1. The first step consists in writing down Eq. 2.24 in a more appropriate form by dividing it for p^0:

$$\frac{\partial f}{\partial t} + v^j \frac{\partial f}{\partial x^j} + \frac{m K^\alpha}{p^0} \frac{\partial f}{\partial p^\alpha} = -\frac{p^\alpha U_\alpha}{\tau p^0} \left(f - f^{\text{eq}} \right) , \tag{2.25}$$

   where $v^j = p^j/p^0$ is particles' velocity. In this form the equation resembles its non-relativistic counterpart.

2. Then, an appropriate polynomial expansion of the Maxwell-Jüttner f^{eq} has to be produced. Since the functional dependency of f^{eq} on the microscopic velocity v^i is not quadratic, Hermite polynomials are not suited for the job.

   A proper set of rank n tensor polynomials $\boldsymbol{J^{(n)}}(p^\mu)$ is therefore built by means of a Gram-Schmidt orthogonalization procedure on the set $\{1, p^\alpha, p^\alpha p^\beta, \dots\}$ (here $\cdot$ represents full tensor contraction).

$$f^{\text{eq}}(p^\mu, U^\mu, T) = \omega(p^0) \sum_{k=0}^{\infty} \boldsymbol{a^{(k)}}(U^\mu, T) \cdot \boldsymbol{J^{(k)}}(p^\mu) \tag{2.26}$$

   with $\omega(p^0)$ a weight function, and $\boldsymbol{a^{(k)}}(U^\mu, T)$ the tensor expansion coefficients

$$\boldsymbol{a^{(k)}}(U^\mu, T) = \int f^{\text{eq}}(p^\mu, U^\mu, T) \boldsymbol{J^{(k)}}(p^\mu) \frac{\mathrm{d}\boldsymbol{p}}{p^0} \tag{2.27}$$

Just like in the LBM, the weight function $\omega(p^0)$ is chosen in such a way that the expansion coefficient of k-th order coincides with the k-th moment of the distribution function, so that truncating Eq. 2.26 to order N preserves its first N moments.

$$f_N^{\text{eq}}(p^\mu, U^\mu, T) = \omega(p^0) \sum_{k=0}^{N} \boldsymbol{a}^{(\boldsymbol{k})}(U^\mu, T) \cdot \boldsymbol{J}^{(\boldsymbol{k})}(p^\mu) \qquad (2.28)$$

3. A quadrature rule has now to be found. By resorting to the method of prescribed abscissae [72], one identifies a set of N_{pop} discrete momenta p_i^μ (with the additional caveat of the corresponding discrete velocities having to sit on the nodes of a Cartesian Grid in order to preserve Perfect Streaming) and related weights w_i. Then one has a set of N_{pop} distribution functions $f_i = f(p_i^\mu, x^\mu)$, N_{pop} discrete versions of Eq. 2.25, N_{pop} equilibrium distribution functions f_{iN}^{eq}

$$f_{iN}^{\text{eq}} = w_i \sum_{k=0}^{N} \boldsymbol{a}^{(\boldsymbol{k})}(U^\mu, T) \cdot \boldsymbol{J}^{(\boldsymbol{k})}(p_i^\mu) \qquad (2.29)$$

4. Very much like it is done in the non-relativistic LBM, the discretization in space and time is done by integrating over characteristics and approximating the integral via a second order Euler scheme, leading to

$$f_i(\boldsymbol{x} + \boldsymbol{v}^i \Delta t, t + \Delta t) = f_i(\boldsymbol{x}, t) - \frac{p_i^\alpha U_\alpha}{\tau} \big(f_i(\boldsymbol{x}, t) - f_{iN}^{\text{eq}} \big) + F_i^{\text{ext}} \qquad (2.30)$$

with F_i^{ext} the discretized version of the external forcing term appearing in Eq. 2.25. Of course, this term has to be properly treated as well, and a description of its discretization will be given in the following pages.

2.2.1 Expansion of the Maxwell-Jüttner distribution

Before detailing how the expansion of the equilibrium distribution is performed, variables have to be made dimensionless. By considering a reference temperature T_0, (note here that in natural units $c = k_{\text{B}} = 1$, temperature, mass, energy and momentum have the same physical units, and velocity is adimensional), one introduces the following variables:

$$\tilde{T} = \frac{T}{T_0} \; , \qquad \tilde{m} = \frac{m}{T_0} \; , \qquad \tilde{p}^\alpha = \frac{p^\alpha}{T_0} \tag{2.31}$$

Then one selects a weight function $\omega(\tilde{p}^0)$ to later define a scalar product on Hilbert space of distribution functions

$$\omega(\tilde{p}^0) = C(\tilde{m}, T_0)e^{-\tilde{p}^0} \; . \tag{2.32}$$

The weight function is selected as the Maxwell-Jüttner distribution in the fluid's rest frame. This choice is crucial as it provides a direct link between the expansion coefficients of the distribution function and its moments. C is a normalization constant selected in such a way that

$$\int \omega(\tilde{p}^0) \frac{\mathrm{d}\boldsymbol{p}}{p^0} = T_0^{d-1} \int \omega(\tilde{p}^0) \frac{\mathrm{d}\tilde{\boldsymbol{p}}}{\tilde{p}^0} = 1 \; , \tag{2.33}$$

implying

$$C(\tilde{m}, T_0) = \left(\frac{1}{T_0}\right)^{d-1} \frac{1}{2^{\frac{d+1}{2}} \pi^{\frac{d-1}{2}} \tilde{m}^{\frac{d-1}{2}} K_{\frac{d-1}{2}}(\tilde{m})} \; . \tag{2.34}$$

This normalization is chosen in order to simplify the process of searching for a quadrature, as it will be shown in the next section.

One then can define a scalar product $(\cdot, \cdot)$ on the Hilbert space of distribution functions

$$(\cdot \; , \cdot) = \int \omega(\tilde{p}^0)(\cdot)(\cdot) \frac{\mathrm{d}\tilde{\boldsymbol{p}}}{\tilde{p}^0} \; , \tag{2.35}$$

in order be able to build the polynomials $\{\boldsymbol{J}^{(i)}(p^\mu), i = 0, \dots, N\}$ via Gram-Schmidt procedure on the set $\{\boldsymbol{b}_k, k = 1, \cdots, \binom{N+d+1}{N}\} = \{1, \tilde{p}^\alpha, \tilde{p}^\alpha \tilde{p}^\beta, \dots\}$. The well known algorithm reads as follow:

$$c_k = b_k - \sum_{j=1}^{k-1} \frac{(b_j, c_j)}{(c_j, c_j)} c_j \ , \qquad e_k = \frac{c_k}{\sqrt{(c_k, c_k)}} \ , \qquad (2.36)$$

where e_k stands for every single independent component of the tensors $\{J^{(i)}(p^\mu), i = 0, \ldots, N\}$. During the application of the Gram-Schmidt algorithm, the results for the integrals from App. B are used.

Then, using the definition given in Eq. 2.27 one can compute the coefficients of the expansion up to the desired order N, again using the results from App. B. The expressions of both the polynomials and coefficients are rather bulky and therefore are given in the appendices.

As an example the first order ($N = 1$) expansion of the (d+1) distribution function is here given:

$$f_1^{\mathrm{eq}} = \frac{cn}{k_B T_0} \ \omega(\tilde{p}^0) \left(\frac{1}{G_{d-2}\tilde{T}} + \frac{(\tilde{p}^0 - \tilde{G}_{d-2})}{\tilde{G}_{d-2}(d - \tilde{G}_{d-2}) + \tilde{m}^2} \left(U^0 - \frac{\tilde{G}_{d-2}}{\tilde{T}\tilde{G}_{d-2}} \right) - \frac{1}{\tilde{G}_{d-2}} \tilde{p}^i U_i \right) \ ,$$

where $\tilde{G}_{d-2} = G_{d-2}(\tilde{m})$. In general, the dimensional information is carried by the expansion coefficients, that are always a product of n/T_0 and adimensional terms depending on $\tilde{p}^\mu, U^\mu, \tilde{T}$. Polynomials are instead written in terms of $\tilde{m}$ and $\tilde{p}^\mu$.

In Fig. 2.1 a graphical comparison between the truncations at various orders N and the original Maxwell-Jüttner distribution is provided for the case at (2+1) dimensions. It is possible to observe that already with $N = 2$ the truncated expansion well reproduces the complete distribution.

Before moving on, one final remark has to be done: the whole procedure highlighted so far has to be modified for the ultra-relativistic case in (1+1) dimensions. In this case in fact the expressions become ill-defined (polynomials and coefficients become divergent in the limit $\tilde{m} \to 0$) if C is computed like Eq. 2.34.

Only in this case then the normalization is chosen to be equal to the physical normalization B used in Eq. 1.37. When one does so, a structure like the one given previously appears, but without ill-defined ultra-relativistic limits.
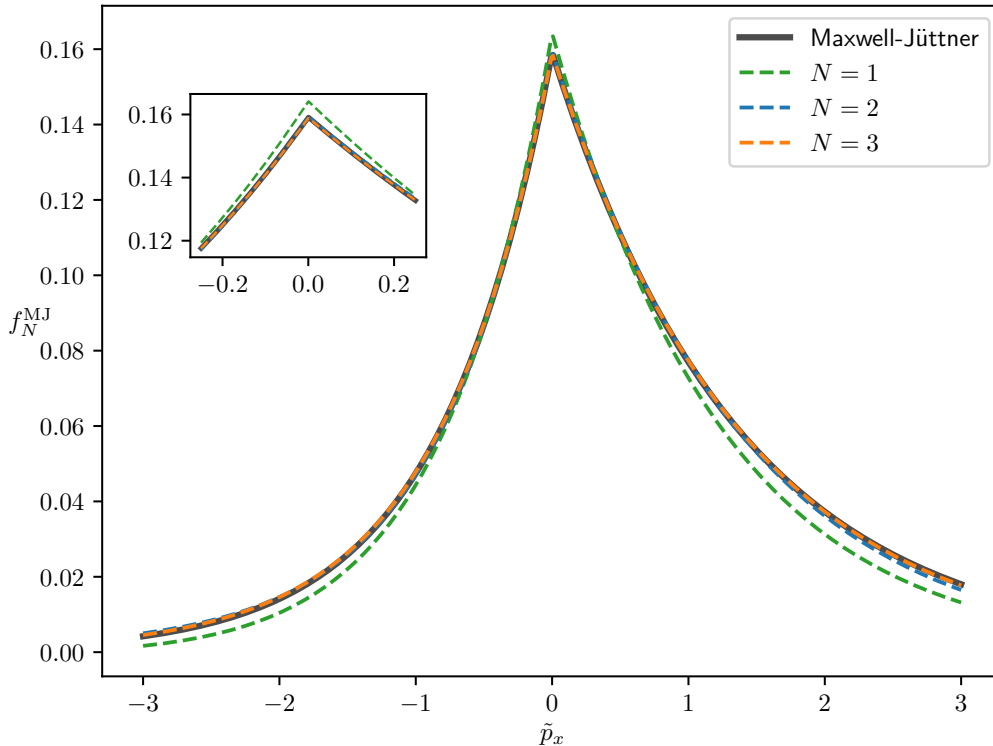
Figure 2.1: *Comparison of the truncated expansions of the equilibrium distribution function for various orders of truncation N against the complete form of the Maxwell-Jüttner distribution. (2+1) dimensional case. The various settings are $\tilde{T} = 1$, $\tilde{m} = 0$, $\tilde{p}_y = \tilde{p}_z = 0$, $U^y = U^z = 0$, and $\beta = U^x/U^0 = 0.25$.*

2.2.2 Quadrature Rule for momentum discretization

The discretization of the momentum-velocity space has a pivotal role in any Lattice Boltzmann scheme, since it allows for the *exact* calculation of the hydrodynamic moments as finite sums over the discrete nodes of the quadrature.

In the framework of RLBM [12, 19, 20], these quadratures are designed to retain one of the main LBM fratures, *perfect streaming*, *i.e.* it is requested that all quadrature points lie on the nodes of a Cartesian grid, so that at every time step information is propagated from one grid cell to the neighboring one. This has two desirable side-effects: i) super luminal propagation is ruled out by construction, and ii) no artificial dissipative effects emerge, since there is no need of interpolation.

It will be seen in the next chapters though that this is not the only possible choice: relaxing the perfect streaming condition brings a number of positive

effects in the simulation of rarefied flows.

For the moment, the method selected in the creation of Gauss-Quadratures is the one of prescribed abscissae [72], that enforces the discretization through the selection of sets of weights w_i satysfing the orthonormality conditions between the polynomials $\boldsymbol{J}^{(i)}(p^\mu)$

$$(\boldsymbol{J}^{(n)}, \boldsymbol{J}^{(m)}) = \int \omega(\tilde{p}^0) J^{(n)}_{\alpha_1 \ldots \alpha_n}(\tilde{p}^\mu) J^{(m)}_{\beta_1 \ldots \beta_m}(\tilde{p}^\mu) \frac{\mathrm{d}\tilde{\boldsymbol{p}}}{\tilde{p}^0} = \delta_{n,m} \prod_{k=1}^{n} \delta_{\alpha_k, \beta_k} , \qquad (2.37)$$

This condition becomes discrete after a set of N^{pop} momenta $\{p_i^\mu\}$ has been selected:

$$(\boldsymbol{J}^{(n)}, \boldsymbol{J}^{(m)}) = \sum_i^{N^{\mathrm{pop}}} w_i J^{(n)}_{\alpha_1 \ldots \alpha_n}(\tilde{p}_i^\mu) J^{(m)}_{\beta_1 \ldots \beta_m}(\tilde{p}_i^\mu) = \delta_{n,m} \prod_{k=1}^{n} \delta_{\alpha_k, \beta_k} . \qquad (2.38)$$

This last condition provides a set of linear equations for the weights w_i, that have to be numerically identified. In order to enforce the condition of perfect streaming, the following parametrization has to be considered for the discrete momenta:

$$\tilde{p}_i^\mu = \tilde{p}_i^0(1, v_0 \boldsymbol{n}_i) , \qquad (2.39)$$

where $\boldsymbol{n}_i \in \mathbb{Z}^d$ represents vectors joining the nodes of a Cartesian grid, and v_0 is a free parameter that has to be chosen in such a way that all discrete velocities $\boldsymbol{v}_i = v_0 \boldsymbol{n}_i$ are less than one (*i.e.* the speed of light in natural units). Additionally, p_i^0 is given as

$$\tilde{p}_i^0 = \frac{\tilde{m}}{\sqrt{1 - |\boldsymbol{v}_i|^2}} . \qquad (2.40)$$

The whole quadrature process can be summarized in the following steps:

1. A value for $\tilde{m}$ is chosen.

2. A value for v_0 is chosen.

3. A set of discrete vectors $\boldsymbol{n}_i \in \mathbb{Z}^d$ is chosen. The vectors are organized in fully symmetric subgroups, each containing vectors of the same length.

Any one of these subsets identifies an unknown weight, and therefore one has to be sure to include enough subgroups in the set in order to have enough unknowns to satisfy the linear independent conditions represented by Eq. 2.38.

4. The system of equations Eq. 2.38 is then numerically solved by finding weights w_i. If no solution is found, then a new value of v_0 is chosen and the procedure starts again. The weights have to be non-negative in order to guarantee numerical stability.

For the ultra-relativistic case a different parametrization has to be used: in fact Eq. 2.39 is not well defined. One thus considers

$$\tilde{p}_{ij}^{\mu} = \tilde{p}_j^0(1, v_0 \boldsymbol{n}_i) \, , \tag{2.41}$$

where the $\tilde{p}_j^0$ are now free parameters and v_0 is a parameter chosen such as the vectors $v_0 \boldsymbol{n}_i$ all have lenght one. The sets $\boldsymbol{n}_i$ are identified by considering the intersections between the surface of a $d - sphere$ and the nodes of the grid. v_0 is then the reciprocal of their common length.

Again, the mass-less quadrature procedure is summarized by the steps:

1. A value for $\tilde{m}$ is chosen.

2. A $d-$sphere with radius R is considered. In this case we set $v_0 = 1/R$.

3. The set of discrete vectors $\in \mathbb{Z}^d$ that have length R is considered. Again, the number of velocities in the set has to be enough to fulfill the independent conditions present in Eq. 2.38.

4. The system of equations Eq. 2.38 is then numerically solved by finding non negative weights w_i and energy shells $\tilde{p}_j^0$. If no solution is found, then a new radius is chosen and the procedure starts again.

In general it is possible to find many different solutions $(v_0, \{p_i^{\mu}, w_i\})$ to the quadrature problem, and some of them are valid for a wide range of $\tilde{m}$. In this way one can cover the whole spectrum of particle masses, from the ultra-relativistic to the classical limit. Fig. 2.2 shows examples of stencils for different dimensions, and different relativistic regimes.
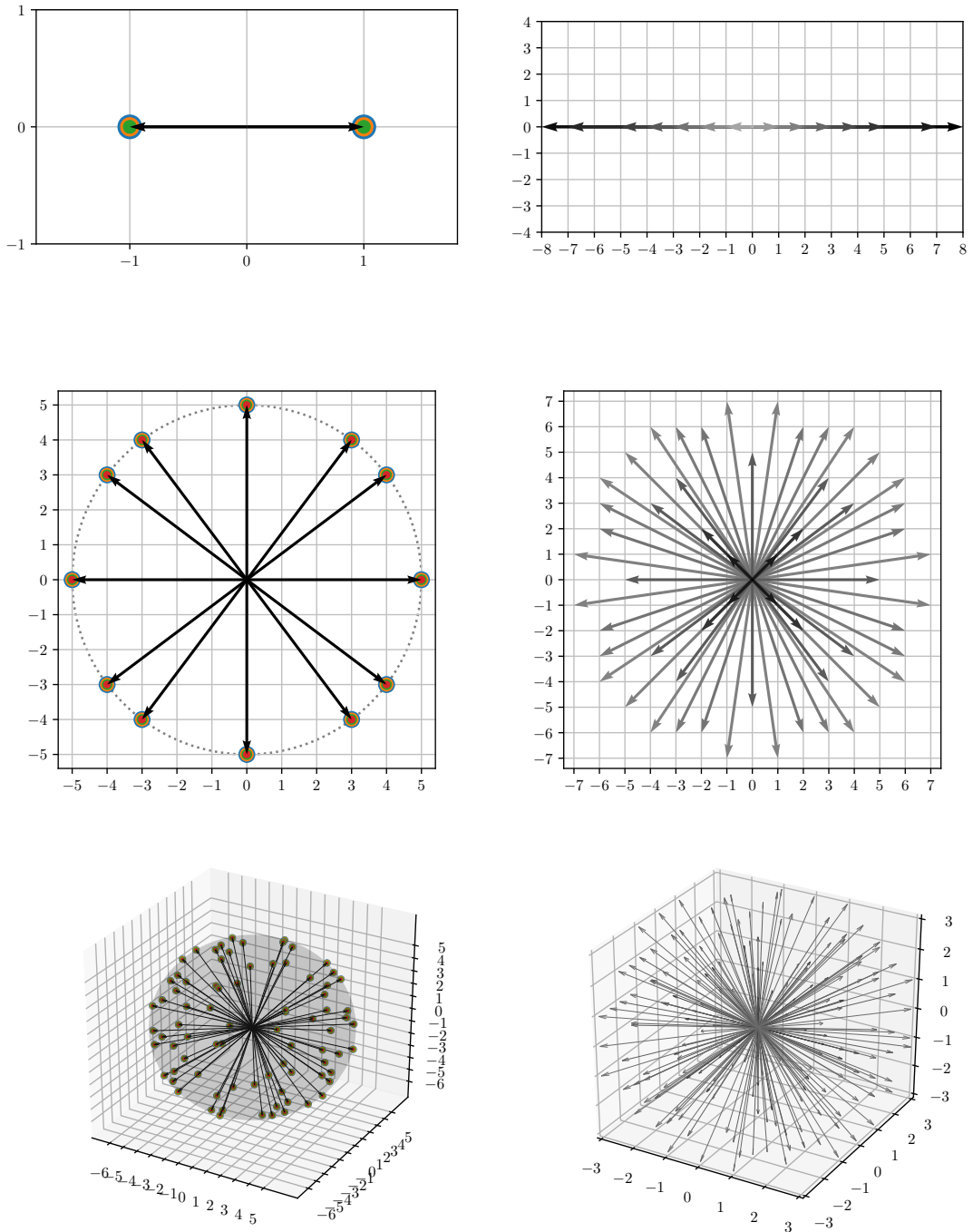
Figure 2.2: *Examples of stencils for the cases $\tilde{m} = 0$ (left column) and $\tilde{m} = 4$ (right column) in (1+1) dimensions (top row), (2+1) dimensions (middle row), and (3+1) dimensions (bottom row). In the ultra-relativistic case, the stencil intersects the surface of a circle (d=2) and a sphere (d=3). The colored dots represent different energy shells. The quadrature order is $N = 3$ for all cases, and N^{pop} ranges from 6 in the (1+1) ultra relativistic case to 182 in the (3+1) massive case.*

2.2.3 Forcing Scheme

In Lattice Boltzmann Methods, definition of Forcing Schemes are nothing more than algorithmic recipes for the discretization of the term in the Boltzmann's Equation describing the volume forces acting on the fluid. In the literature, many different forcing schemes are available for classical LBM [69, 73–76] (see [77] for comparisons), with each of them showing both advantages and disadvantages.

Within RLBM, the forcing scheme is simply derived by taking the forcing term in Eq. 2.24

$$F^{\text{ext}} = mK^\alpha \frac{\partial f}{\partial p^\alpha} \, , \tag{2.42}$$

and by assuming processes close to equilibrium, so that $f \sim f^{\text{eq}}$, and by taking the analytic form of the Maxwell-Jüttner distribution, Eq. 1.35, one gets

$$F^{\text{ext}} = mK^\alpha \frac{\partial f}{\partial p^\alpha} \sim mK^\alpha \frac{\partial f^{\text{eq}}}{\partial p^\alpha} = -\frac{m}{T} K^\alpha U_\alpha f^{\text{eq}} \, , \tag{2.43}$$

and therefore one can easily discretized F^{ext} by simply resorting to the discretization procedure of the equilibrium distribution function. The only thing left to do is to give a proper definition of the Minkowsky force. Following [24], and calling $\boldsymbol{F}$ the classical not-relativistic force, one has that K^α is defined by the following two equations (γ being the Lorentz Factor)

$$K^\alpha p_\alpha = 0 \rightarrow K^0 = \frac{\boldsymbol{K} \cdot \boldsymbol{p}}{p^0} \tag{2.44}$$

$$\boldsymbol{K} = \gamma \boldsymbol{F} \tag{2.45}$$

2.2.4 Conversion to Lattice Units

The last thing left to discuss is a process that is often overlooked when dealing with LBMs: the determination of proper and clear rules for the passage between physical units to lattice units. Some details on the conversions are already been given, but will now be summarized.

In general, every physical quantity can be rendered dimentionless and then brought on the lattice by recurring to some conversion factors C, which are typical parameters of the simulation. Any given quantity χ is converted from

physical to lattice in the following way:

$$\chi_{\mathrm{p}} = C_\chi \chi_\ell \ . \tag{2.46}$$

The first and most obvious step one has to discuss is the conversion of length and time scales. The conversion factor for lengths is provided by the physical distance between two grid nodes in the lattice, computed as the ratio between a typical length scale of the system L and the number N of grid nodes in the lattice

$$C_x = \Delta x_{\mathrm{p}} = \frac{L}{N} \ , \tag{2.47}$$

as a consequence, one has

$$\Delta x_\ell = \frac{\Delta x_{\mathrm{p}}}{C_x} = 1 \ . \tag{2.48}$$

For velocities, one chooses $C_v = v_0$

$$v_{\mathrm{p}} = C_v v_\ell = v_0 v_\ell \ . \tag{2.49}$$

Then the time scaling factor comes straightforward as $C_t = \frac{C_x}{C_v} = \frac{L}{v_0 N}$.

Space and Time steps are directly linked by characteristics used in Eq. 2.30, that require pseudo-particles to move from locations $\boldsymbol{x}$ to $\boldsymbol{x} + \boldsymbol{v}^i \Delta t$. Additionally, these jumps have to be performed between an integer number of grid nodes, implying the following relationship

$$\Delta x_{\mathrm{p}} = v_0 \Delta t_{\mathrm{p}} \ . \tag{2.50}$$

With these choices, one has

$$\Delta t_\ell = \frac{\Delta t_{\mathrm{p}}}{C_t} = \frac{\Delta x_{\mathrm{p}}}{v_0 C_t} = \frac{\Delta x_\ell C_x}{v_0 C_t} = 1 \ . \tag{2.51}$$

Lastly thermal energy, temperature, momentum and mass are all converted

using the same conversion factor $C_T = T_0$, as already stated in Eq. 2.31

With these prescriptions, one can derive every other single conversion factor. Some of them are given as an example in the following summary table:

Lenght	$C_x = L/N$
Velocity	$C_v = v_0$
Temperature	$C_T = T_0$
Time	$C_t = C_x/C_v$
Number Density	$C_n = 1/(C_x)^d$
Pressure (dynamic, static, deviator)	$C_P = C_T C_v^2 C_n$
Energy density	$C_\epsilon = C_T C_n C_v^2$
Shear and Bulk viscosity	$C_\eta = C_\mu = C_t C_P$
Thermal Conductivity	$C_\lambda = C_t C_n$

As a final remark, it can be useful to introduce the lattice values for a couple of adimensional numbers that are commonly encountered in hydrodynamics.

First, we introduce the Knudsen Number Kn, the ratio between the mean free path between collisions Λ and a typical length L of the system. In relativistic systems, the mean free path between collisions is computed as the time relaxation time τ times a relative mean velocity $< v >$, that can be selected as the Møller speed $g_\emptyset$ or the velocity of sound c_s (they all have the same order of magnitude)

$$\Lambda = \tau < v > \tag{2.52}$$

Therefore, considering that $< v >_\ell \sim 1$, one has

$$Kn = \frac{\tau_{\mathrm{p}} < v >_{\mathrm{p}}}{L} = \frac{\tau_\ell}{N} \tag{2.53}$$

This last formula will be used extensively in the next chapters, as the Knudsen number is used to evaluate the level of rarefaction in the fluid.

Another important value is the Reynolds number, that is defined as

$$Re = \frac{\rho_{\mathrm{p}} U_{\mathrm{p}} L}{\eta_{\mathrm{p}}} \tag{2.54}$$

where $\rho_{\mathrm{p}} = m_{\mathrm{p}} n_{\mathrm{p}}$ is the mass density of the fluid. Then one has:

$$Re = \frac{m_{\mathrm{p}} n_{\mathrm{p}} U_{\mathrm{p}} L}{\eta_{\mathrm{p}}} = \frac{\tilde{m} n_\ell U_\ell N}{\eta_\ell} \tag{2.55}$$

where n_ℓ, U_ℓ, $\tilde{m}$ and N are typical values chosen at the start of the simulation, and η_ℓ can be obtained thanks to the estimates given by the Chapman-Enskog expansion.

2.2.5 Algorithm

Having illustrated all the required passages needed to derive a RLBM, I will describe in this section the algorithmic steps that are needed to perform a simulation.

At the start of the simulation, once some initial conditions for the macroscopic fields U_{in}^α, T_{in} and n_{in} are chosen,

$$
\begin{aligned}
U^\alpha(\boldsymbol{x}, t_0) &= U_{\mathrm{in}}^\alpha(\boldsymbol{x}) \ , \\
n(\boldsymbol{x}, t_0) &= n_{\mathrm{in}}(\boldsymbol{x}) \ , \\
T(\boldsymbol{x}, t_0) &= T_{\mathrm{in}}(\boldsymbol{x}) \ ,
\end{aligned}
\tag{2.56}
$$

the populations $f_i(\boldsymbol{x}, t_0)$ are initialized at equilibrium, *i.e.*

$$f_i(\boldsymbol{x}, t_0) = f^{\mathrm{eq}}(n_{\mathrm{in}}(\boldsymbol{x}), U_{\mathrm{in}}^\alpha(\boldsymbol{x}), T_{\mathrm{in}}(\boldsymbol{x})) \ . \tag{2.57}$$

For each time step, at every point of the grid, the following set of operations is performed:

1. Particle flow and energy-momentum tensor are computed as discrete sums over the set of discrete momenta $\tilde{p}_i^\alpha$. If the quadrature has been correctly performed, the sums recover *exactly* the integrals of Eq. 1.17 and Eq. 1.18

$$N^\alpha = \sum_i^{N_{\mathrm{pop}}} f_i \tilde{p}_i^\alpha \ ,$$

$$T^{\alpha\beta} = \sum_i^{N_{\mathrm{pop}}} f_i \tilde{p}_i^\alpha \tilde{p}_i^\beta \ .$$

2. All thermodynamic quantities are obtained and eventually stored on disk, using the relationships of 3.7.

   - ϵ and U^α are obtained solving the eigenvalue problem

     $$\epsilon U^\alpha = T^{\alpha\beta} U_\beta \ .$$

   - n is given by $n = U_\alpha N^\alpha$

   - Temperature T and hydrostatic pressure P are obtained from EOS Eq. 1.40

   - Non equilibrium quantities are obtained from

     $$q^\alpha = -\frac{P+\epsilon}{n} \Delta^{\alpha\beta} N_\beta \ ,$$
     $$\varpi = -P - \frac{1}{d}\Delta_{\alpha\beta} T^{\alpha\beta} \ ,$$
     $$\pi^{<\alpha\beta>} = \left(\Delta^\alpha_\gamma \Delta^\beta_\delta - \frac{1}{d}\Delta^{\alpha\beta}\Delta_{\gamma\delta} \right) T^{\gamma\delta} \ .$$

3. At this point the truncated equilibrium distribution function f_{iN}^{eq} can be computed using the thermodynamic quantities previously obtained.

4. If there is the need, the discrete forcing term is computed (Sec. 2.2.3).

5. The value for the relaxation time τ is provided at every grid node. This value can be chosen to be constant or calculated in such a way that one of the transport coefficients obtained in the Chapman-Enskog expansion (see Ch. 3) is constant.

6. The system is evolved through the Lattice Boltzmann Eq. 2.30

   $$f_i(\boldsymbol{x} + \boldsymbol{v}^i \Delta t, t + \Delta t) = f_i(\boldsymbol{x}, t) - \frac{p_i^\alpha U_\alpha}{c^2 \tau}\left(f_i(\boldsymbol{x}, t) - f_{iN}^{\text{eq}} \right) + F_i^{\text{ext}} \ .$$

   Such a process is usually divided into two steps, according to the *Streaming & Collide* paradigm:

   $$\text{streaming} \quad f_i^*(\boldsymbol{x}, t) = f_i(\boldsymbol{x} - \boldsymbol{v}^i \Delta t, t - \Delta t) \ ,$$
   $$\text{collide} \quad f_i(\boldsymbol{x}, t) = f_i^*(\boldsymbol{x}, t) - \frac{p_i^\alpha U_\alpha}{c^2 \tau}\left(f_i^*(\boldsymbol{x}, t) - f_{iN}^{\text{eq}} \right) + F_i^{\text{ext}} \ .$$

3

Derivation and Calibration of Transport Coefficients

This chapter describes two independent analytic procedures that can be employed for the derivation of a macroscopic dissipative relativistic theory. These alternative methods build directly on the description of the fluid at the kinetic layer, and expand it to the hydrodynamic layer by means of perturbations of the distribution function f. It will be seen how these two procedures, that in classical non-relativistic theories give coherent results, are discordant in the relativistic framework.

Also, these techniques are important calibration tools for numerical schemes based on the kinetic layer, since they provide a description of the transport coefficients λ, η, μ in terms of the parameters at the mesoscopic layer, which at that point can opportunely be tuned to describe fluids with the desired macroscopic properties.

Traditionally, two methods have been used to derive hydrodynamics from a kinetic description of a fluid: Chapman-Enskog's expansion [78] (CE) and Grad's method of moments [79]. In non-relativistic theories both these two methods provide a theoretical link between the Navier-Stokes-Fourier equations and Boltzmann's equation, giving at the same time an equivalent description of the transport coefficients of a fluid.

Everything is more complicated when moving to relativistic regimes: not only the hydrodynamic layer is not well defined, but also CE and Grad give different results for the transport coefficients, this last detail posing not only a theoretical problem but also a serious obstacle to the development of a relativistic kinetic scheme.

While theoretical shortcomings have been highlighted in Grad's method also

in non-relativistic theories [80–83], the main aspect that makes the method less reliable is the fact that it consists in an arbitrary truncation of distribution function's expansion around its equilibrium value, without resorting to any control parameter, while CE is a method that is controlled by powers of the Knudsen number, that carefully controls the validity of the hydrodynamic description.

CE on the other hand does not cure the causality problems highlighted in the previous section, but nevertheless seems to be the correct approach at determining the transport coefficients. It has been shown, in fact, that the same results obtained in CE can be also obtained with Grad once its core expansion is truncated with more than the canonical 14 moments [6, 84, 85], or when it is augmented with entropic arguments [86]. Furthermore, totally different approaches also present results equal to those of CE expansion [87–90].

It is also worth to point out that different approaches other than the one considered here for Grad's method could be considered, namely exspansions of the distribution function based on irriducible tensors of momenta [6]. Here I mantain the more semplicistic procedure also used in [24].

In the next sections the main steps of CE and Grad methods are presented according to the derivation shown in [24]. For what follows, the Anderson-Witting relaxation time approximation introduced in Eq. 1.10 is used.

The results of this chapter have already been shown in [18, 26, 27, 91] and presented in their most general form in [25]. Here I just give a brief account on the material of [25].

3.1 Chapman-Enskog expansion

The Chapman-Enskog expansion stems from a perturbation in the Knudsen number Kn (the ratio between the mean free path ℓ of particles between two subsequent collisions and a typical length scale L of the system) of the distribution function around its equilibrium value:

$$f = \sum_{n=0}^{\infty} \epsilon^n f^{(n)} , \quad \epsilon = \epsilon(\text{Kn}) , \tag{3.1}$$

where $f^{(0)} = f^{\text{eq}}$. Since hydrodynamics is the theory of fluids which are close to equilibrium, I will be considering perturbations only up to the first order in

Kn. Once the order 1 parameter $\phi = \epsilon(f^{(1)}/f^{(0)})$ is defined, one has

$$f \sim f^{\text{eq}} + \phi f^{\text{eq}} \, , \tag{3.2}$$

An intermediate goal is to determine the deviation from equilibrium ϕ. To do so, take Eq. 1.5 without forcing terms and using the Anderson-Witting collision model (Eq. 1.10):

$$p^\alpha \frac{\partial f}{\partial x^\alpha} = -\frac{p^\alpha U_\alpha}{c^2 \tau}\left(f - f^{\text{eq}}\right) \, . \tag{3.3}$$

The first step is to insert Eq. 3.2 into Eq. 3.3, and ignore all $O(\epsilon^2)$ contributions:

$$p^\alpha \frac{\partial f^{\text{eq}}}{\partial x^\alpha} = -\frac{p^\alpha U_\alpha}{c^2 \tau}\phi f^{\text{eq}} \, . \tag{3.4}$$

This yields ϕ in terms of the derivative of the Maxwell-Jüttner (Eq. 1.35) distribution, that can be expressed in the following way after some lengthy calculations

$$\phi = -\frac{c^2 \tau}{(p^\mu U_\mu) f^{\text{eq}}} p^\nu \partial_\nu f^{\text{eq}} =$$
$$= -\frac{c^2 \tau}{(p^\mu U_\mu)} p^\nu \left[\frac{\partial_\nu n}{n} + (1 - G_d)\frac{\partial_\nu T}{T} + \frac{p^\mu U_\mu}{k_{\text{B}} T^2}\partial_\nu T - \frac{p_\mu \partial_\nu U^\mu}{k_{\text{B}} T}\right] \, . \tag{3.5}$$

Then one can use the above equation to compute the macroscopic fields:

$$N^\beta = c \int p^\beta f^{\text{eq}}(1 + \phi)\frac{\partial \boldsymbol{p}}{p^0} \, , \qquad T^{\alpha\beta} = c \int p^\alpha p^\beta f^{\text{eq}}(1 + \phi)\frac{\partial \boldsymbol{p}}{p^0} \, , \tag{3.6}$$

and by inserting Eq. 3.5 into the macroscopic fields one gets

$$N^\beta = cBZ^\beta - c^3 \tau \left[\frac{\partial_\nu n}{n}K^{\nu\beta} + (1 - G_d)\frac{\partial_\nu T}{T}K^{\nu\beta} + \frac{\partial_\nu T}{k_{\text{B}} T^2}BZ^{\beta\nu} - \frac{\partial_\nu U_\delta}{k_{\text{B}} T}K^{\delta\nu\beta}\right] \, ,$$
$$T^{\alpha\beta} = cBZ^{\alpha\beta} - c^3 \tau \left[\frac{\partial_\nu n}{n}K^{\nu\alpha\beta} + (1 - G_d)\frac{\partial_\nu T}{T}K^{\nu\alpha\beta} + \frac{\partial_\nu T}{k_{\text{B}} T^2}BZ^{\nu\alpha\beta} - \frac{\partial_\nu U_\delta}{k_{\text{B}} T}K^{\delta\nu\alpha\beta}\right] \, ,$$

where the integrals $Z^{\alpha_1 \dots \alpha_n}$, $K^{\alpha_1 \dots \alpha_n}$ are given in Appendix B (the formula for a_{22} and a_{43} are also given in the Appendix).

By resorting to equations given in 3.7 for Landau-Lifshitz decomposition

$$\varpi = -P - \frac{1}{d}\Delta_{\alpha\beta}T^{\alpha\beta} \ ,$$

$$\pi^{<\alpha\beta>} = \left(\Delta_\gamma^\alpha \Delta_\delta^\beta - \frac{1}{d}\Delta^{\alpha\beta}\Delta_{\gamma\delta}\right)T^{\gamma\delta} \ , \tag{3.7}$$

$$q^\alpha = -\frac{P+\epsilon}{n}\Delta^{\alpha\beta}N_\beta \ ,$$

one can then determine the non equilibrium fluxes q^α, ϖ and $\pi^{<\alpha\beta>}$ and confront them with the transport equations Eq. 1.66, Eq. 1.67 and Eq. 1.68, obtaining a formula for the transport coefficients λ, μ and η (check [25] for more detailed calculations)

$$\lambda = -c^2 k_{\mathrm{B}} n\tau G_d \left(a_{22}G_d + 1\right) \ ,$$

$$\mu = P\tau \left[a_{43}\left(1+\frac{2}{d}\right) - \frac{\zeta^2 - G_d^2 + (d+2)G_d}{\zeta^2 - G_d^2 + (d+2)G_d - 1}\right] \ , \tag{3.8}$$

$$\eta = P\tau a_{43} \ .$$

The ultra relativistic limit reads as follow:

$$\lambda_{\mathrm{ur}} = \frac{d+1}{d}c^2 k_{\mathrm{B}} n\tau \ , \qquad \mu_{\mathrm{ur}} = 0 \ , \qquad \eta_{\mathrm{ur}} = \frac{d+1}{d+2}P\tau \ . \tag{3.9}$$

3.2 Grad's Method of Moments

Also in Grad's method the distribution function f is expanded around its equilibrium value f^{eq}. This time, however, the expansion is theoretically thought as a generic expansion in Hilbert's space of momenta

$$f = f^{\mathrm{eq}}(1 + \lambda_\alpha p^\alpha + \lambda_{\alpha\beta}p^\alpha p^\beta + \dots) \ . \tag{3.10}$$

We remark here that better expansions, built on irreducible tensors of the

momenta, might be preferable in order to derive more detailed expressions of the transport coefficients [6].

Since the order of the expansion is not controlled by any parameter (contrary to CE), a somewhat arbitrary truncation has to be performed on this expansion. Usually, the order of the truncation is given by the number of constrains one manages to get using the known conditions on the fields n, U_α, T, q_α, ϖ, $\pi^{<\alpha\beta>}$, so that one obtains a closed system of equations for the unknowns λ, $\lambda_{\alpha\beta}$, etc.

In the derivation I follow, based on [24], a 14 unknowns truncation of Eq. 3.10 is obtained by means of constraints derived by the integral definitions of N^α, $T^{\alpha\beta}$, and the third order moment of the distribution function $T^{\alpha\beta\gamma}$.

The starting point in the derivation is given by the definition of the entropy density s (combine Eq. 1.20, Eq. *1.3.1* and Eq. 1.62), the moment defining equations Eq. 1.17, Eq. 1.18, and the definition of the third order moment of the distribution function (here taken trace-less, symmetric, U^α orthogonal for simplicity)

$$s[f] = -\frac{k_\mathrm{B}}{c} U^\alpha \int p_\alpha f \log f \frac{\mathrm{d}\boldsymbol{p}}{p_0} \ , \tag{3.11}$$

$$g[f] = U_\alpha N^\alpha - c U_\alpha \int p^\alpha f \frac{\mathrm{d}\boldsymbol{p}}{p_0} \ , \tag{3.12}$$

$$g^\beta[f] = U_\alpha T^{\alpha\beta} - c U_\alpha \int p^\alpha p^\beta f \frac{\mathrm{d}\boldsymbol{p}}{p_0} \ , \tag{3.13}$$

$$g^{<\gamma\beta>}[f] = U_\alpha T^{\alpha<\beta\gamma>} - c U_\alpha \int p^\alpha p^{<\beta} p^{\gamma>} f \frac{\mathrm{d}\boldsymbol{p}}{p_0} \ . \tag{3.14}$$

Then, according to Lagrange's multipliers method, one defines the functional

$$F[f] = s[f] + \lambda g[f] + \lambda_\beta g^\beta[f] + \lambda_{\gamma\beta} g^{<\gamma\beta>}[f] \tag{3.15}$$

and minimizes it putting

$$0 = \frac{\partial F[f]}{\partial f} = -\int p_\alpha U^\alpha \left[\frac{k_\mathrm{B}}{c} \left(\ln f + 1 \right) + c \left(\lambda + \lambda_\beta p^\beta + \lambda_{\gamma\beta} p^{<\gamma} p^{\beta>} \right) \right] \frac{\mathrm{d}\boldsymbol{p}}{p_0} \ ,$$

$$f = \exp\left(-1 - \frac{c^2}{k_{\mathrm{B}}}(\lambda + \lambda_\beta p^\beta + \lambda_{\gamma\beta} p^{<\gamma} p^{\beta>})\right) \quad . \tag{3.16}$$

By splitting all the unknowns into an equilibrium and non equilibrium part, one realizes that the equilibrium part has to be equal to the Maxwell-Jüttner distribution, and therefore 3.16 can be written as

$$
\begin{aligned}
f &= f^{\mathrm{eq}} \exp\left(-\frac{c^2}{k_{\mathrm{B}}}(\lambda^{\mathrm{neq}} + \lambda_\beta^{\mathrm{neq}} p^\beta + \lambda_{\gamma\beta}^{\mathrm{neq}} p^{<\gamma} p^{\beta>})\right) \\
&\sim f^{\mathrm{eq}} \left[-\frac{c^2}{k_{\mathrm{B}}}(\lambda^{\mathrm{neq}} + \lambda_\beta^{\mathrm{neq}} p^\beta + \lambda_{\gamma\beta}^{\mathrm{neq}} p^{<\gamma} p^{\beta>})\right] ,
\end{aligned}
\tag{3.17}
$$

where the Taylor approximation of the exponential in the last equality has been carried since one assumes to have processes close to equilibrium. With this definition, the distribution function is not yet defined. The λ coefficients can be written in terms of the non equilibrium fields by inserting Eq. 3.17 into the definitions Eq. 1.17 and Eq. 1.18 of N^α and $T^{\alpha\beta}$, and by computing Eq. 3.7.

All the expressions are rather cumbersome, and therefore are not shown here. We refer to [25] for the full calculations. Suffice to say that with a complete expression of the distribution function f in terms of q^α, ϖ and $\pi^{<\alpha\beta>}$, one can derive the third order moment

$$T^{\alpha\beta\gamma} = c \int p^\alpha p^\beta p^\gamma f \frac{\mathrm{d}\boldsymbol{p}}{p^0} , \tag{3.18}$$

and insert it into the relativistic Boltzmann equation, multiplied by $\psi = cp^\beta p^\gamma$ and integrated in momentum space, leading to:

$$U_\alpha(T^{\alpha\beta\gamma} - T^{\alpha\beta\gamma}_{\mathrm{eq}}) = -c^2\tau\partial_\alpha T^{\alpha\beta\gamma} , \tag{3.19}$$

and use the Maxwellian iteration method so that only the equilibrium part of $T^{\alpha\beta\gamma}$ is left in the derivative:

$$U_\alpha(T^{\alpha\beta\gamma} - T^{\alpha\beta\gamma}_{\mathrm{eq}}) = -c^2\tau\partial_\alpha T^{\alpha\beta\gamma}_{\mathrm{eq}} . \tag{3.20}$$

Note that the third order moment at the equilibrium, $T^{\alpha\beta\gamma}_{\mathrm{eq}}$, can be obtained

directly from $T^{\alpha\beta\gamma}$ by setting to zero the non-equilibrium quantities $q^\alpha = 0$, $\varpi = 0$ and $\pi^{<\alpha\beta>} = 0$.

By multiplying Eq. 3.20 by respectively $\Delta^\delta_\beta U_\gamma$, $\Delta_{\beta\gamma}$, and $\Delta^{(\delta}_\beta \Delta^{\epsilon)}_\gamma - \frac{1}{d}\Delta_{\beta\gamma}\Delta^{\delta\epsilon}$, one can determine the non equilibrium fluxes q^α, ϖ and $\pi^{<\alpha\beta>}$ and confront them with the transport equations Eq. 1.66, Eq. 1.67 and Eq. 1.68, obtaining a formula for the transport coefficients λ, μ and η:

$$\lambda = -c^2 k_{\mathrm{B}} n \tau G_d \frac{\left((d+2)G_d + \zeta^2 - G_d^2\right)^2}{-G_d^2\left(d + \zeta^2 + 2\right) + (d+2)\zeta^2 G_d + \zeta^4} \ , \tag{3.21}$$

$$\mu = P\tau \frac{1}{d\left(G_d(d - G_d + 2) + \zeta^2 - 1\right)} \times \tag{3.22}$$

$$\frac{\left(\zeta^2(d - 2G_d) + G_d(-d + G_d - 1)(-d + 2G_d - 2)\right)^2}{G_d^2\left(d^2 + 8d - 2\zeta^2 + 12\right) - G_d\left(d^2 + d(5 - 3\zeta^2) - 10\zeta^2 + 6\right) + \zeta^2\left(-d + 2\zeta^2 - 2\right) - (d+6)G_d^3} \ ,$$

$$\eta = \frac{G_d^2 P\tau}{(d+3)G_d + \zeta^2} \ . \tag{3.23}$$

The ultra-relativistic limit ($\zeta \to 0$) of the above expressions writes as:

$$\lambda_{\mathrm{ur}} = \frac{d+1}{d+2}c^2\tau n k_{\mathrm{B}} \ , \qquad \mu_{\mathrm{ur}} = 0 \ , \qquad \eta_{\mathrm{ur}} = \frac{d+1}{d+3}P\tau \ . \tag{3.24}$$

In Fig. 3.1 the behavior of η, μ and λ with respect to the Relativistic Coldness ζ is shown for both Chapman-Enskog's expansion and Grad's method of moments. It is possible to appreciate that the two procedures give sensibly different results (with Grad underestimating all values), with differences that are bigger toward the ultra-relativistic regime, and disappear in the non-relativistic regime. Later in this thesis it will be seen how to address this problem of identifying what's the correct analysis among the two.

Two additional remarks have to be done: (1), it is worth to note that there is a ζ region where the bulk viscosity is unexpectedly different than zero. This is a result that could explain some behaviors in mildly relativistic gases, like those encountered in relativistic heavy ion collisions [92–96]. (2), the thermal conductivity, as it is evident by looking at Fig. 3.1, goes to zero in the non-relativistic limit ($\zeta \to \infty$, even though one would expect to have a non zero value in classical fluids.

This is due to the fact that when one takes the non-relativistic limit λ has to be correctly made non dimensional:
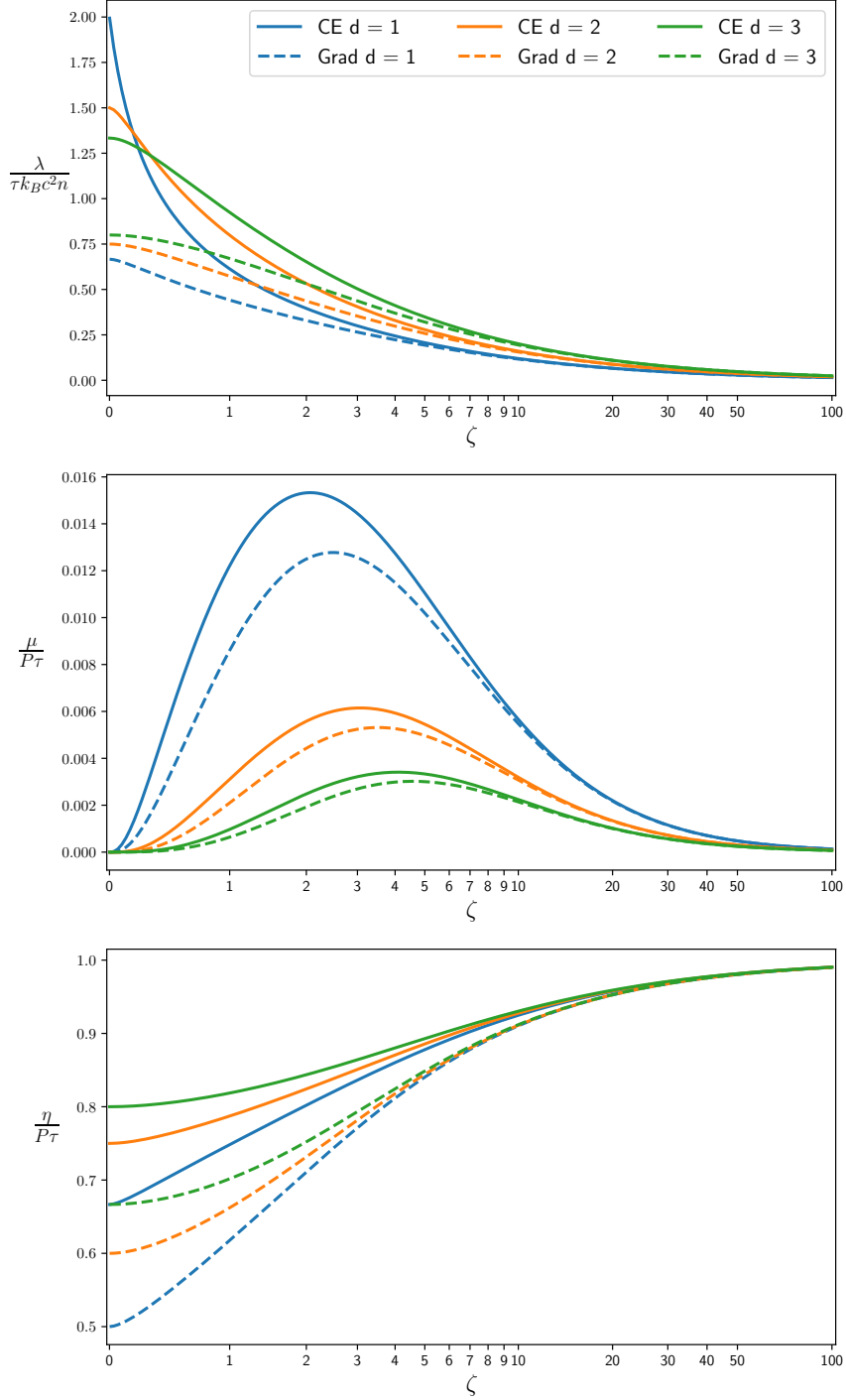
Figure 3.1: *Comparison of the transport coefficients in $1, 2, 3$-dimensions obtained using CE and Grad's method of moments within the Anderson-Witting relaxation time approximation. From top to bottom, one has thermal conductivity λ, bulk viscosity μ, shear viscosity η. All quantities are opportunely made dimensionless.*

$$\lambda_{\text{nr}} = \lim_{\zeta \to \infty} \left[c^2 n k_{\text{B}} \tau f(\zeta) \right] = \lim_{\zeta \to \infty} \left[\frac{c^2 n k_{\text{B}} \tau}{\zeta} \zeta f(\zeta) \right]$$

$$= \lim_{\zeta \to \infty} \left[\frac{P k_{\text{B}} \tau}{m} \zeta f(\zeta) \right] = \frac{P k_{\text{B}} \tau}{m} \frac{d+2}{d} \ , \tag{3.25}$$

Which is exactly the well-known non-relativistic value.

3.3 Calibration of Transport Coefficients

In the previous two sections it has been shown that there is a discrepancy in the connection of the macroscopic transport coefficients to the kinetic parameters: the analytical expressions for λ, μ and η as a function of the relativistic coldness ζ come out differently depending on the expansion method used to derive hydrodynamics starting from the kinetic layer.

This poses a theoretical problem, and more than that, in Lattice Boltzmann simulations a firm grasp and control on the transport coefficients is strongly advised in order to be able to reproduce dynamical systems with the desired macroscopic properties by simply tuning the kinetic parameters of the simulation.

For this reason a numerical approach to the determination of the correct expansion method has been adopted through the years [18, 26, 27, 91]. In this context, a RLBM (like the ones discussed in Ch. 2) is used to numerically evaluate the transport coefficients with a number of different benchmarks.

In the next sections the results presented in the previous articles have been summarized and extended to $1, 2, 3$ spatial dimensions, using third order quadratures for the velocity stencils and truncation of equilibrium distribution function.

3.3.1 Thermal Conductivity

First, the thermal conductivity λ has been measured. The chosen benchmark, inspired by [18], consists in considering the following initial conditions along one single space coordinates x:
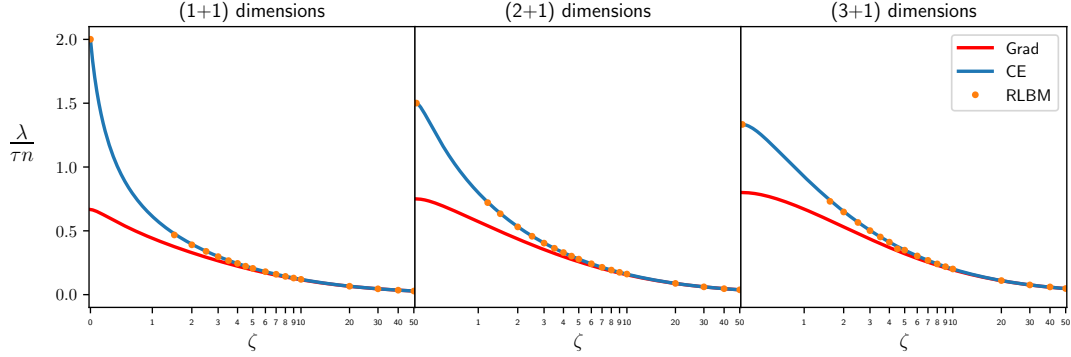
Figure 3.2: *Numerical estimate of the (non-dimensional) thermal viscosity for a relativistic gas in (1 + 1), (2 + 1) and (3 + 1) dimensions, shown respectively from left to right. The results are in agreement with CE analysis.*

$$
\begin{aligned}
T(0, t_0) &= T_{\mathrm{u}} \\
T(L, t_0) &= T_{\mathrm{d}} \\
T(x, t_0) &= 0 \qquad x \in]0, L[\ ,
\end{aligned}
\tag{3.26}
$$

The macroscopic velocity U^α is set at rest, and the particle density n is set to a fixed costant value. Through time, a thermal flux develops from one end of the domain to the other. If $\Delta T = T_{\mathrm{u}} - T_{\mathrm{d}}$ is chosen sufficiently small, then Eq. 1.68 becomes the non-relativistic Fourier equation

$$
q^x = \lambda \nabla^x T \ ,
\tag{3.27}
$$

and the system reaches a steady state where the temperature gradient becomes almost constant and the heat flux (also almost constant) is evaluated from the formula provided in 2.2.5:

$$
q^\alpha = -h_{\mathrm{e}} \Delta^{\alpha\beta} N_\beta \ .
\tag{3.28}
$$

Therefore by performing spatial averages over the whole spatial domain one is able to measure the thermal conductivity λ

$$\lambda = \frac{<q^x>_x}{<\nabla^x T>_x} \ . \tag{3.29}$$

By performing several simulations, each time taking different values for the relativistic coldness ζ, it is possible to extract functional dependencies $\lambda = \lambda(\zeta)$ for every number of spatial dimensions d. The results shown in Fig. 3.2 show once again that the numerical data are compatible with the CE analysis.
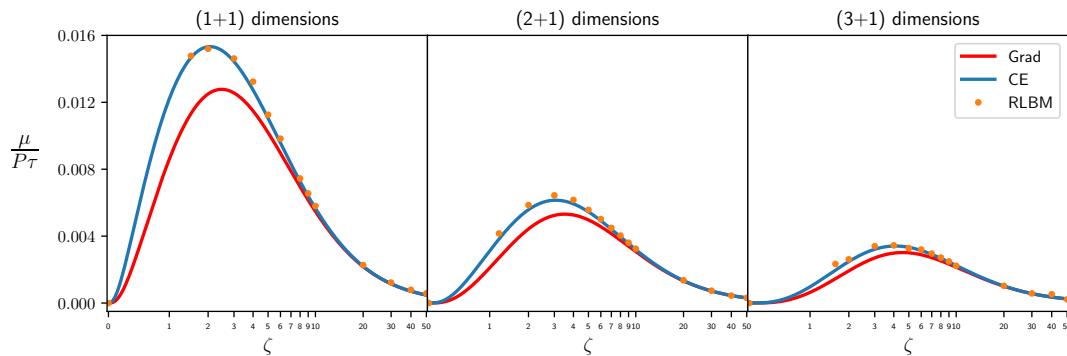
3.3.2 Bulk Viscosity

Figure 3.3: *Numerical estimate of the (non-dimensional) bulk viscosity for a relativistic gas in (1 + 1), (2 + 1) and (3 + 1) dimensions, shown respectively from left to right. The results are in agreement with CE analysis.*

In order to provide a numerical measure of the bulk viscosity, a particular benchmark considering a simple flow describing a mono-dimensional time-decaying sinusoidal wave in a d dimensional periodic domain is considered; this flow is characterized by sizeable velocity gradients, *i.e.* tangible compressibility effects, that allow for the detection of bulk viscosity effects.

The initial conditions for such flow are the following: along one single space coordinate x one considers

$$u_x = \frac{U^x}{U^0} = u_0 \sin\left(\frac{2\pi x}{L}\right) \qquad x \in [0, L] \ , \tag{3.30}$$

and all other components of the macroscopic velocity are initialized to 0. Temperature and density are provided a constant initial value.

With such initial conditions, the sinusoidal wave decays with time, until the fluid goes at rest.

At an intermediate time step in the evolution, a measure of the dynamic pressure is obtained according to the formula provided in *2.2.5*

$$\varpi = -P - \frac{1}{d}\Delta_{\alpha\beta}T^{\alpha\beta} \ , \tag{3.31}$$

Then, provided that sufficiently low velocities are considered (by properly setting the value v_0 in Eq. *3.30*), the relativistic divergence appearing in Eq. *1.66* can be replaced with its non-relativistic counterpart, that can be evaluated via finite differences methods

$$\varpi = -\mu\nabla_\alpha U^\alpha \sim -\mu\partial_i u_i = -\mu\partial_x u_x \ . \tag{3.32}$$

It follows that at each time step of the simulation μ can be estimated with good accuracy by taking spatial averages over the whole domain

$$\mu = -\frac{<\varpi>_x}{<\partial_x u_x>_x} \ . \tag{3.33}$$

By performing several simulations, each time taking different values for the relativistic coldness ζ, it is possible to extract functional dependencies $\mu = \mu(\zeta)$ for every number of spatial dimensions d. The results shown in Fig. *3.3* show once again that the numerical data are compatible with the CE analysis.

3.3.3 *Shear Viscosity*

Lastly, one can turn the attention to the shear viscosity η. The exercise that follows is directly inspired by the one found in [91], and the benchmark adopted in this case is an iteration of the Taylor-Green vortexes [97], that is a well known test for hydrodynamic solvers in the non-relativistic regime as well.

Once a periodic bi-dimensional domain $(x, y) \in [0, L]\text{x}[0, L]$ is taken, the initial conditions for such flow read as
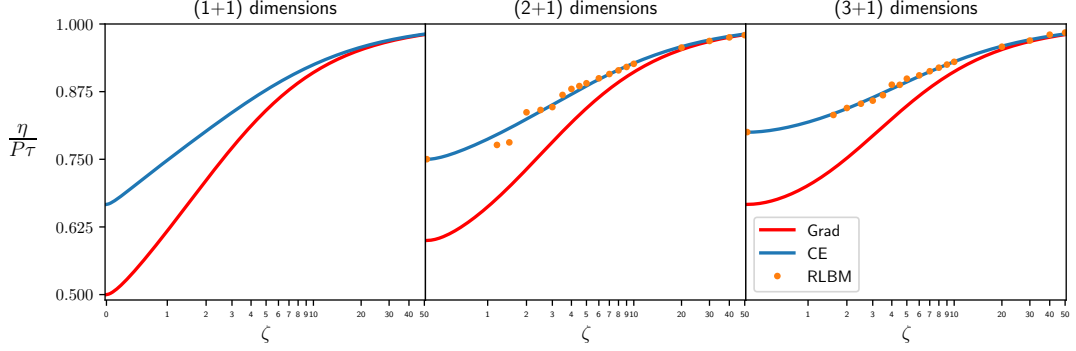
Figure 3.4: *Numerical estimate of the (non-dimensional) shear viscosity for a relativistic gas in $(1 + 1)$, $(2 + 1)$ and $(3 + 1)$ dimensions, shown respectively from left to right. The results are in agreement with CE analysis. The results for the $(1+1)$ dimensional case are not available since the Taylor-Green benchmark is expressed on a bi-dimensional domain.*

$$u_x(x, y, t_0) = \frac{U^x}{U^0} = +u_0 \cos\left(\frac{2\pi x}{L}\right) \sin\left(\frac{2\pi y}{L}\right) ,$$

$$u_y(x, y, t_0) = \frac{U^y}{U^0} = -u_0 \sin\left(\frac{2\pi x}{L}\right) \cos\left(\frac{2\pi y}{L}\right) , \tag{3.34}$$

with all the other components of the macroscopic velocity U^α equal to zero, density n and temperature T set to a constant fixed value. If u_0 is taken sufficiently small, the flux is almost non-relativistic, and the solution can be taken similar to the classical one:

$$u_x = F(t)u_x(x, y, t_0) \tag{3.35}$$

$$u_y = F(t)u_y(x, y, t_0) , \tag{3.36}$$

The task is now the determination of the time dependency $F(t)$. If the flow is almost non-relativistic, then it is divergence-free ($\Delta^\alpha U_\alpha = O(u_0^2)$) and the dynamic pressure gives no contribution to the energy-momentum tensor. $T^{\alpha\beta}$ can then be written as

$$T^{\alpha\beta} = (P + \epsilon)U^\alpha U^\beta - P\eta^{\alpha\beta} + \pi^{<\alpha\beta>} . \tag{3.37}$$

Then, by setting the balance equation Eq. 1.19

$$\partial_\alpha T^{\alpha\beta} = 0 \; , \tag{3.38}$$

one derives the following differential equation (for sufficiently small u_0, one can ignore all terms that are $O(u_0^2)$)

$$2\eta F(t) + F'(t)(P + \epsilon) = 0 \; , \tag{3.39}$$

that has solution

$$F(t) = exp\left(-\frac{2\eta}{P + \epsilon}t\right) \tag{3.40}$$

considering that $P + \epsilon$ stays approximately constant through time. One can then integrate over the spatial domain to obtain the averaged quantity $< u^2 >_{xy} = u_x^2 + u_y^2$ (obtained combining Eq. 3.35 and Eq. 3.40) in order to get

$$< u^2 >_{xy} = \frac{1}{L^2} \int_0^L \int_0^L (u_x^2 + u_y^2) \mathrm{dxdy} = \frac{u_0^2}{2} \exp\left(-\frac{4\eta}{P + \epsilon} t\right) \tag{3.41}$$

which gives a way to compute the shear viscosity

$$\eta = \left(\frac{P + \epsilon}{4t}\right) \log\left(\frac{u_0^2}{2 < u^2 >_{xy}}\right) \; . \tag{3.42}$$

By performing several simulations, each time taking different values for the relativistic coldness ζ, it is possible to extract functional dependencies $\eta = \eta(\zeta)$ for every number of spatial dimensions d. The results shown in Fig. 3.4 show once again that the numerical data are compliant with the CE analysis.

As a final remark, one can also point out that the previous analysis can be used to also evaluate the range of validity of the hydrodynamic approximation. The forecast made by both CE and Grad is valid as long as the small Knudsen number hypothesis remain valid, *i.e.* as long as the hydrodynamic regime is valid $(\mathrm{Kn} \leq 10^{-2})$. As already seen, Kn is computed on the lattice by setting the value of the relaxation time τ (Eq. 2.53), and therefore this highlights an important
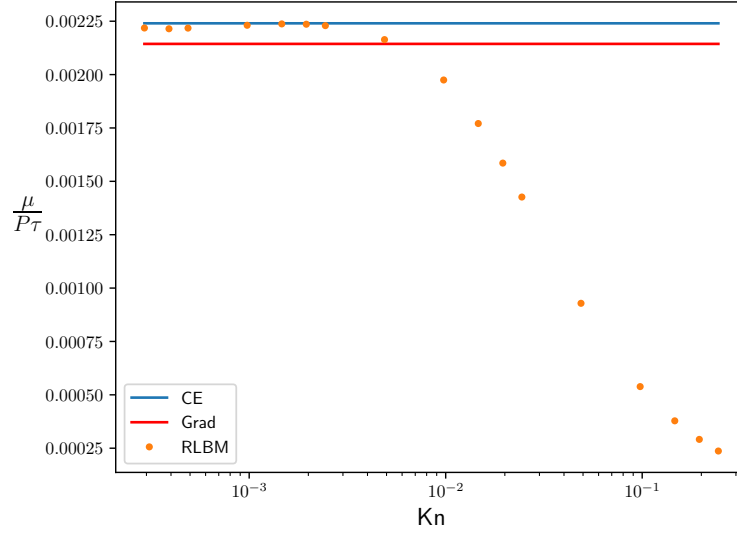
Figure 3.5: *Comparison between the dimensionless bulk viscosity and the Knudsen number Kn. As soon as $Kn \gtrsim 10^{-2}$, the linear relationships forecast by CE and Grad's analysis breaks down, and there is not anymore a firm connection to the transport coefficients.*

factor to keep in mind when doing simulations.

Evidence of what has been said is visible in Fig. 3.5, where the dimensionless bulk viscosity $\mu/P\tau$ has been plotted against the Knudsen number Kn, as computed in Eq. 2.53. The value of the relativistic coldness ζ is set at a fixed value $\zeta = 10$, and the measure is performed for different values of the relaxation time. It is immediately evident that the functional dependency on ζ departs from linearity as soon as one abandons hydrodynamic values of the Knudsen number.

4

Numerical Benchmarks

In this section we provide a couple of numerical benchmarks for the verification of the scheme shown in Ch. 2. The first is a popular iteration of the Bjorken flow, also called the mono-dimensional boost invariant expansion model [98]. This benchmark is common in the community of Heavy-Ion collisions, because it mimics in a basic way the hydrodynamic evolution of the Quark-Gluon Plasma (QGP) that are formed during said collisions, and that at a set stage of the evolution can be described by recurring to relativistic hydrodynamics.

In this thesis work it is the first time that RLBM is shown to correctly repo

In Sec. 4.1, after introducing the curvilinear Milne coordinates, I give a brief introduction on the analytical solution of the benchmark (discussed in [13] and here extended and generalized), discuss how said solution has to be adapted in Cartesian coordinates, and then show the comparison with the results provided by RLBM, in the case of ultra-relativistic inviscid gases in (d+1) dimensions. The verification of RLBM on such flow is shown in this thesis work for the first time.

The second benchmark is the relativistic iteration of the Riemann problem, also called Sod's Shock Tube or mono-dimensional shock wave. This test is widely used in computational fluid dynamics to benchmark solvers in the presence of strong gradients and discontinuities, both in the classical case [99] and in the relativistic one [1, 100]. The results shown here can also be found in [25, 28].

4.1 Bjorken Flow

The Bjorken flow is a toy model realized to mimic the behavior of QGP in experiments of heavy-ion collisions, where two rays of heavy ions are made to collide with each other. The collision develops a hot soup of unconfined quarks, that can be described via hydrodynamics at a set stage of the evolution.

4.1.1 Milne coordinates

In flat space-time the most natural set of coordinates to describe the space is the Cartesian one, which is used for the development of the RLBM. A generic position vector is therefore described as (only one spatial coordinates z is highlighted since only one coordinate is interested in the dynamics, namely the longitudinal coordinate along which the two rays of particles travel)

$$x^\mu = (t, z) \ . \tag{4.1}$$

The boost invariant flow is usually described in the literature by recurring to Milne coordinates [101], as the flow is at rest in said curvilinear coordinates, and therefore the solution can be more easily found. From now on, every tilded quantity will be considered as expressed within the Milne basis:

$$\tilde{x}^\mu = (\tau, w) \tag{4.2}$$

The change of coordinates from Cartesian to Milne is given by the following transformation rule (No change is implied on the transverse space coordinates):

$$\begin{cases} \tau &= \sqrt{t^2 - z^2} \\ w &= \operatorname{arctanh}\left(\frac{z}{t}\right) \end{cases} \qquad \begin{cases} t &= \tau \cosh(w) \\ z &= \tau \sinh(w) \end{cases} \ . \tag{4.3}$$

One can therefore obtain the transformation matrix $\Lambda^\mu{}_\nu = \frac{\partial \tilde{x}^\mu}{\partial x^\nu}$ between the two reference frames, which among other things will provide an expression for

the metric in the new basis:

$$\tilde{\eta}_{\alpha\beta} = (\Lambda^{-1})^\mu{}_\alpha (\Lambda^{-1})^\nu{}_\beta\ \eta_{\mu\nu} = \mathrm{diag}\left(+1, -\tau^2\right) \tag{4.4}$$

$$\tilde{\eta}^{\alpha\beta} = \Lambda^\alpha_\mu\ \Lambda^\beta_\nu\ \eta^{\mu\nu}\, . = \mathrm{diag}\left(+1, -\frac{1}{\tau^2}\right) \tag{4.5}$$

Additionally, the curvilinear coordinates define connection coefficients $\Gamma^\alpha_{\beta\gamma}$, and the usual derivative has to be replaced with the covariant derivative:

$$A^\alpha_{;\beta} = \partial_\beta A^\alpha + \Gamma^\alpha_{\beta\gamma} A^\gamma\, . \tag{4.6}$$

Milne's connection coefficients are defined by

$$\tilde{\Gamma}^\alpha_{\beta\gamma} = \frac{1}{2}\tilde{\eta}^{\alpha\mu}\left(\partial_\beta \tilde{\eta}_{\mu\gamma} + \partial_\gamma \tilde{\eta}_{\beta\mu} - \partial_\mu \tilde{\eta}_{\gamma\beta}\right)\ , \tag{4.7}$$

$$\tilde{\Gamma}^0_{dd} = \tau \qquad \tilde{\Gamma}^d_{0d} = \frac{1}{\tau} \qquad \tilde{\Gamma}^d_{d0} = \frac{1}{\tau}\ , \tag{4.8}$$

all other connections are zero.

The Bjorken flow is the description of a fluid which is expanding along one spatial dimension (the z-axis) with velocity $\beta = \frac{z}{t}$ for $|z| \le t$, starting from an initial time t_0.

The Cartesian macroscopic velocity U^α can then be written as

$$U^\alpha = \frac{1}{\sqrt{t^2 - z^2}}\left(t, z\right)\ . \tag{4.9}$$

One can then use the transformation matrix $\Lambda^\mu{}_\nu$ to obtain the corresponding Milne macroscopic velocity $\tilde{U}^\alpha$:

$$\tilde{U}^\mu = \Lambda^\mu{}_\nu U^\nu = (c, 0)\ . \tag{4.10}$$

This prescription dictates how to solve for the particle number density n, the energy density ϵ, and the temperature T.

4.1.2 Analytic Solution (ideal ultra-relativistic fluid)

In the inviscid regime, no dissipative contribution is given to the particle flow N^α and energy-momentum tensor $T^{\alpha\beta}$ (meaning that the non-equilibrium quantities in the two moments are set to zero). Note that in the Milne framework, one has:

$$\tilde{N}^\alpha = n\tilde{U}^\alpha \ , \tag{4.11}$$

$$\tilde{T}^{\alpha\beta} = (\epsilon + P)\tilde{U}^\alpha\tilde{U}^\beta - P\tilde{\eta}^{\alpha\beta} \ . \tag{4.12}$$

The balance equations 1.19 in Milne coordinates assume the form

$$0 = N^\alpha_{;\alpha} = \partial_\alpha N^\alpha + \Gamma^\beta_{\beta\alpha}N^\alpha \ , \tag{4.13}$$

$$0 = T^{\alpha\beta}_{;\alpha} = \partial_\alpha T^{\alpha\beta} + \Gamma^\beta_{\mu\alpha}T^{\mu\alpha} + \Gamma^\alpha_{\mu\alpha}T^{\mu\beta} \ . \tag{4.14}$$

By imposing such conservation equations, considering Eq. 4.10 and Eq. 4.11 one gets:

$$0 = \partial_\tau(n\tau) \ ,$$
$$0 = \partial_\tau(\epsilon) + \frac{P + \epsilon}{\tau} \ , \tag{4.15}$$
$$0 = \partial_w(P) \ ,$$

that has to be solved once the initial conditions

$$n_0 = n(\tau_0) \ , \qquad \epsilon_0 = \epsilon(\tau_0) \ , \qquad P_0 = P(\tau_0) \ , \qquad T_0 = T(\tau_0) \ , \tag{4.16}$$

are provided. In the ultra-relativistic case, Eqs. 4.15 can be solved analytically by coupling them with the ideal EOS (Eq. 1.40), since in the ultra-relativistic limit one has $G_d = d + 1$:

$$P = nT \ ,$$
$$\epsilon = dP \ , \tag{4.17}$$

and one then obtains the solution

$$n(\tau) = n_0 \frac{\tau_0}{\tau} \ ,$$

$$\epsilon(\tau) = \epsilon_0 \left(\frac{\tau_0}{\tau}\right)^{\frac{d+1}{d}} \ ,$$

$$P(\tau) = P_0 \left(\frac{\tau_0}{\tau}\right)^{\frac{d+1}{d}} \ , \tag{4.18}$$

$$T(\tau) = T_0 \left(\frac{\tau_0}{\tau}\right)^{\frac{1}{d}} \ .$$

On the other hand, in the more general case of massive particles, the additional dependency of the ideal EOS on temperature ($\epsilon = P(G_d(T) - 1)$) does not make the system of equations analytically solvable. One can though solve numerically for temperature, by expressing the second equation in 4.15 as

$$\partial_\tau \left(T(G_d(T) - 1)\right) + \frac{T}{\tau} = 0 \ . \tag{4.19}$$

The particle density stays unchanged, and therefore once the temperature is obtained the energy density and the pressure can be derived from the EOS.

4.1.3   RLBM results

In order to simulate the (ultrarelativistic) Bjorken flow within the framework of the RLBM, the initial conditions given previously in Milne coordinates have to be expressed back into Cartesian coordinates. Once a domain $z \in [-\frac{L}{2}, \frac{L}{2}]$ and an initial time $t = t_0$ are selected, the initial value τ_0 is given by

$$\tau_0 = \sqrt{t_0^2 - \frac{L^2}{4}} \ . \tag{4.20}$$

Therefore to set the initial thermodynamic quantities at $t = t_0$ for all the points $-\frac{L}{2} < z < \frac{L}{2}$ (that give values of $\tau > \tau_0$) one will have to refer to Eq. 4.18. The populations are initialized at equilibrium f^{eq} as usual. The solution Eq. 4.18 reads in Cartesian coordinates as
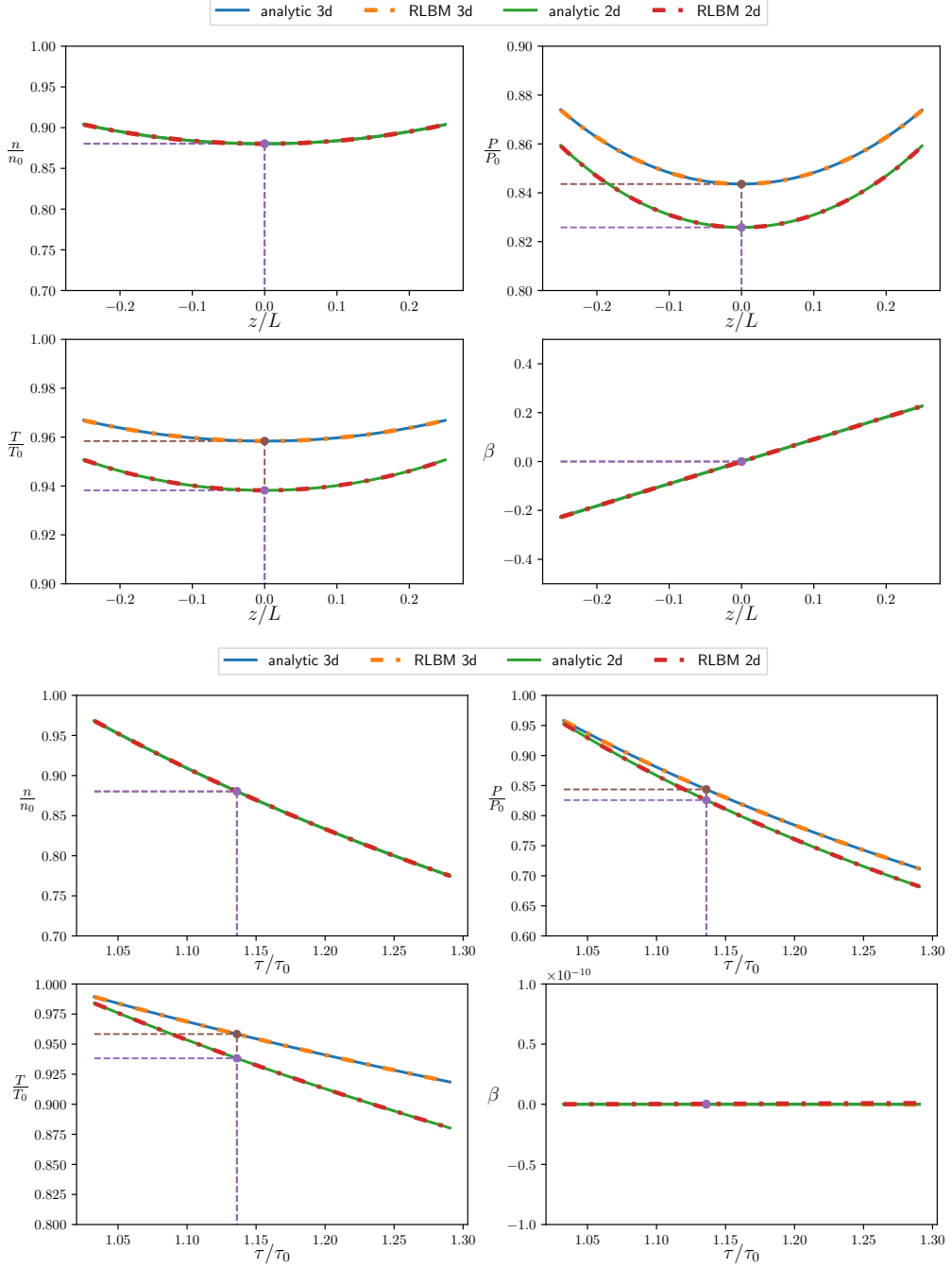
Figure 4.1: *Comparison of numerical results for the Bjorken flow of an ultra relativistic inviscid gas of particles in (2+1) and (3+1) dimensions with the analytic solutions Eq. 4.18 and Eq. 4.21. The initial settings of the flow are $t_0 = 1.0 fm/c$, $L = 0.5 fm$, $N = 1000$. On the top panel, four snapshots at $t = 1.1 fm/c$ are shown against the spatial coordinate z. In the bottom panel the values of the thermodynamic quantities taken at $z = 0$ are plotted against τ, and in both cases there is a perfect match with the analytic solutions. As density and velocity do not depend on dimension, all the curves in the respective plots are overlapped. The purple and brown marker identify the same points in the two different coordinate systems.*

$$n(t,z) = n_0 \left(\frac{t_0^2 - L^2/4}{t^2 - z^2} \right)^{\frac{1}{2}}$$ (4.21)

$$P(t,z) = P_0 \left(\frac{t_0^2 - L^2/4}{t^2 - z^2} \right)^{\frac{d+1}{2d}}$$

$$T(t,z) = T_0 \left(\frac{t_0^2 - L^2/4}{t^2 - z^2} \right)^{\frac{1}{2d}}$$

$$\beta(t,z) = \frac{z}{t}$$

No further trick has to be taken, except for an implementation of boundary conditions. In fact, while in the Milne coordinate system the dynamic is periodic in space (all thermodynamic variables are constant with respect to the space coordinate w, and the macroscopic velocity $\tilde{U}^\alpha$ is always at rest), in Cartesian coordinates there is the need for a prescription for the ghost nodes immediately outside of the domain.

At every time step the populations in the left ghost node and right ghost node are set to be composed of two parts: the equilibrium part is simply the Maxwell-Jüttner equilibrium computed using the thermodynamic quantities in Eq. 4.18, while the non equilibrium part is computed using a linear interpolation with the nearest inner nodes.

Lastly, one final remark on the simulation has to be provided. In order to compare the thermodynamics quantities against the value of τ, at every time step t one picks the values of the thermodynamic quantities at $z = 0$, so that $\tau(z = 0, t) = t$ and $w(z = 0, t) = 0$.

In Fig. 4.1 the results of the simulations in Cartesian and Milne coordinates are provided, and a perfect matching with the analytic solutions Eq. 4.18 and Eq. 4.21 is shown.

4.2 Mono-dimensional Shock Wave

A second test for the validity of the RLBM scheme is provided by the popular Sod's shock tube, or mono-dimensional shock wave (also known as Riemann Problem). This test is widely used in computational fluid dynamics to benchmark solvers in the presence of strong gradients and discontinuities, both in the classical

case [99] and in the relativistic one [1, 100].

The dynamic develops along one spatial dimension, characterized by the coordinate $x \in [-L/2, L/2]$. At $x = 0$, a layer splits the fluid, initially at rest, into two different thermodynamical states

$$\left(P, \; n, \; T, \; \beta = \frac{U^x}{U^0} \right) = \begin{cases} (P_L, \; n_L, \; T_L, \; 0) & x \leq 0 \\ (P_R, \; n_R, \; T_R, \; 0) & x > 0 \end{cases}, \qquad (4.22)$$

where the left quantities are taken bigger than the right ones.

Once the layer is removed, the discontinuity at $x = 0$ develops into a shock-/rarefaction wave, that travels through the medium decaying with time. An analytical solution for the problem exists for ultra relativistic gases, in the inviscid regime ($Kn \to 0$) or in the free-streaming regime ($Kn \to \infty$). In order to characterize the regime - in addition to Kn - it is customary to introduce the quantity η/s, the shear viscosity to entropy density ratio, where s is usually computed as [24]

$$s = n \left(G_d - \log \left(\frac{n}{n^{\text{eq}}} \right) \right) \qquad (4.23)$$

$$n^{\text{eq}} = \int f^{\text{eq}} \frac{\mathrm{d}\boldsymbol{p}}{p^0} = B(n, T) Z \qquad (4.24)$$

(with the usual definition of the integral Z given in App.B and the coefficient $B(n, T)$ defined in Eq. 1.37). In what follows both the two methods will be used to classify the regime.

As the iteration of RLBM shown in the previous chapters has been thought as a solver for hydrodynamics, no perfect results are expected for this benchmark in the free-streaming regime. Nonetheless, in Ch.5 an extension of RLBM specifically realized to treat this regime will be discussed.

For the moment though only the hydrodynamic regime is examined, meaning that only low values of η/s are considered, and the other case is left for later treatment.

In the inviscid case as the wave travels through the medium different zones with distinctive features appear:

- In the unperturbed zones (L) and (R), all fields keep their initial values.

- In the zone (*) a rarefaction wave with head at coordinate x_{H} and tail at coordinate x_{T} travels to the left.
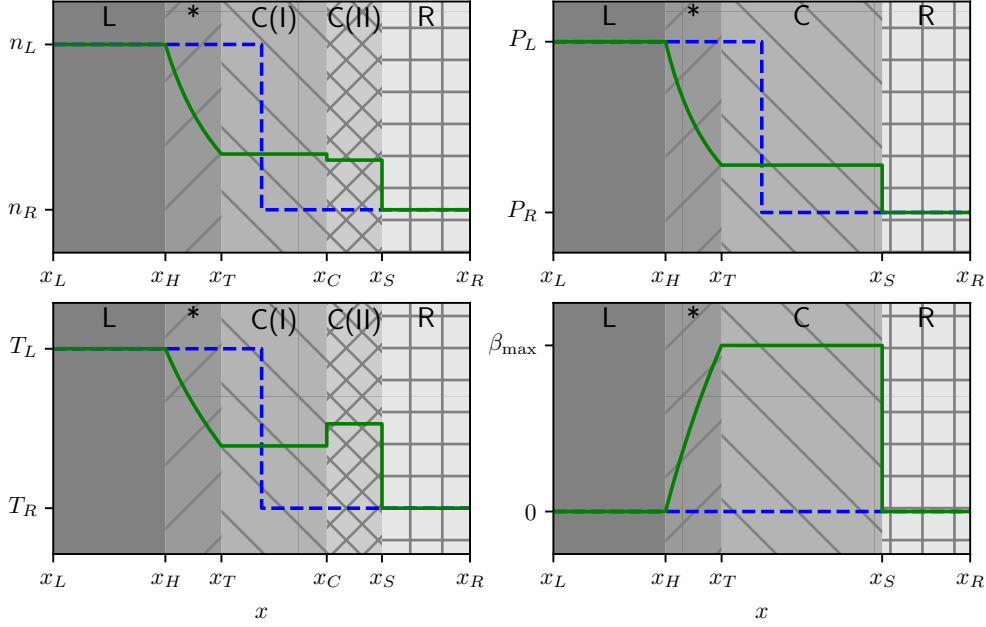
Figure 4.2: *Example of the dynamic of a shock/rarefaction wave for a inviscid fluid, when the initial conditions considered are the ones in Eq. 4.22 (here represented by the dashed blue line). A later stage of the evolution is shown by the green line, and the various zones presented in the main text are clearly visible.*

- In the shock zone (C), characterized by the presence of the shock wave, there is the presence of a discontinuity at $x = x_{\mathrm{C}}$ for density and temperature, that will therefore be labelled with I and II. Pressure and velocity, that do not exhibit a discontinuity, are instead labelled as $P_I = P_{II} = P_{\mathrm{C}}$ and $\beta_I = \beta_{II} = \beta_{\mathrm{C}}$.

An example of the dynamics is provided in Fig. 4.2, and in Sec. 4.2.1 the analytic solution for the ultra-relativistic regime is presented.

When considering viscous flows this same scenario appears only with profiles that are smoothed due to dissipation. As the solutions of the viscid and/or massive cases would be semi-analytical, and require expensive numerical work, RLBM results are compared against another numerical solver that is though based on different working principles:

- Relativistic Boltzmann Equation - Test Particle (RLB-TP) [102–109], a Monte Carlo-enabled solution of the full kernel of the Boltzmann equation based on test particles method.

4.2.1   Analytic Solution (ideal ultra-relativistic fluid)

The starting step for the derivation of the solution in the rarefaction zone $*$ are the constitutive equations for an ideal fluid, Euler's equations Eq. 1.31, that are greatly simplified in the case of massless particles ($\zeta = 0$). By introducing the variable $w = \frac{x}{t}$, one writes these equations as

$$(\beta - w)\, \partial_w n = -\frac{n}{1 - \beta^2}\, (1 - \beta w)\, \partial_w \beta \ , \tag{4.25}$$

$$(\beta - w)\, \partial_w \beta = -\frac{1 - \beta^2}{P + \epsilon}\, (1 - \beta w)\, \partial_w P \ , \tag{4.26}$$

$$(\beta - w)\, \partial_w P = -\frac{\Gamma P}{1 - \beta^2}\, (1 - \beta w)\, \partial_w \beta \ , \tag{4.27}$$

where

$$\Gamma = \frac{c_P}{c_v} = \left(1 + \frac{1}{d}\right)$$

is the ultra-relativistic adiabatic index. Combining the Eq. 4.26 and Eq. 4.27, and using the ideal EOS, it is possible to eliminate the pressure derivative

$$(\beta - w)^2 = (1 - \beta w)\, c_s^2 \ , \qquad c_s = 1/\sqrt{d} \ , \tag{4.28}$$

and to get as a solution

$$w_\pm = \left(\frac{\beta \mp c_s}{1 \mp c_s \beta}\right) \ . \tag{4.29}$$

In what follows only w_+ is considered, as it represents a rarefaction wave traveling to the left. By inserting w_+ into equations Eq. 4.25 and Eq. 4.27 one derives equations for n and P that when are integrated in w give out the following Riemann invariants:

$$n \left(\frac{1 + \beta}{1 - \beta} \right)^{\frac{\sqrt{d}}{2}} = \text{cost.} \ , \tag{4.30}$$

$$P \left(\frac{1 + \beta}{1 - \beta} \right)^{\frac{d+1}{2\sqrt{d}}} = \text{cost.} \ . \tag{4.31}$$

By computing these invariants at the coordinate x_H, the values for density and pressure in the rarefaction zone are readily obtained

$$n_* = n_{\mathrm{L}} \ \left(\frac{1 - \beta_*}{1 + \beta_*} \right)^{\frac{\sqrt{d}}{2}} \ , \tag{4.32}$$

$$P_* = P_{\mathrm{L}} \ \left(\frac{1 - \beta_*}{1 + \beta_*} \right)^{\frac{d+1}{2\sqrt{d}}} \ , \tag{4.33}$$

with

$$\beta_* = \frac{w_+ + c_s}{1 + c_s w_+} \ . \tag{4.34}$$

In order to determine the solution in the shock zone C, the Rankine-Hugoniot conditions [110] are applied on the interface between zones $C(II)$ and R. These conditions express the continuity of the normal component of the energy momentum-tensor, and after some manipulations write as

$$\frac{n_{II} \beta'_{\mathrm{C}}}{\sqrt{1 - \beta'^2_{\mathrm{C}}}} = \frac{n_R \beta'_{\mathrm{R}}}{\sqrt{1 - \beta'^2_{\mathrm{R}}}} \ , \tag{4.35}$$

$$\frac{P_{\mathrm{C}} \left(1 + \beta'^2_{\mathrm{C}} d \right)}{1 - \beta'^2_{\mathrm{C}}} = \frac{P_{\mathrm{R}} \left(1 + \beta'^2_{\mathrm{R}} d \right)}{1 - \beta'^2_{\mathrm{R}}} \ , \tag{4.36}$$

$$\frac{P_C \beta'_{\mathrm{C}}}{\sqrt{1 - \beta'^2_{\mathrm{C}}}} = \frac{P_R \beta'_{\mathrm{R}}}{\sqrt{1 - \beta'^2_{\mathrm{R}}}} \ , \tag{4.37}$$

where all the primed quantities are given in a reference frame where the shock front is at rest. By applying a Lorentz boost from this frame to the lab frame one gets

$$\beta'_{\mathrm{C}} = \frac{\beta_{\mathrm{C}} - \beta_s}{1 - \beta_s \beta_{\mathrm{C}}} \quad , \quad \beta'_{\mathrm{R}} = -\beta_s \ . \tag{4.38}$$

Where β_s is the shock front velocity in the lab frame. By inserting this into Eq. 4.35, Eq. 4.36 and Eq. 4.37 one obtains

$$\beta_s = \sqrt{\frac{P_{\mathrm{R}} + dP_{\mathrm{C}}}{d[P_{\mathrm{C}} + dP_{\mathrm{R}}]}} \ , \quad \beta_{\mathrm{C}} = \sqrt{\frac{d(P_{\mathrm{C}} - P_{\mathrm{R}})^2}{[P_{\mathrm{R}} + dP_{\mathrm{C}}][P_{\mathrm{C}} + dP_{\mathrm{R}}]}} \ , \tag{4.39}$$

and

$$n_{II} = n_{\mathrm{R}} \sqrt{\frac{P_{\mathrm{C}}[P_{\mathrm{R}} + dP_{\mathrm{C}}]}{P_{\mathrm{R}}[P_{\mathrm{C}} + dP_{\mathrm{R}}]}} \quad . \tag{4.40}$$

Next, by considering the interface between zones $*$ and $C(I)$ and Eq. 4.33, the contact point $w_{\mathrm{T}} = x_{\mathrm{T}}/t$ is found.

$$w_{\mathrm{T}} = \frac{1 - c_s - (1 + c_s)\left(\frac{P_{\mathrm{C}}}{P_{\mathrm{L}}}\right)^{\frac{2\sqrt{d}}{d+1}}}{1 - c_s + (1 + c_s)\left(\frac{P_{\mathrm{C}}}{P_{\mathrm{L}}}\right)^{\frac{2\sqrt{d}}{d+1}}} \quad . \tag{4.41}$$

The pressure on the central plateau P_{C} can be found by numerically solving the equation $\beta_*(w_{\mathrm{T}}) = \beta_{\mathrm{C}}$, thus:

$$\frac{\left(\frac{P_{\mathrm{L}}}{P_{\mathrm{C}}}\right)^{\frac{2\sqrt{d}}{d+1}} - 1}{\left(\frac{P_{\mathrm{L}}}{P_{\mathrm{C}}}\right)^{\frac{2\sqrt{d}}{d+1}} + 1} - \sqrt{\frac{d(P_{\mathrm{C}} - P_{\mathrm{R}})^2}{[P_{\mathrm{R}} + dP_{\mathrm{C}}][P_{\mathrm{C}} + dP_{\mathrm{R}}]}} = 0 \ . \tag{4.42}$$

Finally, the density field n_I can be obtained from Eq. 4.32:

$$n_I = n_*(w_{\mathrm{T}}) = n_{\mathrm{L}} \left(\frac{P_{\mathrm{C}}}{P_{\mathrm{L}}}\right)^{\frac{d}{d+1}} \quad . \tag{4.43}$$

A summary of the presented solution is given below.

$$x_{\mathrm{H}} = -c_s\, t\,, \qquad x_{\mathrm{T}} = \frac{\beta_{\mathrm{C}} - c_s}{1 - \beta_{\mathrm{C}} c_s} t\,, \qquad x_{\mathrm{C}} = \beta_{\mathrm{C}}\, t\,, \qquad x_{\mathrm{S}} = \beta_s\, t$$

$$\beta(x,t) = \begin{cases} \beta_L & x < x_{\mathrm{H}} \\ \beta_* = \frac{w + c_s}{1 + c_s w} & x_{\mathrm{H}} < x < x_{\mathrm{T}} \\ \beta_{\mathrm{C}} = \sqrt{\frac{d(P_{\mathrm{C}} - P_{\mathrm{R}})^2}{[P_{\mathrm{R}} + dP_{\mathrm{C}}][P_{\mathrm{C}} + dP_{\mathrm{R}}]}} & x_{\mathrm{T}} < x < x_{\mathrm{S}} \\ \beta_{\mathrm{R}} & x > x_{\mathrm{S}} \end{cases}$$

$$n(x,t) = \begin{cases} n_L & x < x_{\mathrm{H}} \\ n_* = n_L \left(\frac{(1 - c_s)(1 - w)}{(1 + c_s)(1 + w)} \right)^{\frac{\sqrt{d}}{2}} & x_{\mathrm{H}} < x < x_{\mathrm{T}} \\ n_I = n_L \left(\frac{P_{\mathrm{C}}}{P_{\mathrm{L}}} \right)^{\frac{d}{d+1}} & x_{\mathrm{T}} < x < x_{\mathrm{C}} \\ n_{II} = n_{\mathrm{R}} \sqrt{\frac{P_{\mathrm{C}}[P_{\mathrm{R}} + dP_{\mathrm{C}}]}{P_{\mathrm{R}}[P_{\mathrm{C}} + dP_{\mathrm{R}}]}} & x_{\mathrm{C}} < x < x_{\mathrm{S}} \\ n_{\mathrm{R}} & x > x_{\mathrm{S}} \end{cases}$$

$$P(x,t) = \begin{cases} P_{\mathrm{L}} & x < x_{\mathrm{H}} \\ P_* = P_{\mathrm{L}} \left(\frac{(1 - c_s)(1 - w)}{(1 + c_s)(1 + w)} \right)^{\frac{d+1}{2\sqrt{d}}} & x_{\mathrm{H}} < x < x_{\mathrm{T}} \\ P_{\mathrm{C}} & x_{\mathrm{T}} < x < x_{\mathrm{S}} \\ P_{\mathrm{R}} & x > x_{\mathrm{S}} \end{cases}$$

where $w = \frac{x}{t}$, β_s is

$$\beta_s = \sqrt{\frac{P_{\mathrm{R}} + dP_{\mathrm{C}}}{d[P_{\mathrm{C}} + dP_{\mathrm{R}}]}}$$

and the pressure value P_{C} can be found by numerically solving the equation:

$$\frac{\left(\frac{P_{\mathrm{L}}}{P_{\mathrm{C}}} \right)^{\frac{2\sqrt{d}}{d+1}} - 1}{\left(\frac{P_{\mathrm{L}}}{P_{\mathrm{C}}} \right)^{\frac{2\sqrt{d}}{d+1}} + 1} = \sqrt{\frac{d(P_{\mathrm{C}} - P_{\mathrm{R}})^2}{[P_{\mathrm{R}} + dP_{\mathrm{C}}][P_{\mathrm{C}} + dP_{\mathrm{R}}]}}$$
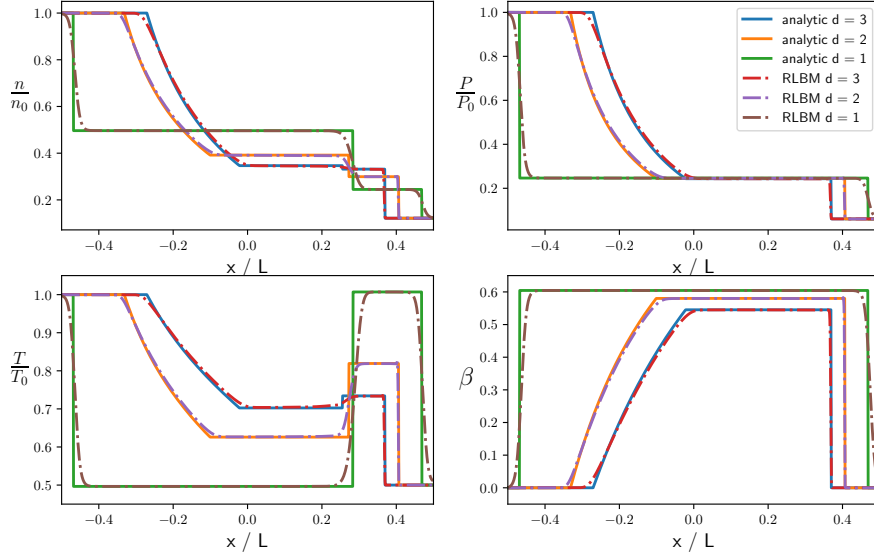
Figure 4.3: *Comparison of RLBM with the analytic solution of the ideal ultra-relativistic Sod shock tube, for different spatial dimensions. The fields of density (top-left panel), pressure (top-right panel), temperature (bottom-left panel) and velocity (bottom-right panel) are shown. All quantities are opportunely made dimensionless. The RLBM agrees nicely with the analytic solution.*

4.2.2 RLBM results

As a first result of RLBM, a comparison against the analytical solution for ideal ultra relativistic fluids is provided in Fig. 4.3, for different values of the spatial dimensions d. The initial conditions for the flow are the following:

$$(P, \ T, \ \beta) = \begin{cases} \left(5.4 \ \ GeV/fm^d, \ 400 \ \ MeV, \ 0\right) & x \leq 0 \\ \left(0.3 \ \ GeV/fm^d, \ 200 \ \ MeV, \ 0\right) & x > 0 \end{cases} , \qquad (4.44)$$

and density is chosen accordingly to EOS (the reference values for P, T and n are taken to be the values of the unperturbed left zone). All simulations are conducted on a grid with $N = 6400$ lattice points, representing a domain of $L = 6.4$ fm. The presented snapshots are taken at $t = 3.0$ fm/c, and the value of the lattice relaxation time is chosen reasonably small, so that the value of the Knudsen number computed as of Eq. 2.53 is reasonably small (for stability reason the Lattice Boltzmann method can not simulate completely inviscid flows, as the lattice relaxation time τ can not be chosen $< 1/2$). The value chosen for τ is 2, and with the chosen spatial discretization that translates to Kn$= \tau/N \sim 3 \times 10^{-4}$, which is an acceptable value for an almost inviscid flow.
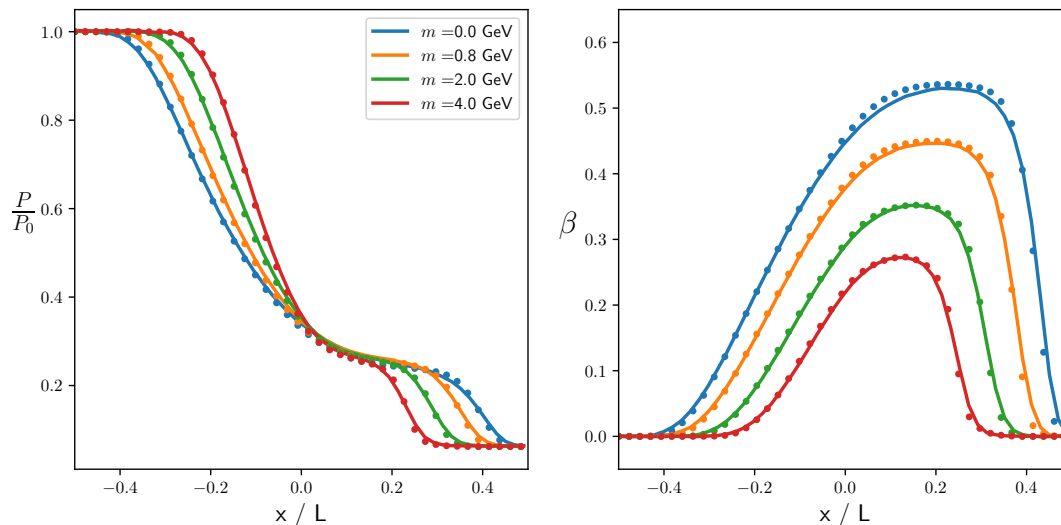
Figure 4.4: *RLBM results (dots) for different masses versus the ideal ultra-relativistic analytic solution of the Relativistic Riemann problem ($m = 0$) and RLB-TP results ($m \neq 0$) in (3+1) spatial dimensions (represented by the lines). The setup is the same used for the fig. 4.3 (Eq. 4.44 and following), and the value of η/s is set to 0.1. For the whole set of particle masses considered, the agreement with the reference solutions is good.*

There is a good match between the numerics and the analytical solutions, showing that RLBM is capable of reproducing the dynamics with these parameters at every spatial dimension.

In Fig. 4.4 different masses are considered in the (3+1) dimensional case. In this case the comparison is performed against other numerical solvers, namely the previously cited RLB-TP. In this case the parameter that characterizes the viscous regime is the shear viscosity to entropy ratio η/s, as this is the usual quantity employed to characterize flows in QGP simulations. The setting for the flows are the ones previously stated, and the value of η/s is chosen at $\eta/s = 0.1$, that represents a value for Kn well into the hydrodynamic regime. Again, good agreement between RLBM and the reference results is found.

Lastly, I show in Fig. 4.5 the results for RLBM when changing the regime of the flow, from ideal to free-streaming. As the Knudsen number (here again represented by the value of η/s) increases, RLBM struggles to reproduce the solution, and even though the general behavior of the curves is reproduced, a staircase effect appears. This is the main motivation for the development of an extension of RLBM that is suited to the reproduction of beyond-hydrodynamic flows and that will be detailed in the next chapter.
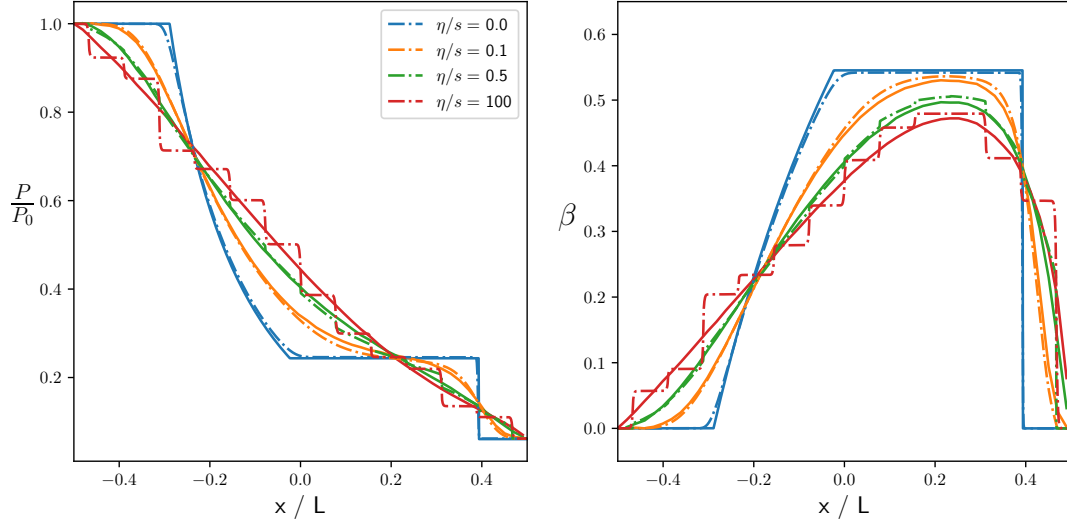
Figure 4.5: *Comparison of RLBM results (dash-dotted) against reference results (analytic in the inviscid case in blue, and RLB-TP otherwise) across all ranges of the Knudsen number, from ideal to the free-streaming regime. The value of the rest mass is set to zero. For large values of Kn, i.e. beyond the hydrodynamic regime, RLBM struggles to reproduce the solution (because it has been designed for the hydrodynamic regime), but still shows its general behaviour.*

5

Extension of the model to Weakly Interacting Regimes

Beyond-hydro regimes (characterized by values of the Knudsen number beyond 0.1) are very relevant for QGP, especially with regard to their long-time evolution after the hydrodynamic epoch [111]. Furthermore, electron conduction in pure enough materials is almost ballistic [112], and therefore more attuned to beyond-hydrodynamic descriptions.

As it has been seen in Ch. 4, the RLBM method presented in Ch. 2 fails in reproducing the dynamics whenever interactions are not strong enough to ensure the hydrodynamic condition $Kn \ll 1$. In this regime (beyond hydrodynamics), the increasing range of interactions between particles (represented by the decrease in the relative magnitude of the RHS in Eq. 1.5) does not correct eventual errors in the streaming dynamics along the (pseudo-)particle trajectories selected by the discrete velocity stencils.

All in all, being the previously shown RLBM based on a kinetic description of relativistic gases (which in principle is valid across the whole Knudsen spectrum), an extension of the algorithm to simulate beyond hydrodynamic regimes should in theory be possible, and indeed it will be shown in the remaining part of this chapter that by modifying the momentum space discretization this task can be achieved.

The final goal of the optimized discretization is the implementation of a more isotropic velocity stencil, capable of covering homogeneously the momentum space. This goal is achieved at the expense of a very desirable property of lattice kinetic schemes: perfect streaming, namely the fact that the discrete streaming along trajectories has to connect the nodes of a Cartesian Grid.

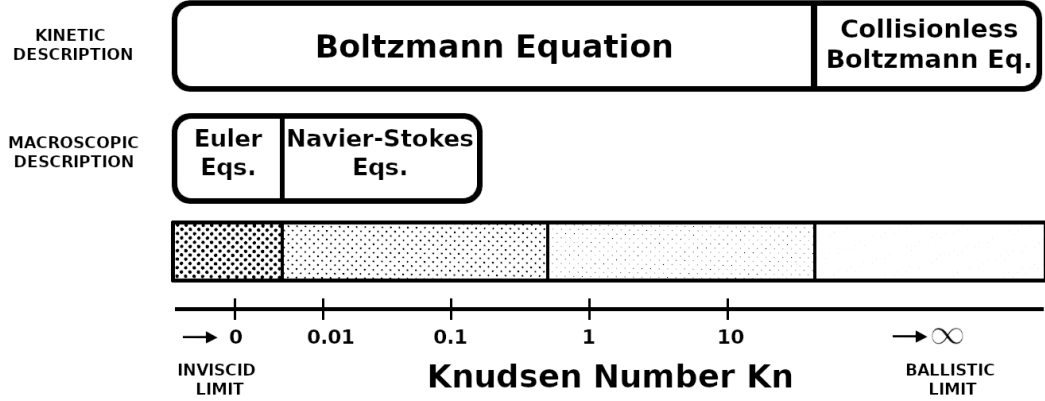This tradeoff enables though the realization of the aforementioned velocity

Figure 5.1: *The Knudsen Spectrum and the ranges of validity of the different fluid descriptions. As RLBM is a kinetic numerical scheme based on a description of the dynamics at the Boltzmann level, it should in principle be able to reproduce the whole Knudsen spectrum. On the other hand, the RLBM iteration described in Ch. 2 has been designed to resolve the hydrodynamic picture ($Kn << 1$) and therefore has to be modified in order to work at high Kn regimes.*

stencils, and opens the possibility of simulating weakly interacting regimes up to the free-streaming phase ($Kn \to \infty$), also called ballistic regime.

This extension of RLBM to the study of high Knudsen flows is inspired by the work of Ambruş and Blaga [13], and consists in employing off-lattice product-based quadrature rules in the momentum space discretization, instead of the on-lattice quadrature process described in 2.2.2. All the other algorithmic steps of RLBM remain untouched, and therefore in Sec. 5.1 only this new procedure will be detailed. Next, in section 5.2 results with this new iteration of the scheme will be presented on the mono-dimensional shock wave benchmark. In [29] there is a detailed explanation of the technique employed for the momentum discretization in the ultrarelativistic (2+1)-dimensional case, and in the next sections I will be generalizing the discussion to the massive case, as well as the (3+1) dimensional case.

5.1   *Momentum Space Discretization*

In this section a detailed discussion of the new momentum space discretization is provided to open the possibility of handling beyond hydrodynamic regimes via

the development of off-lattice isotropic stencils that better cover the momentum space.

The starting point of the new development is the orthogonality condition, Eq. 2.37, that has to be correctly conserved when moving from continuous integrals to discrete sums. As the $\boldsymbol{J^{(}n)}$ are polynomials of the momentum variable $\tilde{p}^\mu$, this means that proper quadrature rules have to discretize exactly the integrals

$$I^{\alpha_1\dots\alpha_k} = \int \omega(\tilde{p}^0) \prod_{i=1}^{k} (\tilde{p}^{\alpha_i}) \frac{\mathrm{d}\tilde{\mathrm{p}}}{\tilde{p}^0} \, , \tag{5.1}$$

with $\forall k \leq 2N$ (N being the order of the quadrature, equal or bigger than the truncation order of the equilibrium distribution function expansion). At this point it is beneficial to focus on the $(2+1)$ and $(3+1)$ dimensional cases separately, as the procedures, while similar in theory, differ for some practical aspects.

We note here that the following procedure is not immediately extended to the $(1+1)$ dimensional case, while it should in principle be working for all dimensions higher than 3.

5.1.1 (2+1) dimensions

By switching to polar coordinates, and by considering the mass-shell condition $\tilde{p}^0 = \sqrt{\tilde{p}^2 + m^2}$, the integral in Eq. 5.1 can be decomposed into a product of two different integrals, which are named radial integral $I_{\tilde{p}}^{\alpha_1\dots\alpha_k}$ and angular integral $I_{\Omega}^{\alpha_1\dots\alpha_k}$:

$$I^{\alpha_1\dots\alpha_k} = I_{\tilde{p}}^{\alpha_1\dots\alpha_k} \times I_{\Omega}^{\alpha_1\dots\alpha_k} \, , \tag{5.2}$$

$$I_{\tilde{p}}^{\alpha_1\dots\alpha_k} = \int_0^{+\infty} w(\tilde{p})(\tilde{p}^2 + \tilde{m}^2)^{\frac{k_0}{2}} \tilde{p}^{k_x+k_y} \mathrm{d}\tilde{p} \, , \tag{5.3}$$

$$I_{\Omega}^{\alpha_1\dots\alpha_k} = \int_0^{2\pi} (\cos\theta)^{k_x}(\sin\theta)^{k_y} \mathrm{d}\theta \, , \tag{5.4}$$

with

$$w(\tilde{p}) = \tilde{p}\frac{\omega(\sqrt{\tilde{p}^2 + \tilde{m}^2})}{\sqrt{\tilde{p}^2 + \tilde{m}^2}} \ , \tag{5.5}$$

and k_0, k_x and k_y accounting for the number of occurrences of the various degrees of freedom in $I^{\alpha_1...\alpha_k}$, with $k_0 + k_x + k_y = k$.

This splitting suggests that a possible strategy might be represented by the adoption of a Gauss-product rule between a radial quadrature discretizing $I_{\tilde{p}}^{\alpha_1...\alpha_k}$, and an angular quadrature discretizing $I_{\Omega}^{\alpha_1...\alpha_k}$.

The radial quadrature can be obtained by considering the change of variables $y = \sqrt{\tilde{p}^2 + \tilde{m}^2} - \tilde{m}$, that sets the radial integral to

$$I_{\tilde{p}}^{\alpha_1...\alpha_k} = \int_0^{+\infty} W(y)Q(y)\mathrm{dy} \ , \tag{5.6}$$

with the new weight function

$$W(y) = \omega(y + \tilde{m}) = \frac{1}{2\pi}e^{-y+\tilde{m}} \ , \tag{5.7}$$

and $Q(y)$ a polynomial of degree k if the value $k_x + k_y$ is even. If it is odd, then for symmetry reason the angular integral is zero, therefore in this case one does not have to consider the radial discretization.

As the new weight function is just a rescaled exponential, it is immediately evident that the correct named quadrature to adopt in this case is the Gauss-Laguerre quadrature of order $2N$:

$$\text{abscissae } y_i \qquad \text{roots of } L_{N+2}(y) = 0 \tag{5.8}$$

$$\text{weights } w_i^{(\tilde{p})} \qquad \frac{y_i}{2\pi[(N+2)^2 L_{N+2}(y_i)]^2} \tag{5.9}$$

The corresponding values for $\tilde{p}_i$ and $\tilde{p}_i^0$ can be obtained from y_i with back substitution ($\tilde{p}_0^i = y_i + \tilde{m}$, $\tilde{p}_i = \sqrt{\tilde{p}_0^{i2} - \tilde{m}^2}$). The total number of radial nodes comes out to be $N + 1$.

The angular integral (independent of the mass) is promptly discretized by considering that the integrand can be recast into a sum of circular functions of maximum degree $k_x + k_y$. Any circular function of degree K is exactly integrated
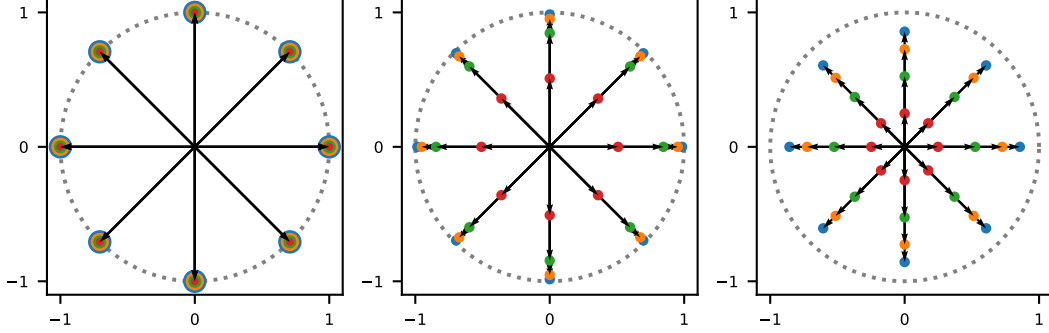
Figure 5.2: *Some example for the off-lattice stencils depicted in the previous pages. The quadrature values chosen are $N = 3$, $K = 10$, and $\tilde{m} = 0.0$, 2.0 and 10.0 (from left to right).*

on the circle by employing K equally spaced absicissae and fixed weights:

$$\text{abscissae } \theta_j \qquad j\frac{2\pi}{K} \; , \tag{5.10}$$

$$\text{weights } w_j^{(\theta)} \qquad \frac{2\pi}{K} \; , \quad j = 1 \ldots K \quad . \tag{5.11}$$

Since the maximum value of $k_x + k_y$ is $2N$, one needs to have at least $K \geq 2N + 1$. The quadrature rule can thus be built as the following product:

$$\tilde{p}_{ij}^{\mu} = \begin{pmatrix} \sqrt{\tilde{p}_i + \tilde{m}^2} \\ \tilde{p}_i \cos\theta_j \\ \tilde{p}_i \sin\theta_j \end{pmatrix} \quad , \tag{5.12}$$

$$w_{ij} = w_i^{(\tilde{p})} w_j^{(\theta)} \quad , \qquad \begin{matrix} i = 1 \ldots N+1 \\ j = 1 \ldots K \end{matrix} \quad . \tag{5.13}$$

with total number of populations $N^{\text{pop}} = K(N + 1)$. In Fig.5.2 the stencils for a set of different mass values are depicted.

As these stencils require the perfect streaming condition to be relaxed, the usual stream & collide paradigm has to be modified in order to collect information from the nodes of the Cartesian grid. In two dimensions, a simple bilinear interpolation is adopted:

$$f_i(\boldsymbol{x} - \boldsymbol{v}^i \Delta t, t - \Delta t) = \frac{1}{\Delta x \Delta y} \Bigg\{$$

$$f_i(\boldsymbol{x} - \boldsymbol{r_x} - \boldsymbol{r_y}, t - \Delta t) \Big(\qquad \Delta t |v_x^i| \Big) \Big(\qquad \Delta t |v_y^i| \Big)$$

$$f_i(\boldsymbol{x} \qquad - \boldsymbol{r_y}, t - \Delta t) \Big(\Delta x - \Delta t |v_x^i| \Big) \Big(\qquad \Delta t |v_y^i| \Big)$$

$$f_i(\boldsymbol{x} - \boldsymbol{r_x} \qquad , t - \Delta t) \Big(\qquad \Delta t |v_x^i| \Big) \Big(\Delta y - \Delta t |v_y^i| \Big)$$

$$f_i(\boldsymbol{x} \qquad , t - \Delta t) \Big(\Delta x - \Delta t |v_x^i| \Big) \Big(\Delta y - \Delta t |v_y^i| \Big) \Bigg\} \tag{5.14}$$

with

$$\boldsymbol{r_x} = sgn(v_x^i) \Delta x \hat{\boldsymbol{x}} \tag{5.15}$$

$$\boldsymbol{r_y} = sgn(v_y^i) \Delta y \hat{\boldsymbol{y}} \tag{5.16}$$

5.1.2 (3+1) dimensions

The procedure in (3+1) dimensions starts from the same steps: by switching to spherical coordinates, and by employing the mass-shell condition, one writes

$$I^{\alpha_1 \dots \alpha_k} = I_{\tilde{p}}^{\alpha_1 \dots \alpha_k} \times I_{\Omega}^{\alpha_1 \dots \alpha_k} \,, \tag{5.17}$$

$$I_{\tilde{p}}^{\alpha_1 \dots \alpha_k} = \int_0^{+\infty} w(\tilde{p})(\tilde{p}^2 + \tilde{m}^2)^{\frac{k_0}{2}} \tilde{p}^{k_x + k_y + k_z} \mathrm{d}\tilde{p} \,, \tag{5.18}$$

$$I_{\Omega}^{\alpha_1 \dots \alpha_k} = \int_{\Omega} (\sin\theta \cos\varphi)^{k_x} (\sin\theta \cos\varphi)^{k_y} (\cos\theta)^{k_z} \mathrm{d}\Omega \,, \tag{5.19}$$

with

$$w(\tilde{p}) = \tilde{p}^2 \frac{\omega(\sqrt{\tilde{p}^2 + \tilde{m}^2})}{\sqrt{\tilde{p}^2 + \tilde{m}^2}} \,, \tag{5.20}$$

Going through the same change of variable of before, one finds

$$I_{\tilde{p}}^{\alpha_1\ldots\alpha_k} = \int_0^{+\infty} W(y)Q(y)\mathrm{dy} \,, \qquad (5.21)$$

with the new weight function

$$W(y) = \omega(y+\tilde{m})\sqrt{(y^2+2\tilde{m}y)} = \frac{\sqrt{y^2+2\tilde{m}y}}{2\pi}e^{-y+\tilde{m}} \,, \qquad (5.22)$$

This time though the shape of the new weight function does not suggest any kind of named quadrature to be adopted, therefore one has to create from scratch the rule. Such task is possible once a set of polynomials $P_k(y)$ orthogonal with respect to the weight function $W(y)$ is found. It turns out that such polynomials are the $0\ldots0$ entries of the set of polynomials $\boldsymbol{J}^{(k)}$, that depend only on $\tilde{p}_0$ meaning that

$$P_0(y) = J^{(0)} = 1 \qquad (5.23)$$
$$P_1(y) = J_0^{(1)}(y+m)$$
$$P_2(y) = J_{00}^{(2)}(y+m)$$
$$\ldots$$
$$P_{N+1}(y) = J_{0\ldots0}^{(N+1)}(y+m)$$

From which one builds the following quadrature rule:

$$\text{abscissae } y_i \qquad \text{roots of } P_{N+1}(y) = 0 \qquad (5.24)$$

$$\text{weights } w_i^{(\tilde{p})} \qquad \int_0^\infty W(y)\frac{P_{N+1}(y)}{(y-y_i)\,P'_{N+1}(y_i)}\mathrm{dy} \qquad (5.25)$$

The angular quadrature is more complicated. The integrand in $I_\Omega^{\alpha_1\ldots\alpha_k}$ can be recast into a sum of spherical harmonics $Y_\ell^m(\theta,\varphi)$ of maximum degree $\ell_{max} = k_x + k_y + k_z$, therefore one has now to exactly discretize the integral

$$\int_\Omega Y_\ell^m(\theta,\varphi)\mathrm{d}\Omega = \sum_{k=1}^{N_{pop}} \mathrm{w_k} Y_\ell^{\mathrm{m}}(\theta_{\mathrm{k}},\varphi_{\mathrm{k}}), \quad \forall \ell \leq \ell_{max} \leq 2\mathrm{N}\,. \qquad (5.26)$$

There is a number of different discretizations to be adopted in order to exactly integrate the spherical harmonics on the sphere. Here I describe three of them: the Gauss-Legendre rule, the Lebedev rule, and the spherical-design rule, all needing a quadrature order of degree $K \geq 2N$.

- In the Gauss-Legendre quadrature, the integration over the solid angle is split in the coordinates θ and φ, and while the integration over the φ variable is discretized using a simple mid-point rule, the integration over the θ variable gets discretized using a Gauss-Legendre quadrature. In this way one does not obtain minimal sets of abscissae, and moreover the nodes are not distributed uniformly on the surface of the sphere.

- The Lebedev quadrature relies instead on the rotational symmetries of the ochtaedral [113] and ichosaedral [114] group, that if imposed on the final stencil greatly reduce the number of non linear equations to be solved to determine nodes and weights. These stencils are a great improvement over Gauss-Legendre, but still show some overlaps.

- The spherical-design quadrature [115], that is the rule that has been used in this work, is instead built on the numerical solution of Eq. 5.26, once the weights are all taken to be equal. Here the set of stencils freely available in [116] has been used.

All in all, after the set $\{\theta_j, \varphi_j, w_j^{(\theta, \varphi)}\}$ has been selected, the stencil reads as

$$
\tilde{p}_{ij}^{\mu} = \begin{pmatrix} \sqrt{\tilde{p}_i + m^2} \\ \tilde{p}_i \sin \theta_j \cos \varphi_j \\ \tilde{p}_i \sin \theta_j \sin \varphi_j \\ \tilde{p}_i \cos \theta_j \end{pmatrix} \quad , \tag{5.27}
$$

$$
w_{ij} = w_i^{(\tilde{p})} w_j^{(\theta, \varphi)} \quad , \quad \begin{matrix} i = 1 \dots N + 1 \\ j = 1 \dots N_K \end{matrix} \quad . \tag{5.28}
$$

where N_K is the number of nodes in the angular quadrature, dependent on the order K chosen. The total number of points in the quadrature is $N^{\text{pop}} = N_K(N+1)$.

Also in this case the scheme has to be modified at the streaming step with the addition of a trilinear interpolation scheme:

$$f_i(\boldsymbol{x} - \boldsymbol{v}^i \Delta t, t - \Delta t) = \frac{1}{\Delta x \Delta y \Delta z} \Bigg\{ \tag{5.29}$$

$$f_i(\boldsymbol{x} - \boldsymbol{r_x} - \boldsymbol{r_y} - \boldsymbol{r_z}, t - \Delta t) \Big(\quad \Delta t |v_x^i| \Big) \Big(\quad \Delta t |v_y^i| \Big) \Big(\quad \Delta t |v_z^i| \Big)$$

$$f_i(\boldsymbol{x} \quad\quad - \boldsymbol{r_y} - \boldsymbol{r_z}, t - \Delta t) \Big(\Delta x - \Delta t |v_x^i| \Big) \Big(\quad \Delta t |v_y^i| \Big) \Big(\quad \Delta t |v_z^i| \Big)$$

$$f_i(\boldsymbol{x} - \boldsymbol{r_x} \quad\quad - \boldsymbol{r_z}, t - \Delta t) \Big(\quad \Delta t |v_x^i| \Big) \Big(\Delta y - \Delta t |v_y^i| \Big) \Big(\quad \Delta t |v_z^i| \Big)$$

$$f_i(\boldsymbol{x} - \boldsymbol{r_x} - \boldsymbol{r_y} \quad\quad , t - \Delta t) \Big(\quad \Delta t |v_x^i| \Big) \Big(\quad \Delta t |v_y^i| \Big) \Big(\Delta z - \Delta t |v_z^i| \Big)$$

$$f_i(\boldsymbol{x} - \boldsymbol{r_x} \quad\quad\quad , t - \Delta t) \Big(\quad \Delta t |v_x^i| \Big) \Big(\Delta y - \Delta t |v_y^i| \Big) \Big(\Delta z - \Delta t |v_z^i| \Big)$$

$$f_i(\boldsymbol{x} \quad\quad - \boldsymbol{r_y} \quad\quad , t - \Delta t) \Big(\Delta x - \Delta t |v_x^i| \Big) \Big(\quad \Delta t |v_y^i| \Big) \Big(\Delta z - \Delta t |v_z^i| \Big)$$

$$f_i(\boldsymbol{x} \quad\quad\quad - \boldsymbol{r_z}, t - \Delta t) \Big(\Delta x - \Delta t |v_x^i| \Big) \Big(\Delta y - \Delta t |v_y^i| \Big) \Big(\quad \Delta t |v_z^i| \Big)$$

$$f_i(\boldsymbol{x} \quad\quad\quad\quad , t - \Delta t) \Big(\Delta x - \Delta t |v_x^i| \Big) \Big(\Delta y - \Delta t |v_y^i| \Big) \Big(\Delta z - \Delta t |v_z^i| \Big) \Bigg\}$$

with

$$\boldsymbol{r_x} = sgn(v_x^i) \Delta x \hat{\boldsymbol{x}} \tag{5.30}$$

$$\boldsymbol{r_y} = sgn(v_y^i) \Delta y \hat{\boldsymbol{y}} \tag{5.31}$$

$$\boldsymbol{r_z} = sgn(v_z^i) \Delta z \hat{\boldsymbol{z}} \tag{5.32}$$

5.1.3 Decoupling of radial and angular quadratures

With the procedures explained in the previous sections, one opens the possibility of increasing the isotropy of the stencil by individually tuning the parameters N, K or N_K. This is crucial when moving to regimes characterized by high values of the Knudsen number, since as the gas becomes more and more rarefied, even small errors in the velocities space become increasingly detrimental to the numerical solution.

Increases in the isotropy can also be achieved by decoupling the radial and the angular abscissae; this means that when building the product rule, one can rotate with different angles the sub-stencils related to different energy shells.

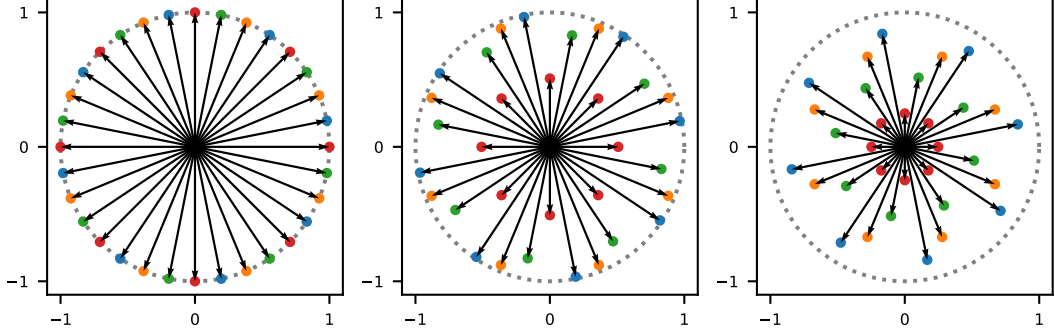In $(2+1)$ dimensions this can be easily done by replacing the angular nodes in Eq. 5.10 with the following:

Figure 5.3: *Some example for the off-lattice stencils depicted in the previous pages. The quadrature values chosen are $N = 3$, $K = 8$, and $\tilde{m} = 0.0$, 2.0 and 10.0 (from left to right).*

$$\theta_{ij} = \left(j + \frac{i}{N+1} \right) \frac{2\pi}{K} \quad . \tag{5.33}$$

In Fig. 5.3 various stencils decoupled with this technique are shown.

The task is less trivial in $(3+1)$ dimensions, as in this case there is a lot more freedom when specifying the rotations between the sub-stencils.

In fact, having considered an initial velocity set derived using the spherical design quadrature rule described above, then one has, for a radial quadrature of order N, $N + 1$ overlapped shells of vectors G_i belonging to the set $G = \bigcup_i G_i$.

Then one has to determine the set of angles $\{\alpha_i, \gamma_i\}$, with $i = 1 \ldots N + 1$, that defines the rotation matrix

$$R(\alpha_i, \gamma_i) = \begin{pmatrix} \cos\alpha_i \cos\gamma_i & -\sin\alpha_i & \cos\alpha_i \sin\gamma_i \\ \sin\alpha_i \cos\gamma_i & \cos\alpha_i & \sin\alpha_i \sin\gamma_i \\ -\sin\gamma_i & 0 & \cos\gamma_i \end{pmatrix} \quad . \tag{5.34}$$

The new stencil G' is then defined as $G' = \bigcup_i R(\alpha_i, \gamma_i) \cdot G_i$.

The approach used to devise this operation can be defined in multiple ways. In this thesis work the following two methods are considered:

- The different rotation matrices $R(\alpha_i, \gamma_i)$ can be determined by numerically solving the Thomson problem [117], that consists in the determination of the position on the surface of a sphere of electrons such that the electrostatic energy is minimized. By taking the nodes of the quadrature as the positions of the electrons, the matrices $R(\alpha_i, \gamma_i)$ are iteratively determined by joining

the substencils G_i and solving the associated Thomson problem. As an example, we propose the iterative process that solves the case $N = 3$:

1. the substencils G_1, G_2, G_3 are identified using the spherical design quadrature rule, and are represented by the overlapping set of points on the sphere.

2. G_2 is rotated using a rotation $R(\alpha_2, \gamma_2)$, with (α_2, γ_2) parameters to be determined.

3. The set $G' = G_1 \cup G_2$ is considered, and the parameters (α_2, γ_2) are determined by numerically solving the Thomson problem (*i.e.* by minimizing the electrostatic energy between the electrons sitting on the sphere at the positions given by G').

4. G_3 is rotated using a rotation $R(\alpha_3, \gamma_3)$, with (α_3, γ_3) parameters to be determined.

5. The set $G'' = G' \cup G_3$ is considered, and the parameters (α_3, γ_3) are determined by numerically solving the Thomson problem (*i.e.* by minimizing the electrostatic energy between the electrons sitting on the sphere at the positions given by G''). G'' is the desired stencil.

- The second method is available only for shell numbers that are equal to vertexes of platonic solids ($N + 1 = (4, 6, 8, 12, 20)$), consists in finding the rotation matrices that map one vertex of the solid (one node of a single substencil) to its other vertexes (the corresponding node on the other substencils).

  For the case $N = 3$ one has for example 4 energy shells, and therefore one considers a tetrahedron (that has four vertexes, dubbed as A,B,C,D). One identifies then the rotation matrices R as the ones that move one vertex to the other:

  1. $R(\alpha_2, \gamma_2)$ = moves A into B
  2. $R(\alpha_3, \gamma_3)$ = moves A into C
  3. $R(\alpha_4, \gamma_4)$ = moves A into D

  When $N + 1 \neq (4, 6, 8, 12, 20)$, this method can be used by identifying as fictitious Platonic solids with $N + 1$ vertexes the results of a $N + 1$ Thomson problem. For example, if $N = 5$ one can numerically solve the Thomson problem with five electrons, and then identify the rotations that move from one vertex to all the other four.

5.2   Mono-dimensional Shock wave

In this section the previously shown quadrature rules are tested on the same mono-dimensional shock wave problem of Ch. 4. I confront the RLBM results with an analytic solution of the ultra-relativistic free-streaming Boltzmann Equation, derived in Sec. 5.2.1, and resort to LBE-TP for the other viscous regimes.

5.2.1   Analytic Solution (free streaming ultra-relativistic fluid)

The calculations here presented are a generalization of the procedures highlighted in [13] for the three-dimensional case to a generic number of spatial dimensions.

In order to find the analytic solution of the Mono-dimensional shock wave for an ultra-relativistic fluid in the free-streaming regime ($Kn \to \infty$), one starts by considering the relativistic Boltzmann equation Eq. 2.25 in the absence of external forces, and in the free-streaming regime:

$$p^\alpha \partial_\alpha f = 0 \ . \tag{5.35}$$

In the mono-dimensional shock wave, the dynamics develop along one single direction, say along the $\hat{\boldsymbol{x}}$ axis, therefore the distribution function $f(\boldsymbol{x}, \boldsymbol{v}, t)$ will be symmetric over the other degrees of freedoms, *i.e.* depend only on the x coordinates.

$$p^0 \partial_t f + p_x \partial_x f = \partial_t f + v_x \partial_x f = 0 \ . \tag{5.36}$$

Additionally, the initial conditions already presented in Eq. 4.22, *i.e.*

$$(P, \ n, \ T, \ \beta) = \begin{cases} (P_L, \ n_L, \ T_L, \ 0) & x \le 0 \\ (P_R, \ n_R, \ T_R, \ 0) & x > 0 \end{cases} \ , \tag{5.37}$$

translate on the distribution function f as

$$f_0 = \theta(-x) f_L^{eq} + \theta(x) f_R^{eq} \ , \tag{5.38}$$

where f_L^{eq} and f_R^{eq} are the equilibrium distribution Eq. 1.35 respectively

computed on the left and right unperturbed zones. By recurring to the method
of characteristics one finds that the solution of Eq. 5.36 is

$$f(x, p, t) = \theta(-x + v_x t) f_L^{eq} + \theta(x - v_x t) f_R^{eq} ,$$ (5.39)

and by introducing $w = x/t$ one can write Eq. 5.39 by distinguishing two
different regions, respectively the unperturbed one for $|w| > 1$, and the perturbed
one at $|w| \leq 1$:

$$f(w, p, v_x) = \begin{cases} f_L^{\text{eq}} & w < -1 \\ f_L^{\text{eq}} + \theta(w - v_x)(f_R^{\text{eq}} - f_L^{\text{eq}}) & |w| \leq 1 \\ f_R^{\text{eq}} & w > 1 \end{cases}$$ (5.40)

In order to define the macroscopic profiles in the perturbed region, one needs
to calculate integrals in the form of Eq. 1.17 and Eq. 1.18. The full form for N^α
and $T^{\alpha\beta}$ in the perturbed region is given by:

$$N^\alpha = N_L^\alpha + i^\alpha(w)\frac{n_R - n_L}{\Omega}$$ (5.41)

$$T^{\alpha\beta} = T_L^{\alpha\beta} + i^{\alpha\beta}(w)\frac{\epsilon_R - \epsilon_L}{\Omega}$$ (5.42)

with $\Omega = \frac{d\pi^{d/2}}{\Gamma\left(1 + \frac{d}{2}\right)}$ and

$$i^0(w) = \int_\Omega \theta(w_x - v_x) d\Omega$$

$$i^x(w) = \int_\Omega v_x \theta(w_x - v_x) d\Omega$$

$$i^{xx}(w) = \int_\Omega v_x^2 \theta(w_x - v_x) d\Omega$$

$$i^{0x}(w) = i^x(w)$$

$$i^{00}(w) = i^0(w)$$

$$i^{ii}(w) = \frac{1}{d-1}(i^{00}(w) - i^{xx}(w)) \qquad \forall i \neq x$$ (5.43)

and all other integrals equal to zero. The quantities $i^0(w)$, $i^0(w)$, and $i^{xx}(w)$

assume different values depending on the dimension d. Here I give results for the most common cases $d = 2$ and $d = 3$

$$i^{(0)}(w) = \begin{cases} 2\pi - 2\arccos(w) & d = 2 \\ 2\pi(w + 1) & d = 3 \end{cases} \tag{5.44}$$

$$i^{(x)}(w) = \begin{cases} -2\sqrt{1 - w^2} & d = 2 \\ \pi(w^2 - 1) & d = 3 \end{cases} \tag{5.45}$$

$$i^{(xx)}(w) = \begin{cases} \pi - w\sqrt{1 - w^2} - \arccos(w) & d = 2 \\ \frac{2\pi}{3}(1 + w^3) & d = 3 \end{cases} \tag{5.46}$$

From the above relations, the thermodynamic quantities can be obtained:
$(2 + 1)$ dimensions:

$$N^0 = n_{\mathrm{L}} + \left(1 - \frac{\arccos(w)}{\pi}\right)(n_{\mathrm{R}} - n_{\mathrm{L}}) \tag{5.47}$$

$$N^x = -\frac{\sqrt{1 - w^2}}{\pi}(n_{\mathrm{R}} - n_{\mathrm{L}}) \tag{5.48}$$

$$T^{00} = \epsilon_{\mathrm{L}} + \left(1 - \frac{\arccos(w)}{\pi}\right)(\epsilon_{\mathrm{R}} - \epsilon_{\mathrm{L}}) \tag{5.49}$$

$$T^{0x} = -\frac{\sqrt{1 - w^2}}{\pi}(\epsilon_{\mathrm{R}} - \epsilon_{\mathrm{L}}) \tag{5.50}$$

$$T^{xx} = P_{\mathrm{L}} + \left(1 - \frac{w\sqrt{1 - w^2}}{\pi} - \frac{\arccos(w)}{\pi}\right)(P_{\mathrm{R}} - P_{\mathrm{L}}) \tag{5.51}$$

$$T^{yy} = P_{\mathrm{L}} + \left(-1 + \frac{w\sqrt{1 - w^2}}{\pi} - \frac{\arccos(w)}{\pi}\right)(P_{\mathrm{R}} - P_{\mathrm{L}}) \tag{5.52}$$

$(3 + 1)$ dimensions:

$$N^0 = n_L + (1 + w)(n_R - n_L) \tag{5.53}$$

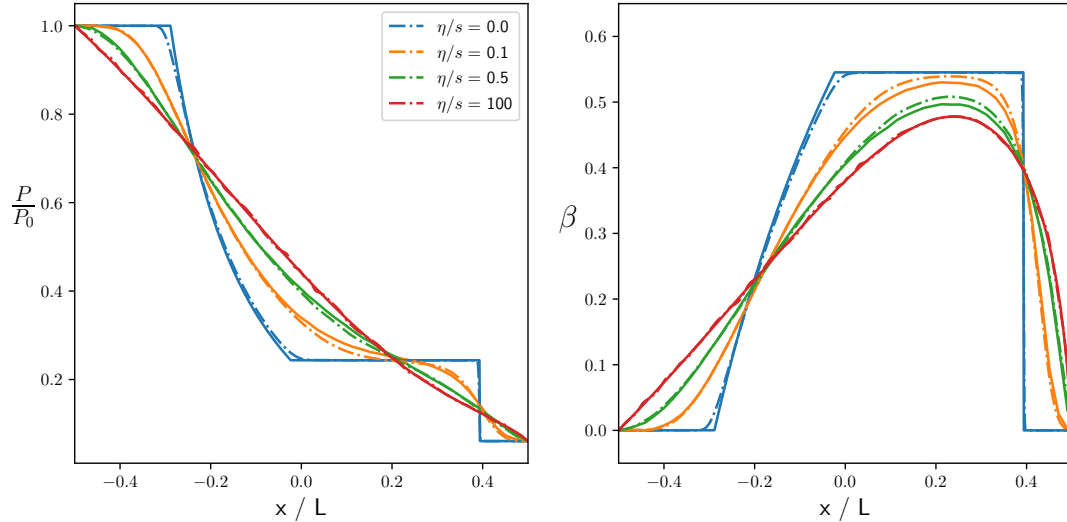$$N^x = \frac{1}{4}(w^2 - 1)(n_R - n_L) \tag{5.54}$$

Figure 5.4: *Comparison of RLBM results against RLB-TP and analytics across all ranges of the Knudsen number, from ideal to the free-streaming regime. The value of the rest mass is set to zero. With the new off-lattice stencils ($N = 3$ and $N_K = 120$), RLBM is more than capable to recover the correct solution even in the free-streaming regime. The comparison with the old on-lattice stencils can be performed by confronting this figure with Fig. 4.5.*

$$T^{00} = \epsilon_L + \frac{1}{2}(1 + w)(\epsilon_R - \epsilon_L) \tag{5.55}$$

$$T^{0x} = \frac{1}{4}(w^2 - 1)(\epsilon_R - \epsilon_L) \tag{5.56}$$

$$T^{xx} = P_L + \frac{1}{2}(1 + w^3)(P_R - P_L) \tag{5.57}$$

$$T^{yy} = T^{zz} = P_L + \frac{1}{4}(-w^3 + w + 2)(P_R - P_L) \tag{5.58}$$

5.2.2 RLBM results

In this section I show the improved results that can be obtained on the mono-dimensional shock wave benchmark by employing the new quadrature rules Fig. 5.4. The comparison of RLBM results is provided in the free streaming regime against the ultra-relativistic ideal solution given in 5.2.1, and for intermediate viscous regimes RLB-TP is used. The comparison is provided in (3+1) dimensions.

The off-lattice stencil adopted for the comparison has $N^{\text{pop}} = 480$ populations, and settings for the quadratures are as follows:
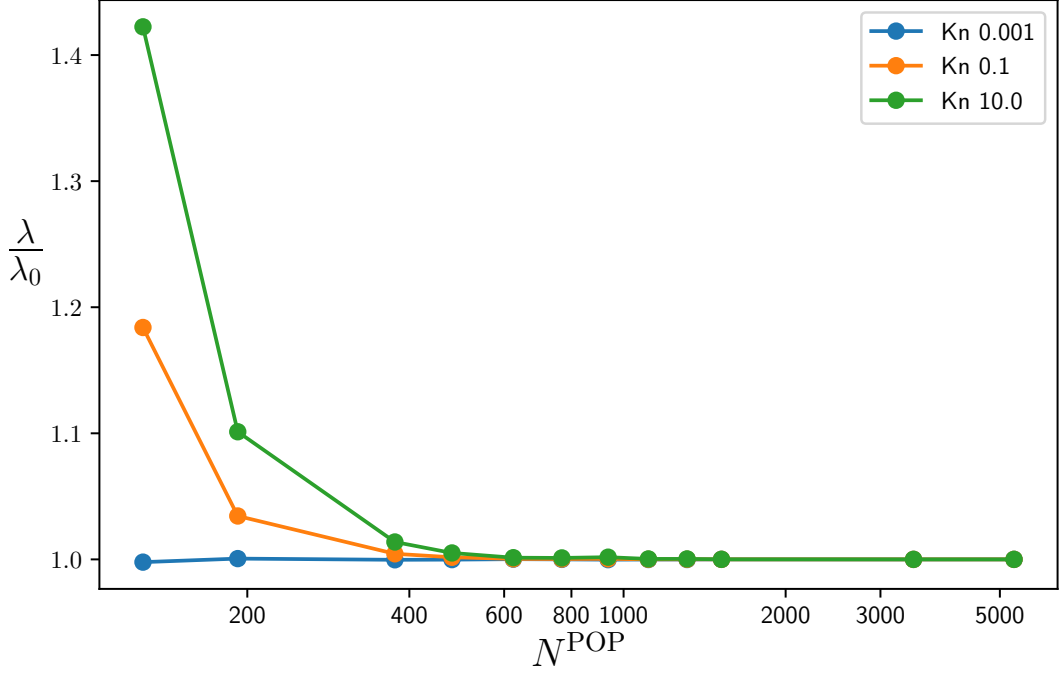
Figure 5.5: *As Kn increases, the number of populations needed to correctly reproduce the dynamics increases as well. Here I show the dependency on the relative error of the solution λ with respect to N^{pop}, showing that after a certain threshold increases in the resolution of the momentum space are not needed anymore. All λ values are rescaled with respect to their asymptotic value λ_0 computed at $N^{pop} \sim 5000$ for better readability.*

$$N = 3 \, , \qquad\qquad (5.59)$$
$$K = 16 \, ,$$
$$N_K = 120 \, ,$$

Obviously this level of discretization is not needed for all viscous regimes, as in the hydrodynamic regime velocity stencils with less nodes are still sufficient to reproduce the dynamics. In order to give a feeling of the scaling of the number of populations with respect to the regime of the flow, in Fig. 5.5 I have reproduced the relative error on the pressure field, computed as

$$\lambda = \frac{||P - P_{\text{ref}}||_2}{||P_{\text{ref}}||_2} \ . \tag{5.60}$$

where P_{ref} is a RLBM numerical solution performed with improved spatial and momentum resolution with respect to the previously examined case. It is possible to appreciate that as one transitions from the hydrodynamic picture to the free streaming regime, the error goes scales with N^{pop}, until a saturation point is reached around the value $N^{\text{pop}} \sim 480$.

6

Relativistic Lattice Boltzmann Method for Radiative Transfer

In numerical astrophysics, the study of radiation transfer is of determinant importance when dealing with phenomena such as neutron stars mergers [21], core-collapses supernovae [22, 23] and accretion disks in black holes, where numerical simulations are vital to compare with experimental findings [118].

Through the years, the need for the study of these phenomena has given rise to a number of numerical schemes [119–128], which can be grouped in two main different categories:

- Hydrodynamic schemes, that solve the "macroscopic" equations for the first order moments of the radiative distribution function, typically the radiation energy density and momentum density. These methods generally resolve only the low order moments, and some of them rely on some assumption to close the set of equations (*leakage scheme* [129, 130], *flux limited diffusion* [131, 132] and *M1 scheme* [133–135]).

- Monte-Carlo methods that solve directly the Boltzmann equation for photons, which suffer from the typical numerical noise [136, 137].

All in all, the fact that radiation (in the form of photons or neutrinos) interacts with a (dynamic) background fluid via emission, absorption and scattering, makes it so that its evolution can be considered at the kinetic level by a Boltzmann equation with said phenomena in place of particle collisions [138].

This opens the possibility for a third approach different than the ones given above: a Relativistic Lattice Boltzmann Method that relies on the scale of the Boltzmann equation and provides solutions for the moments of the radiative distribution function.

The techniques shown in Ch. 5 come into play as radiation has to be correctly handled by the scheme both in the optically thin regimes (when radiation weakly interacts with matter) and in optically thick regimes (strong radiation-matter interaction). Therefore the developments of Ch. 5 are central in this kind of scheme, because in optically thin regimes the radiation is freely streaming, and in order to reproduce the correct behavior in this regime it is important to have isotropically defined stencils.

In this thesis work only a general review on the method is provided, with highlights on where the developments of Ch. 5 have been used: in Sec. *6.1* a brief theoretical background is provided on Radiation Transfer, then the Lattice Boltzmann Method is described in Sec. *6.2*. Then an application of the method to the study of relativistic jets is discussed.

A more in depth description can be found in [30], where numerous test cases that highlight the features of the method are considered.

6.1 Theoretical Background

The governing equation in radiation dynamics is given by the Radiative Transfer Equation (RTE) that can be described through the Boltzmann equation for a gas of massless particles *i.e.* photons or neutrinos moving at the speed of light [138].

Fields are expressed in terms of the distribution function $f_\nu(\boldsymbol{x}, \hat{\boldsymbol{n}}, t)$ that accounts for the energy density carried by photons-neutrinos through an infinitesimal surface located at $\boldsymbol{x}$, in the solid angle $d\Omega$ in direction $\hat{\boldsymbol{n}}$, and in the frequency band $d\nu$; the RTE expresses its evolution in time:

$$\frac{1}{c}\frac{\partial f_\nu}{\partial t} + \hat{\boldsymbol{n}} \cdot \nabla f_\nu = -\kappa_{a,\nu} f_\nu + \eta_\nu + C_s \ , \tag{6.1}$$

where $\kappa_{a,\nu}$ is the coefficient of the absorption interaction with the background fluid, η_ν is the coefficient regulating emission, and C_s represents the scattering term.

After approximating C_s with the first two terms of a Legendre expansion (E_ν and $\boldsymbol{F}_\nu$ are respectively the energy and momentum density and $\kappa_{0/1,\nu}$ are the frequency dependent opacities)

$$C_s \sim -\kappa_{0,\nu} f_\nu + \kappa_{0,\nu} E_\nu + 3\kappa_{1,\nu} \hat{\boldsymbol{n}} \cdot \boldsymbol{F}_\nu \; . \tag{6.2}$$

Integration of Eq. 6.1 into the frequency domain (gray approximation) yields

$$\frac{1}{c}\frac{\partial I}{\partial t} + \hat{\boldsymbol{n}} \cdot \nabla I = -\kappa_a I + \eta + \kappa_0 (E - I) + 3\kappa_1 \hat{\boldsymbol{n}} \cdot \boldsymbol{F} \; . \tag{6.3}$$

This is an evolution equation for the *specific intensity*

$$I(\boldsymbol{x}, \hat{\boldsymbol{n}}, t) = \int_0^{+\infty} \nu^3 f_\nu \mathrm{d}\nu \; , \tag{6.4}$$

and its moments

$$\text{Radiation Energy density} \quad E(\boldsymbol{x}, t) = \int_\Omega I(\boldsymbol{x}, \hat{\boldsymbol{n}}, t) \mathrm{d}\Omega \; , \tag{6.5}$$

$$\text{Radiation Momentum density} \quad \boldsymbol{F}(\boldsymbol{x}, t) = \int_\Omega I(\boldsymbol{x}, \hat{\boldsymbol{n}}, t) \hat{\boldsymbol{n}} \mathrm{d}\Omega \tag{6.6}$$

(all quantities appearing in Eq. 6.3 are frequency integrated). Note that Eq. 6.3 is functionally similar to the dynamic equations which are at the base of lattice kinetic solvers such as RLBM, and therefore the same methodologies used for LBM can be applied to this case study.

6.2 RLBM method

In order to recover a form of Eq. 6.3 more prone to an LB treatment, contributions from absorption and emission are grouped into a source term S, while the scattering terms not containing the specific intensity make up a fictitious equilibrium intensity I^{eq}:

$$S = -\kappa_a I + \eta \; , \tag{6.7}$$

$$I^{\mathrm{eq}} = E + \left(3\frac{\kappa_1}{\kappa_0} \right) \hat{\boldsymbol{n}} \cdot \boldsymbol{F} \; , \tag{6.8}$$

one has then

$$\frac{1}{c}\frac{\partial I}{\partial t} + \hat{\boldsymbol{n}} \cdot \nabla I = -\kappa_0 (I - I^{\mathrm{eq}}) + S \; , \tag{6.9}$$

with κ_0 having the role of a relaxation time in a BGK-like approximation. At this point, a discretization of the "velocity space" (the space where vectors $\hat{\boldsymbol{n}}$, the direction of propagation of the radiation, live) has to be performed.

In order to do so, one has just to realize that the specific intensity I is a function only depending on angles, and that the directions $\hat{\boldsymbol{n}}$ are nothing more than points on the surface of a sphere (in 3d) or a circle (in 2d). Therefore the angular quadratures described in Sec. *5.1.1* and Sec. *5.1.2* can be employed.

One has then a set of N^{pop} weights and abscissae $(w_j, \hat{\boldsymbol{n}}_j)$ to define the discretized version of specific intensity

$$I_j(\boldsymbol{x}, t) = I(\boldsymbol{x}, \hat{\boldsymbol{n}}_j, t) \; , \tag{6.10}$$

to discretize the equilibrium and source term

$$S_j = -\kappa_a I_j + \eta \; , \tag{6.11}$$

$$I_j^{\mathrm{eq}} = E + \left(3\frac{\kappa_1}{\kappa_0} \right) \hat{\boldsymbol{n}}_j \cdot \boldsymbol{F} \; , \tag{6.12}$$

and to compute as discretized sums the energy and momentum density

$$E \sim \sum_j^{N^{\mathrm{pop}}} I_j \; , \tag{6.13}$$

$$\boldsymbol{F} \sim \sum_j^{N^{\mathrm{pop}}} I_j \hat{\boldsymbol{n}}_j \; . \tag{6.14}$$

At this point the usual space and time discretization can be used, and an evolution equation for I_j is obtained:

$$I_j(\boldsymbol{x} + c\hat{\boldsymbol{n}}_j \Delta t, t + \Delta t) = I_j(\boldsymbol{x}, t) - c\kappa_0 \Delta t \left[I_j(\boldsymbol{x}, t) - I_j^{\text{eq}}(\boldsymbol{x}, t) \right] + c\Delta t S_j(\boldsymbol{x}, t) .$$
(6.15)

This equation can be evolved in the algorithm using the usual Stream & Collide paradigm, together with the interpolation schemes shown in Sec. *5.1.1* and Sec. *5.1.2* in order to recover information from the Cartesian nodes of the grid.

6.3   *Simulation of a relativistic jet*

While many test cases are examined in [30], I want to discuss here a test application based on a realistic astrophysical scenario, namely a simulation of a relativistic jet as it propagates through the interstellar medium.

Such simulations are important in the study of active galactic nuclei, where they are produced during the formation of supermassive black holes [31,32], and in magnetized neutron star mergers, where they appear together with gamma-ray bursts [33].

The simulation is set up by coupling the LB scheme previously exposed, that solves for radiation, to the Relativistic Magneto-Hydrodynamic (RMHD) Solver BHAC [139], that solves for the fluid.

The coupling is performed in the following way:

1. At every iteration, fluid's rest mass density ρ, temperature T and three velocity $\mathbf{u}$ are used to compute absorption $\tilde{\kappa}_a$ and emission $\tilde{\eta}$ coefficients, and the scattering opacities $\tilde{\kappa}_0$ and $\tilde{\kappa}_1$ in the fluid rest frame (where they are more easily defined [140]), according to the following:

   - $\tilde{\kappa}_a = \rho^2 T^{-3.5}$, according to Rosseland mean opacity for thermal bremsstrahlung [141]

   - $\tilde{\eta} = \sigma_{\text{SB}} / \pi \tilde{\kappa}_a T^4$, which is emissivity obtained from Kirchhoff's law upon assuming black-body radiation. $\sigma_{\text{SB}} = 0.1$ is chosen to ensure a moderate amount of radiation production.
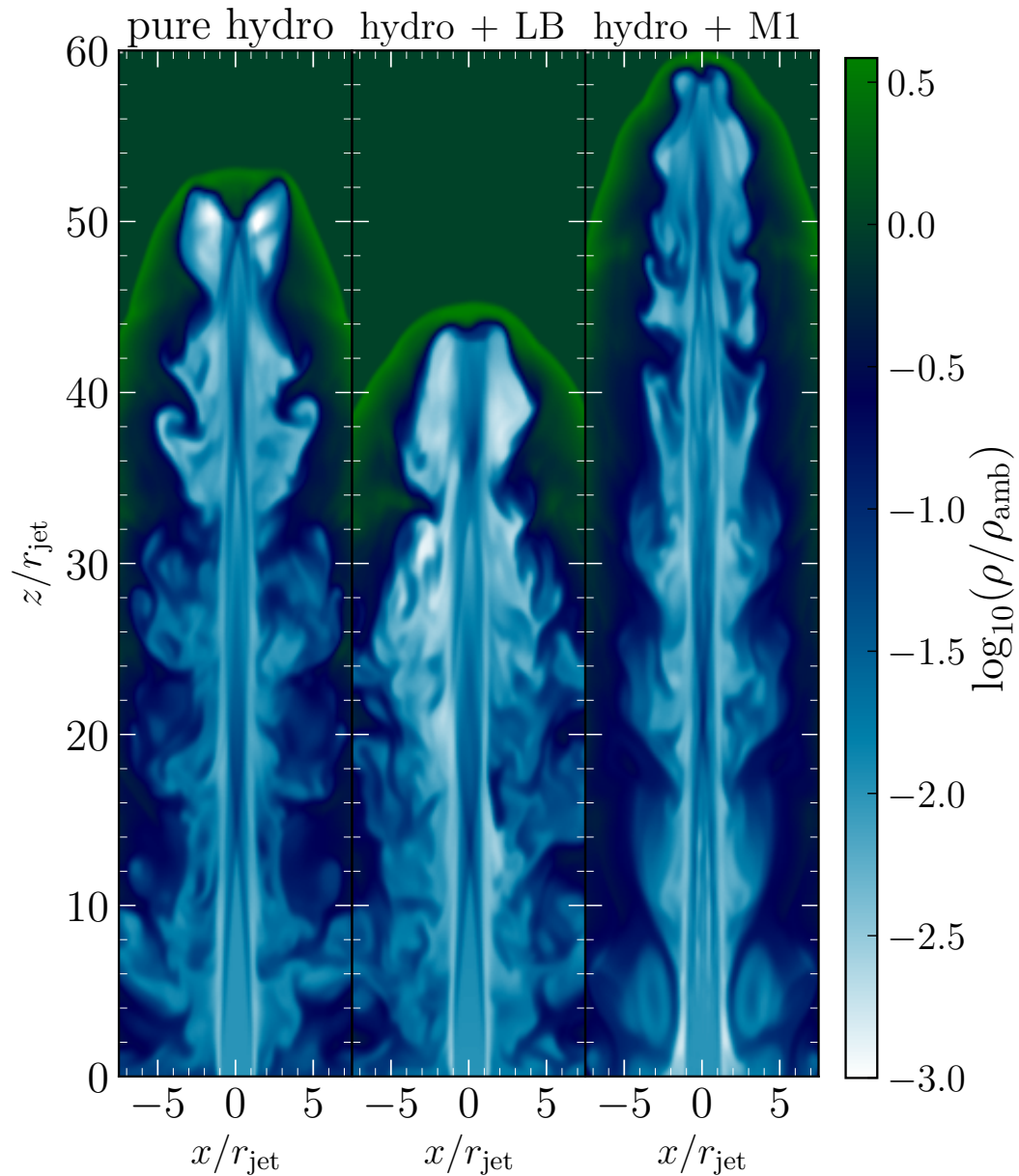
Figure 6.1: *Cut through the (x, z) plane for the relativistic jet after $t = 125cr_{\mathrm{jet}}$. Shown is the mass density for the pure-hydro (left) and the coupled hydro-radiation using LB (center) and M1 (right), over a reference value out of the jet ρ_{amb}*

- $\tilde{\kappa}_0 = 10^{-3}\rho$ and $\tilde{\kappa}_1 = 0$, to simulate Thomson's scattering which is proportional to the number of scatters in the medium (hence to the density of fluid particles) and has no preferred direction.

2. The coefficients are computed in the Eulerian lab frame where the Lattice Boltzmann method performs the evolution of radiation. The transformation between the two frames is the following [30, 140]:

$$\kappa_a = \frac{1 - \boldsymbol{u} \cdot \hat{\boldsymbol{n}}}{\sqrt{1 - (\boldsymbol{u}/c)^2}}\tilde{\kappa_a}, \quad \eta = \frac{(1 - (\boldsymbol{u}/c)^2)^{3/2}}{(1 - \boldsymbol{u} \cdot \hat{\boldsymbol{n}})^3}\tilde{\eta}$$

$$\kappa_0 = \frac{1 - \boldsymbol{u} \cdot \hat{\boldsymbol{n}}}{\sqrt{1 - (\boldsymbol{u}/c)^2}}\tilde{\kappa_0}, \quad \kappa_1 = \frac{(1 - (\boldsymbol{u}/c)^2)^{3/2}}{(1 - \boldsymbol{u} \cdot \hat{\boldsymbol{n}})^3}\tilde{\kappa_1}$$

3. The LB code is now ready to perform a simulation step for every one of the N_{pop} radiation specific intensities, I_i. After collision and streaming are performed, the macroscopic radiation quantities (the energy E and momentum densities $\boldsymbol{F}$) are computed according to 6.13.

4. From theese quantities one computes all the radiative contributions to the energy-momentum tensor that are needed to evolve the fluid in BHAC. BHAC then performs a simulation step, and the process starts again from the first item in this list.

The simulation is arranged following [142]: the jet is injected from the bottom border of the computational domain imposing a costant inlet velocity in a circular nozzle, and propagates along the z-axis coordinate. The grid has size $160 \times 160 \times 640$ grid cells, where the jet is injected at $z = 0$ through a nozzle with radius $r_{\mathrm{jet}} = 10$ lattice nodes.

The results of the simulation are compared with a similar one that instead of the presented LB method uses the M1 code already cited to solve for the radiative part [143]. In Fig. 6.1 the fluid mass density is shown for three different iterations: on the left, a pure Relativistic Magneto Hydrodynamic simulation, without radiation dynamics, is presented. The other two snapshots show instead the iterations with radiation solved through LB (center) and the M1 scheme (right).

It is possible to appreciate that both the simulations look structurally similar to the pure RMHD one, with the exception of the LB one being considerably shorter than the M1. More than being an indication of the fact that the LB

scheme might have some problems, this is due to known errors [143–145] in the M1 scheme, that assumes a closure relation for the evolution equation for the first moment of the specific intensity, and therefore can only track the average direction of radiation momentum.

In particular, they clearly show the ability of the LB method to handle correctly scenarios with physical conditions that are very close to those encountered in relativistic astrophysical phenomena.

Conclusions

In this thesis a new framework for the simulation of relativistic fluids has been presented. The method first proposed in [20] has been expanded and generalized into a mature tool, able to simulate relativistic flows in all relativistic regimes, from ultra-relativistic to non-relativistic, and across the whole Knudsen spectrum.

The algorithmic description has been purposely kept indipendent of the spatial dimension, so that the scheme can be adapted to bi-dimensional or three-dimensional flows with no particular efforts.

I summarize here the main results presented in this work:

- Extension and generalization of the (3+1)-dimensional Relativistic Lattice Boltzmann Method proposed in [20] to a generic number of spatial dimensions. The scheme is tailored for the simulation of flows at every relativistic regime via the definition of a particle mass-tailored discrete velocity set. The scheme preserves the main advantages of classical Lattice schemes, such as Perfect Streaming, or ease of implementation and parallelization.

- Derivation of a link between the kinetic and the hydrodynamic layer, through an analytic expression for all transport coefficients in all spatial dimensions, using both Chapman-Enskog expansion and Grad's method of moments. Then, RLBM has been used to numerically discern between the two methods. The obtained results suggest that the Chapman-Enskog expansion is the correct way of linking the mesoscopic description to hydrodynamics.

  Furthermore, these expansion methods provide a calibration procedure for the Transport Coefficients in the RLBM framework. These are crucial in order to reproduce the desired dissipative properties in the simulated flows.

- Verification of the method in the form of two different test-cases, the Bjorken flow and the mono-dimensional Relativistic Sod Shock Tube. The numerical data have been confronted to analytical results when possible, or to other numerical solvers otherwise.

  Such results have been given for different values of rest masses, spatial dimensions, and viscous regimes.

- Extension of RLBM to cure the incorrect behavior of the scheme when simulating flows in weakly interacting regimes. The extension is based on the implementation of a new discretization procedure for the pseudo-particles' momenta, that results in more isotropic and better distributed velocity vectors.

- Development and test of a new Lattice Kinetic Scheme for the simulation of radiative transfer in astrophysical contexts. The scheme draws from the improvements considered for RLBM and is actually able to reproduce the dynamic of radiation in both the optically thick or thin regime.

This RLBM method can potentially been used now for the simulation of a wealth of different relativistic fluid problems across scales from astrophysics and cosmology to high-energy physics and material science.

There is space for futhure methodological improvements, e.g. on boundary conditions, which have specific importance in the framework of bi-dimensional flows (the electron flows studied in laboratories are always physically bounded). Also, when approaching high macroscopic velocities, LB methods suffer from compressibility effects, so algorithmic developments are expected in this regard.

Furthermore, a careful analysis of the computational costs associated with the new off-lattice discretization is needed, in order to be able to employ this technique on large scale problems. In this context, it would be also interesting to consider equilibrium distributions other than the Jüttner one, in order to implement quantum effects into the flow dynamics.

As to applications, the customization of the RLBM scheme to the detailed study of quark-gluon plasmas dynamics in current and future high-energy experiments, appears a very appealing topic for future research.

With regards to the LB for Radiative Transfer, a natural prospect is the extension of the method to General Relativistic framework. This process is complicated by the curved nature of the Space Time, and by the fact that in this case the collision step would happen in a different frame with respect to the

streaming step (the radiation-matter interaction parameters are defined in the co-moving lab frame, while streaming has to be operated on Eulerian lab frames).

A

Projector $\Delta^{\alpha\beta}$

In this appendix the properties of the Minkowski-orthogonal projector to the fluid velocity U^α, defined as

$$\Delta^{\alpha\beta} = \eta^{\alpha\beta} - \frac{1}{c^2}U^\alpha U^\beta \ , \tag{A.1}$$

$$\Delta_{\alpha\beta} = \eta_{\alpha\beta} - \frac{1}{c^2}U_\alpha U_\beta \ . \tag{A.2}$$

are summarized. In particular, once this tensor introduced, the decompositions of vectors and tensors in U^α parallel-orthogonal components are straightforward.

By construction, the product of $\Delta_{\alpha\beta}$ with the velocity U^β is therefore equal to zero, and its trace equals the number of spatial dimensions:

$$\Delta^{\alpha\beta}U_\beta = \Delta_{\alpha\beta}U^\beta = 0 \ , \tag{A.3}$$

$$\Delta^\alpha_\alpha = d \ . \tag{A.4}$$

It is useful to introduce the short-hand notation

$$\Delta^\alpha_\gamma = \Delta^{\alpha\beta}\Delta_{\beta\gamma} = \delta^\alpha_\gamma - \frac{1}{c^2}U^\alpha U_\gamma \ , \tag{A.5}$$

together with the following easily verifiable properties:

$$\Delta^\gamma_\alpha \Delta_{\gamma\beta} = \Delta_{\alpha\beta} \ , \tag{A.6}$$

$$\Delta^\alpha_\gamma \Delta^\gamma_\beta = \Delta^\alpha_\beta \ . \tag{A.7}$$

These projectors can be applied to express a generic vector A^α as the sum of

two terms, respectively orthogonal and parallel to U^α:

$$A^\alpha = a_1 \frac{U^\alpha}{c} + a_2^\alpha \quad \begin{cases} a_1 & = \frac{1}{c} U^\beta A_\beta \\ a_2^\alpha & = \Delta^{\alpha\beta} A_\beta \end{cases} \tag{A.8}$$

Likewise, any generic tensor $T^{\alpha\beta}$ can be decomposed into different parts by combining it with all possible combinations of U^α and the projector $\Delta^{\alpha\beta}$:

$$T^{\alpha\beta} = t_1 \frac{U^\alpha U^\beta}{c^2} + t_2^\alpha \frac{U^\beta}{c} + t_3^\beta \frac{U^\alpha}{c} + t_4^{\alpha\beta} \tag{A.9}$$

$$t_1 = \frac{1}{c} U^\mu U^\nu T_{\mu\nu} \tag{A.10}$$

$$t_2^\alpha = \Delta_\mu^\alpha U_\nu T^{\mu\nu} \tag{A.11}$$

$$t_3^\beta = \Delta_\nu^\beta U_\mu T^{\mu\nu} \tag{A.12}$$

$$t_4^{\alpha\beta} = \Delta_\mu^\alpha \Delta_\mu^\beta T^{\mu\nu} \tag{A.13}$$

Additionally, one can decompose any U^α-orthogonal tensor (like $t_4^{\alpha\beta}$) into symmetric, antyisimmetric, and simmetric traceless:

$$V^{\alpha\beta} = V^{[\alpha\beta]} + V^{(\alpha\beta)} = V^{[\alpha\beta]} + V^{<\alpha\beta>} + Tr \tag{A.14}$$

where:

$$V^{(\alpha\beta)} = \frac{1}{2} \left(\Delta^{\alpha\gamma} \Delta^{\beta\delta} + \Delta^{\beta\gamma} \Delta^{\alpha\delta} \right) V_{\gamma\delta} \ , \tag{A.15}$$

$$V^{[\alpha\beta]} = \frac{1}{2} \left(\Delta^{\alpha\gamma} \Delta^{\beta\delta} - \Delta^{\beta\gamma} \Delta^{\alpha\delta} \right) V_{\gamma\delta} \ , \tag{A.16}$$

$$V^{<\alpha\beta>} = V^{(\alpha\beta)} - Tr \quad \text{with} \quad Tr = \frac{1}{d} \Delta^{\alpha\beta} \Delta_{\gamma\delta} V^{\gamma\delta} \ , \tag{A.17}$$

The following properties naturally follow from the definitions above:

$$U_\alpha V^{(\alpha\beta)} = 0 \qquad \eta_{\alpha\beta} V^{(\alpha\beta)} = \Delta_{\mu\nu} V^{\mu\nu} \qquad \Delta_{\alpha\beta} V^{(\alpha\beta)} = \Delta_{\mu\nu} V^{\mu\nu} \ , \tag{A.18}$$

$$U_\alpha V^{[\alpha\beta]} = 0 \qquad \eta_{\alpha\beta} V^{[\alpha\beta]} = 0 \qquad \Delta_{\alpha\beta} V^{[\alpha\beta]} = 0 \ , \tag{A.19}$$

$$U_\alpha V^{<\alpha\beta>} = 0 \qquad \eta_{\alpha\beta} V^{<\alpha\beta>} = 0 \qquad \Delta_{\alpha\beta} V^{<\alpha\beta>} = 0 \ . \tag{A.20}$$

It is at times useful to introduce a decomposition also for the gradient ∂_α, by

defining the convective time derivative D and its orthogonal component ∇^α:

$$\partial^\alpha = \Delta^{\alpha\beta}\partial_\beta + \frac{1}{c^2}U^\alpha U^\beta \partial_\beta = \nabla^\alpha + \frac{1}{c^2}U^\alpha D , \tag{A.21}$$

with the following useful properties:

$$U_\alpha \nabla^\alpha = 0 , \tag{A.22}$$

$$\nabla^\alpha U_\alpha = \partial^\alpha U_\alpha . \tag{A.23}$$

B

Integrals of the Maxwell-Jüttner distribution

Computed here are some integrals often used in the development of the numerical methods presented in this work and in the definition of the transport coefficients.

2.1 Integrals $Z^{\alpha_1...\alpha_n}$

Define

$$Z = \int e^{-\frac{p_\mu U^\mu}{k_B T}} \frac{\mathrm{d}\boldsymbol{p}}{p_0} \tag{B.1}$$

$$Z^{\alpha_1...\alpha_n} = \int e^{-\frac{p_\mu U^\mu}{k_B T}} p^{\alpha_1}\dots p^{\alpha_n} \frac{\mathrm{d}\boldsymbol{p}}{p_0} . \tag{B.2}$$

All integrals $Z^{\alpha_1...\alpha_n}$ can be obtained by subsequent derivations of Z with respect to macroscopic velocity

$$Z^{\alpha_1...\alpha_n} = (-k_B T)^n \frac{\partial Z}{\partial U_{\alpha_1}\dots\partial U_{\alpha_n}} , \tag{B.3}$$

therefore one will only have to correctly compute this quantity in order to obtain all the required structures. Z is a Lorentz-invariant quantity which depends only on $U_\alpha U^\alpha = c^2$, and therefore can be computed in every frame of reference. Choosing fluid's rest frame is of course the best option. Further, since one needs to compute the derivatives in Eq. B.3, one first derive Z for an

unconstrained $U_\alpha U^\alpha$ and, after performing the derivatives, evaluate the result for $U_\alpha U^\alpha = c^2$:

$$Z = \int e^{-\frac{p_0 \sqrt{U^\mu U_\mu}}{k_{\rm B} T}} \frac{d^d p}{p_0} = \int e^{-\frac{\sqrt{U^\mu U_\mu}}{k_{\rm B} T} \sqrt{m^2 c^2 + p^2}} \frac{d^d p}{\sqrt{m^2 c^2 + p^2}} \ , \qquad \text{(B.4)}$$

and then switch to spherical coordinates:

$$d^d p = p^{d-1} dp \ d\Omega \qquad \text{with} \qquad \int d\Omega = \frac{d\pi^{\frac{d}{2}}}{\Gamma\left(1 + \frac{d}{2}\right)} \ ,$$

giving

$$Z = \frac{d\pi^{\frac{d}{2}}}{\Gamma\left(1 + \frac{d}{2}\right)} \int_0^{+\infty} e^{-\frac{\sqrt{U^\mu U_\mu}}{k_{\rm B} T} \sqrt{m^2 c^2 + p^2}} \frac{p^{d-1} dp}{\sqrt{m^2 c^2 + p^2}} \ .$$

Changing integration variable $p = mc\sqrt{t^2 - 1}$ and defining $\zeta = mc^2/k_{\rm B} T$, one has

$$Z = \frac{d\pi^{\frac{d}{2}}}{\Gamma\left(1 + \frac{d}{2}\right)} (mc)^{d-1} \int_1^{+\infty} (t^2 - 1)^{\frac{d-1}{2} - \frac{1}{2}} e^{-\frac{\zeta t}{c} \sqrt{U^\mu U_\mu}} dt \ .$$

Recalling one useful definition of the modified Bessel function of the second kind [71]:

$$K_\nu(z) = \frac{\pi^{1/2}(z/2)^\nu}{\Gamma\left(\nu + 1/2\right)} \int_1^{+\infty} e^{-zt}(t^2 - 1)^{\nu - 1/2} dt \ ,$$

one finally obtains:

$$Z = \pi^{\frac{d-1}{2}} 2^{\frac{d+1}{2}} \zeta^{\frac{d-1}{2}} \left(\frac{k_{\rm B} T}{\sqrt{c}}\right)^{d-1} \frac{K_{\frac{d-1}{2}}\left(\frac{\zeta}{c} \sqrt{U^\mu U_\mu}\right)}{(U^\mu U_\mu)^{\frac{d-1}{4}}} \ .$$

All integrals can now be obtained using Eq. B.3; tedious but straightforward manipulations yield a nice and regular structure. Indeed, defining the coefficients A_n:

$$A_n = 2^{\frac{d+1}{2}} \pi^{\frac{d-1}{2}} \zeta^{n+\frac{d-1}{2}} K_{n+\frac{d-1}{2}}(\zeta) \,, \tag{B.5}$$

one obtains:

$$Z = \left(\frac{k_B T}{c}\right)^{d-1} A_0$$

$$Z^\alpha = \left(\frac{k_B T}{c}\right)^{d} A_1 \frac{U^\alpha}{c}$$

$$Z^{\alpha\beta} = \left(\frac{k_B T}{c}\right)^{d+1} \left[A_2 \frac{U^\alpha U^\beta}{c^2} - A_1 \eta^{\alpha\beta}\right]$$

$$Z^{\alpha\beta\gamma} = \left(\frac{k_B T}{c}\right)^{d+2} \left[A_3 \frac{U^\alpha U^\beta U^\gamma}{c^3} - A_2 \left(\frac{\eta^{\alpha\beta} U^\gamma + \eta^{\gamma\beta} U^\alpha + \eta^{\alpha\gamma} U^\beta}{c}\right)\right]$$

$$\ldots$$

$$Z^{\alpha_1 \alpha_2 \ldots \alpha_n} = \left(\frac{k_B T}{c}\right)^{d+n-1} \sum_{k=0}^{\lfloor \frac{n}{2} \rfloor} (-1)^k A_{n-k} \frac{\prec U_{n-2k} \eta_k \succ}{c^{n-2k}}$$

Where

$$\prec U_{n-2k} \eta_k \succ = \underbrace{\eta^{\alpha_1 \alpha_2} \ldots \eta^{\alpha_{2k-1} \alpha_{2k}}}_{k \text{ terms}} \underbrace{U^{\alpha_{2k+1}} U^{\alpha_{2k+2}} \ldots U^{\alpha_n}}_{(n\text{-}2k) \text{ terms}} + \text{permutations of indexes.}$$

In the above, terms like $\eta^{\alpha\beta}$, $\eta^{\beta\alpha}$ and $U^\alpha U^\beta$, $U^\beta U^\alpha$ are counted only once. To give an example, for $n = 4$, $k = 1$, we have:

$$\prec U_2 \eta_1 \succ = \eta^{\alpha_1 \alpha_2} U^{\alpha_3} U^{\alpha_4} + \eta^{\alpha_1 \alpha_3} U^{\alpha_2} U^{\alpha_4} + \eta^{\alpha_2 \alpha_3} U^{\alpha_1} U^{\alpha_4}$$
$$+ \eta^{\alpha_1 \alpha_4} U^{\alpha_3} U^{\alpha_2} + \eta^{\alpha_4 \alpha_3} U^{\alpha_2} U^{\alpha_1} + \eta^{\alpha_2 \alpha_4} U^{\alpha_1} U^{\alpha_3} \,.$$

2.2   Integrals $K^{\alpha_1 \ldots \alpha_n}$

In the derivation of the Chapman-Enskog expansion, the integrals defined as

$$K = B(n,T) \int \frac{e^{-\frac{p_\mu U^\mu}{k_B T}}}{p_\mu U^\mu} \frac{\mathrm{d}\boldsymbol{p}}{p_0} \ , \tag{B.6}$$

$$K^{\alpha_1 \dots \alpha_n} = B(n,T) \int e^{-\frac{p_\mu U^\mu}{k_B T}} \frac{p^{\alpha_1} \dots p^{\alpha_n}}{p_\mu U^\mu} \frac{\mathrm{d}\boldsymbol{p}}{p_0} \ , \tag{B.7}$$

have been encountered. The tensorial structure of said integrals has to be similar to the one of the $Z^{\alpha_1 \dots \alpha_n}$, therefore one can write down:

$$K^\alpha = \frac{n}{k_B T} a_{11} \frac{U^\alpha}{c}$$

$$K^{\alpha\beta} = \frac{n}{c} \left[a_{21} \frac{U^\alpha U^\beta}{c^2} - a_{22} \eta^{\alpha\beta} \right]$$

$$K^{\alpha\beta\gamma} = \frac{n k_B T}{c^2} \left[a_{31} \frac{U^\alpha U^\beta U^\gamma}{c^3} - a_{32} \left(\frac{\eta^{\alpha\beta} U^\gamma + \eta^{\gamma\beta} U^\alpha + \eta^{\alpha\gamma} U^\beta}{c} \right) \right]$$

$$\dots$$

$$K^{\alpha_1 \dots \alpha_n} = \frac{n(k_B T)^{n-2}}{c^{n-1}} \sum_{k=0}^{\lfloor \frac{n}{2} \rfloor} (-1)^k a_{n(k+1)} \frac{\prec U_{n-2k} \eta_k \succ}{c^{n-2k}}$$

where the $1 + \lfloor \frac{n}{2} \rfloor$ coefficients $a_{n(k+1)}$ are to be determined. From the definition, one gets the following property

$$U_{\alpha_n} K^{\alpha_1 \dots \alpha_n} = B(n,T) Z^{\alpha_1 \dots \alpha_{n-1}} \ . \tag{B.8}$$

that gives $\lfloor \frac{n+1}{2} \rfloor$ equations for the unknown coefficients, obtained by matching equal tensorial terms in both $U_{\alpha_n} K^{\alpha_1 \dots \alpha_n}$ and $B(n,T) Z^{\alpha_1 \dots \alpha_{n-1}}$:

$$\frac{a_{n(k+1)}}{(n-2k-1)!} - \frac{a_{n(k+2)}}{(n-2k-2)!} \theta \left(\lfloor \frac{n}{2} \rfloor - 1 - k \right) = \frac{2^k k!}{(n-1)!} \frac{A_{n-1-k}}{A_1} \ , \tag{B.9}$$

which is valid for $0 \leq k \leq \lfloor \frac{n-1}{2} \rfloor$. The remaining condition to close the system of equations (needed only for even values of n) is given by observing that

$$K^{\alpha_1 \dots \alpha_n}{}_{\alpha_n} = (mc)^2 K^{\alpha_1 \dots \alpha_{n-2}} \ . \tag{B.10}$$

By applying multiple times this property, one gets for the case n even:

$$K^{\alpha_1 \ldots \alpha_{n/2}}{}_{\alpha_1 \ldots \alpha_{n/2}} = (mc)^n K \ , \tag{B.11}$$

that means that one has to be able to correctly compute the integral K to be able to define all the $K^{\alpha_1 \ldots \alpha_n}$ with n even. To do so, one can proceed in the same way employed for the integral Z

$$K = B(n,T) \int \frac{e^{-\frac{p_\mu U^\mu}{k_{\mathrm{B}}T}}}{p_\mu U^\mu} \frac{\mathrm{d}\boldsymbol{p}}{p_0} = \frac{n\zeta^d d\pi^{\frac{d}{2}}}{cA_1(mc)^2\Gamma(1 + \frac{d}{2})} \int_1^\infty \frac{e^{-\zeta t}(t^2 - 1)^{\frac{d-1}{2}}}{t}\mathrm{dt} \tag{B.12}$$

and go on with the calculation by splitting the cases d even and odd, using Newton's binomial rule, and re-expressing everything in term of a single formula

$$\chi = \frac{m^2 c^3}{n}K = \frac{\zeta^d d\pi^{\frac{d}{2}}}{A_1\Gamma(1 + \frac{d}{2})} \sum_{k=0}^{\lfloor\frac{d-1}{2}\rfloor} \binom{\lfloor\frac{d-1}{2}\rfloor}{k}(-1)^{\lfloor\frac{d-1}{2}\rfloor-k}\mathrm{I}_{1-2\mathrm{k}}(\zeta) \ , \tag{B.13}$$

with

$$\mathrm{I}_{1-2\mathrm{k}}(\zeta) = \begin{cases} E_{1-2k}(\zeta) = \int_1^\infty \frac{e^{-\zeta t}}{t^{1-2k}}\mathrm{dt} & \text{d even} \\ Ki_{1-2k}(\zeta) = \int_1^\infty \frac{e^{-\zeta t}}{t^{1-2k}\sqrt{t^2-1}}\mathrm{dt} & \text{d odd} \end{cases} \ , \tag{B.14}$$

which are respectively the *Generalized Exponential Integral Function* and the *Bickley-Naylor Function*.

We give here the first coefficients, already factorized in terms of the previously defined value $G_d = \frac{A_2}{A_1}$

$$a_{11} = \frac{1}{\zeta^2}(G_d - (d+1))$$

$$a_{21} = 1 + \frac{1}{d}(\chi - 1) \qquad\qquad a_{22} = \frac{1}{d}(\chi - 1)$$

$$a_{31} = G_d + 2 \qquad\qquad a_{32} = 1$$

$$a_{41} = \frac{3dG_d - 3\zeta^2\chi + 3\zeta^2}{d(d+2)} + (d+6)G_d + \zeta^2 \quad a_{42} = \frac{d(3d+7)G_d - \zeta^2\chi + \zeta^2}{d(d+2)} \quad a_{43} = \frac{G_d - \zeta^2\chi + \zeta^2}{d(d+2)} \ .$$

Note here that in order to get the transport coefficients in the Chapman-

Enskog procedure only a_{22} and a_{43} are needed.

Bibliography

[1] L. Rezzolla and O. Zanotti. *Relativistic Hydrodynamics.* 2013.

[2] P. Romatschke and U. Romatschke. *Relativistic Fluid Dynamics In and Out of Equilibrium: And Applications to Relativistic Nuclear Collisions.* Cambridge Monographs on Mathematical Physics. Cambridge University Press, 2019.

[3] Lucas A. and Fong K.C. Hydrodynamics of electrons in graphene. *Journal of Physics: Condensed Matter*, 30(5):053001, jan 2018.

[4] W. Israel. Nonstationary irreversible thermodynamics: A Causal relativistic theory. *Annals Phys.*, 100:310–331, 1976.

[5] W. Israel and J. M. Stewart. Transient relativistic thermodynamics and kinetic theory. *Annals Phys.*, 118:341–372, 1979.

[6] G. Denicol, H. Niemi, E. Molnar, and D. Rischke. Derivation of transient relativistic fluid dynamics from the boltzmann equation. *Physical Review D*, 85, 02 2012.

[7] M. Mendoza, B. M. Boghosian, H. J. Herrmann, and S. Succi. Fast lattice boltzmann solver for relativistic hydrodynamics. *Phys. Rev. Lett.*, 105:014502, Jun 2010.

[8] M. Mendoza, B.M. Boghosian, H.J. Herrmann, and S. Succi. Derivation of the lattice boltzmann model for relativistic hydrodynamics. *Phys. Rev. D*, 82:105008, Nov 2010.

[9] P. Romatschke, M. Mendoza, and S. Succi. Fully relativistic lattice boltzmann algorithm. *Phys. Rev. C*, 84:034903, Sep 2011.

[10] Q. Li, K. H. Luo, and X. J. Li. Lattice boltzmann method for relativistic hydrodynamics: Issues on conservation law of particle number and discontinuities. *Phys. Rev. D*, 86:085044, Oct 2012.

[11] F. Mohseni, M. Mendoza, S. Succi, and H. J. Herrmann. Lattice boltzmann model for ultrarelativistic flows. *Phys. Rev. D*, 87:083003, Apr 2013.

[12] M. Mendoza, I. Karlin, S. Succi, and H. J. Herrmann. Relativistic lattice boltzmann model with improved dissipation. *Phys. Rev. D*, 87:065027, Mar 2013.

[13] V.E. Ambruş and R. Blaga. High-order quadrature-based lattice boltzmann models for the flow of ultrarelativistic rarefied gases. *Phys. Rev. C*, 98:035201, Sep 2018.

[14] R. Blaga and V.E. Ambruş. Quadrature-based lattice boltzmann model for relativistic flows. *AIP Conference Proceedings*, 1796(1):020010, 2017.

[15] D. Oettinger, M. Mendoza, and H. J. Herrmann. Gaussian quadrature and lattice discretization of the fermi-dirac distribution for graphene. *Phys. Rev. E*, 88:013302, Jul 2013.

[16] O. Furtmaier, M. Mendoza, I. Karlin, S. Succi, and H. J. Herrmann. Rayleigh-bénard instability in graphene. *Phys. Rev. B*, 91:085401, Feb 2015.

[17] R.C.V. Coelho, M. Mendoza, M.M. Doria, and H.J. Herrmann. Kelvin-helmholtz instability of the dirac fluid of charge carriers on graphene. *Phys. Rev. B*, 96:184307, Nov 2017.

[18] R.C.V. Coelho, M. Mendoza, M.M. Doria, and H.J. Herrmann. Fully dissipative relativistic lattice boltzmann method in two dimensions. *Computers & Fluids*, 172:318–331, 2018.

[19] A. Gabbana, M. Mendoza, S. Succi, and R. Tripiccione. Numerical evidence of electron hydrodynamic whirlpools in graphene samples. *Computers and Fluids*, 172:644–650, 2018.

[20] A. Gabbana, M. Mendoza, S. Succi, and R. Tripiccione. Towards a unified lattice kinetic scheme for relativistic hydrodynamics. *Phys. Rev. E*, 95:053304, May 2017.

[21] Luca Baiotti and Luciano Rezzolla. Binary neutron star mergers: a review of einstein's richest laboratory. *Reports on Progress in Physics*, 80(9):096901, jul 2017.

[22] S.A. Colgate and R.H. White. The Hydrodynamic Behavior of Supernovae Explosions. *Astrophysics Journal*, 143:626, mar 1966.

[23] H.-Th. Janka, K. Langanke, A. Marek, G. Martínez-Pinedo, and B. Müller. Theory of core-collapse supernovae. *Physics Reports*, 442(1):38–74, 2007. The Hans Bethe Centennial Volume 1906-2006.

[24] C. Cercignani and G. M. Kremer. *The Relativistic Boltzmann Equation: Theory and Applications*. Birkhäuser Basel, 2002.

[25] A. Gabbana, D. Simeoni, S. Succi, and R. Tripiccione. Relativistic lattice boltzmann methods: Theory and applications. *Physics Reports*, 863:1–63, 2020.

[26] A. Gabbana, D. Simeoni, S. Succi, and R. Tripiccione. Relativistic dissipation obeys chapman-enskog asymptotics: Analytical and numerical evidence as a basis for accurate kinetic simulations. *Phys. Rev. E*, 99:052126, May 2019.

[27] A. Gabbana, D. Simeoni, S. Succi, and R. Tripiccione. Probing bulk viscosity in relativistic flows. *Philosophical Transactions of the Royal Society A: Mathematical, Physical and Engineering Sciences*, 378(2175):20190409, 2020.

[28] A. Gabbana, S. Plumari, G. Galesi, V. Greco, D. Simeoni, S. Succi, and R. Tripiccione. Dissipative hydrodynamics of relativistic shock waves in a quark gluon plasma: Comparing and benchmarking alternate numerical methods. *Phys. Rev. C*, 101:064904, Jun 2020.

[29] L. Bazzanini, A. Gabbana, D. Simeoni, S. Succi, and R. Tripiccione. A lattice boltzmann method for relativistic rarefied flows in (2+1) dimensions. *Journal of Computational Science*, 51:101320, 2021.

[30] L R Weih, A Gabbana, D Simeoni, L Rezzolla, S Succi, and R Tripiccione. Beyond moments: relativistic lattice Boltzmann methods for radiative transport in computational astrophysics. *Monthly Notices of the Royal Astronomical Society*, 498(3):3374–3394, 08 2020.

[31] Manel Perucho. Dissipative processes and their role in the evolution of radio galaxies. *Galaxies*, 7(3), 2019.

[32] Oliver Porth, Koushik Chatterjee, and Event Horizon Telescope Collaboration. The Event Horizon General Relativistic Magnetohydrodynamic Code Comparison Project. *Astrophys. J. Supp.*, 243(2):26, aug 2019.

[33] L. Rezzolla, B. Giacomazzo, L. Baiotti, J. Granot, C. Kouveliotou, and M. A. Aloy. The Missing Link: Merging Neutron Stars Naturally Produce Jet-like Structures and Can Power Short Gamma-ray Bursts. *Astrophys. J. Letters*, 732:L6, may 2011.

[34] P.L. Bhatnagar, E.P. Gross, and M. Krook. A model for collision processes in gases. i. small amplitude processes in charged and neutral one-component systems. *Phys. Rev.*, 94:511–525, May 1954.

[35] C. Cercignani. *The Boltzmann Equation and Its Applications*. Springer New York, 1988.

[36] C.M. Marle. Modèle cinetique pour l'etablissement des lois de la conduction de la chaleur et de la viscosite en théorie de la relativite. *C. R. Acad. Sci., Paris*, 260:6539–6541, 1965.

[37] C.M. Marle. Sur l'établissement des équations de l'hydrodynamique des fluides relativistes dissipatifs. i. -l'équation de boltzmann relativiste. *Annales de l'I.H.P. Physique théorique*, 10(1):67–126, 1969.

[38] C.M. Marle. Sur l'établissement des équations de l'hydrodynamique des fluides relativistes dissipatifs. ii. - méthodes de résolution approchée de l'équation de boltzmann relativiste. *Annales de l'I.H.P. Physique théorique*, 10(2):127–194, 1969.

[39] J.L. Anderson and H.R. Witting. A relativistic relaxation-time model for the boltzmann equation. *Physica*, 74(3):466 – 488, 1974.

[40] R.H. Boyer. Some Uses of Hyperbolic Velocity Space. *American Journal of Physics*, 33(11):910–916, nov 1965.

[41] N.A. Chernikov. The relativistic collision integral. *Soviet Phys. (Doklady)*, 2, 5 1957.

[42] C. Cercignani and G. M. Kremer. Trend to equilibrium of a degenerate relativistic gas. *Journal of Statistical Physics*, 98(1/2):441–456, 2000.

[43] European Mathematical Society. Uniform boundedness. In *Encyclopedia of Mathematics*. EMS Press, feb 2011.

[44] European Mathematical Society. Equicontinuity. In *Encyclopedia of Mathematics*. EMS Press, feb 2011.

[45] F. Jüttner. Das maxwellsche gesetz der geschwindigkeitsverteilung in der relativtheorie. *Annalen der Physik*, 339(5):856–882, 1911.

[46] S.R. de Groot, W.A. van Leeuwen, and Ch.G. van Weert. *Relativistic kinetic theory : Principles and applications*. Amsterdam, North-Holland Pub. Co., 1980.

[47] C. Eckart. The thermodynamics of irreversible processes. iii. relativistic theory of the simple fluid. *Phys. Rev.*, 58:919–924, Nov 1940.

[48] L.D. Landau and E.M. Lifshitz. *Fluid Mechanics*. Elsevier Science, 1987.

[49] W. Israel and J.M. Stewart. Thermodynamics of nonstationary and transient effects in a relativistic gas. *Physics Letters A*, 58(4):213–215, 1976.

[50] I. Müller. Zum paradoxon der wärmeleitungstheorie. *Zeitschrift fur Physik*, 198(4):329–344, aug 1967.

[51] T. Koide, G. S. Denicol, Ph. Mota, and T. Kodama. Relativistic dissipative hydrodynamics: A minimal causal theory. *Phys. Rev. C*, 75:034909, 2007.

[52] C. Cattaneo. *Sulla Conduzione Del Calore*. Springer Berlin Heidelberg, Berlin, Heidelberg, 2011.

[53] W. Israel. Thermodynamics of relativistic systems. *Physica A: Statistical Mechanics and its Applications*, 106(1):204–214, 1981.

[54] I. Müller and T. Ruggeri. *Rational Extended Thermodynamics*. Springer New York, 1998.

[55] D. Jou, J. Casas-Vázquez, and G. Lebon. *Extended Irreversible Thermodynamics*. Springer Berlin Heidelberg, 2001.

[56] P. Huovinen and D. Molnar. Applicability of causal dissipative hydrodynamics to relativistic heavy ion collisions. *Phys. Rev. C*, 79:014906, Jan 2009.

[57] I. Bouras, E. Molnár, H. Niemi, Z. Xu, A. El, O. Fochler, C. Greiner, and D. H. Rischke. Investigation of shock waves in the relativistic riemann problem: A comparison of viscous fluid dynamics to kinetic theory. *Phys. Rev. C*, 82:024910, Aug 2010.

[58] P. Romatschke. Relativistic (lattice) boltzmann equation with nonideal equation of state. *Phys. Rev. D*, 85:065012, Mar 2012.

[59] S. Succi. *The Lattice Boltzmann Equation: For Complex States of Flowing Matter*. OUP Oxford, 2018.

[60] T. Krüger, H. Kusumaatmaja, A. Kuzmin, O. Shardt, G. Silva, and E.M. Viggen. *The Lattice Boltzmann Method - Principles and Practice*. 10 2016.

[61] J. Hardy, Y. Pomeau, and O. de Pazzis. Time evolution of a two-dimensional classical lattice system. *Phys. Rev. Lett.*, 31:276–279, Jul 1973.

[62] U. Frisch, B. Hasslacher, and Y. Pomeau. Lattice-gas automata for the navier-stokes equation. *Phys. Rev. Lett.*, 56:1505–1508, Apr 1986.

[63] G.R. McNamara and G. Zanetti. Use of the boltzmann equation to simulate lattice-gas automata. *Physical review letters*, 61:2332–2335, 12 1988.

[64] F.J. Higuera and J. Jiménez. Boltzmann approach to lattice gas simulations. *Europhysics Letters (EPL)*, 9(7):663–668, aug 1989.

[65] F.J. Higuera, S. Succi, and R. Benzi. Lattice gas dynamics with enhanced collisions. *Europhysics Letters (EPL)*, 9(4):345–349, jun 1989.

[66] H. Chen, S. Chen, and W.H. Matthaeus. Recovery of the navier-stokes equations using a lattice-gas boltzmann method. *Phys. Rev. A*, 45:R5339–R5342, Apr 1992.

[67] R. Benzi, S. Succi, and M. Vergassola. The lattice boltzmann equation: theory and applications. *Physics Reports*, 222(3):145–197, 1992.

[68] X. He and L.S. Luo. Theory of the lattice boltzmann method: From the boltzmann equation to the lattice boltzmann equation. *Physical Review E*, 56:6811–6817, 12 1997.

[69] X. Shan and X. He. Discretization of the velocity space in the solution of the boltzmann equation. *Phys. Rev. Lett.*, 80:65–68, Jan 1998.

[70] X. Shan. General solution of lattices for cartesian lattice bhatanagar-gross-krook models. *Phys. Rev. E*, 81:036702, Mar 2010.

[71] M. Abramowitz and I.A. Stegun. *Handbook of Mathematical Functions with Formulas, Graphs, and Mathematical Tables.* Dover, New York, ninth dover printing, tenth gpo printing edition, 1964.

[72] P.C. Philippi, L.A. Hegele, L.O.E. dos Santos, and R. Surmas. From the continuous to the lattice boltzmann equation: The discretization problem and thermal models. *Phys. Rev. E*, 73:056702, May 2006.

[73] X. Shan and H. Chen. Lattice boltzmann model for simulating flows with multiple phases and components. *Phys. Rev. E*, 47:1815–1819, Mar 1993.

[74] Z. Guo, C. Zheng, and B. Shi. Discrete lattice effects on the forcing term in the lattice boltzmann method. *Phys. Rev. E*, 65:046308, Apr 2002.

[75] X. He, X. Shan, and G.D. Doolen. Discrete boltzmann equation model for nonideal gases. *Phys. Rev. E*, 57:R13–R16, Jan 1998.

[76] A.L. Kupershtokh, D.A. Medvedev, and D.I. Karpov. On equations of state in a lattice boltzmann method. *Computers & Mathematics with Applications*, 58(5):965–974, 2009. Mesoscopic Methods in Engineering and Science.

[77] H. Huang, M. Krafczyk, and X. Lu. Forcing term in single-phase and shan-chen-type multiphase lattice boltzmann models. *Phys. Rev. E*, 84:046710, Oct 2011.

[78] S. Chapman and T. G. Cowling. *The Mathematical Theory of Non-uniform Gases (An Account of the Kinetic Theory of Viscosity, Thermal Conduction and Diffusion in Gases).* Cambridge University Press, paperback edition, 1 1991.

[79] H. Grad. On the kinetic theory of rarefied gases. *Communications on Pure and Applied Mathematics*, 2(4):331–407, 1949.

[80] H.C. Öttinger. Thermodynamically admissible 13 moment equations from the boltzmann equation. *Phys. Rev. Lett.*, 104:120601, Mar 2010.

[81] H. Struchtrup and M. Torrilhon. Regularization of grad's 13 moment equations: Derivation and linear analysis. *Physics of Fluids*, 15(9):2668–2680, 2003.

[82] R. M. Velasco, F. J. Uribe, and L.S. García-Colín. Inconsistencies in moment methods. *Phys. Rev. E*, 66:032103, Sep 2002.

[83] M. Torrilhon. Modeling nonequilibrium gas flow based on moment equations. *Annual Review of Fluid Mechanics*, 48(1):429–458, 2016.

[84] G. S. Denicol, T. Koide, and D. H. Rischke. Dissipative relativistic fluid dynamics: A new way to derive the equations of motion from kinetic theory. *Phys. Rev. Lett.*, 105:162501, Oct 2010.

[85] G.S. Denicol, H. Niemi, I. Bouras, E. Molnár, Z. Xu, D.H. Rischke, and C. Greiner. Solving the heat-flow problem with transient relativistic fluid dynamics. *Phys. Rev. D*, 89:074005, Mar 2014.

[86] A. Jaiswal, R.S. Bhalerao, and S. Pal. Complete relativistic second-order dissipative hydrodynamics from the entropy principle. *Phys. Rev. C*, 87:021901, Feb 2013.

[87] K. Tsumura and T. Kunihiro. Derivation of relativistic hydrodynamic equations consistent with relativistic boltzmann equation by renormalization-group method. *The European Physical Journal A*, 48(11), nov 2012.

[88] K. Tsumura, Y. Kikuchi, and T. Kunihiro. Relativistic causal hydrodynamics derived from boltzmann equation: A novel reduction theoretical approach. *Phys. Rev. D*, 92:085048, Oct 2015.

[89] Y. Kikuchi, K. Tsumura, and T. Kunihiro. Derivation of second-order relativistic hydrodynamics for reactive multicomponent systems. *Phys. Rev. C*, 92:064909, Dec 2015.

[90] Y. Kikuchi, K. Tsumura, and T. Kunihiro. Mesoscopic dynamics of fermionic cold atoms — quantitative analysis of transport coefficients and relaxation times. *Physics Letters A*, 380(24):2075–2080, 2016.

[91] A. Gabbana, M. Mendoza, S. Succi, and R. Tripiccione. Kinetic approach to relativistic dissipation. *Phys. Rev. E*, 96:023305, Aug 2017.

[92] F. Karsch, D. Kharzeev, and K. Tuchin. Universal properties of bulk viscosity near the qcd phase transition. *Physics Letters B*, 663(3):217–221, 2008.

[93] G.S. Denicol, T. Kodama, T. Koide, and Ph. Mota. Effect of bulk viscosity on elliptic flow near the qcd phase transition. *Phys. Rev. C*, 80:064901, Dec 2009.

[94] A. Dobado and J.M. Torres-Rincon. Bulk viscosity and the phase transition of the linear sigma model. *Phys. Rev. D*, 86:074021, Oct 2012.

[95] J. Noronha-Hostler, G.S. Denicol, J. Noronha, R.P.G. Andrade, and F. Grassi. Bulk viscosity effects in event-by-event relativistic hydrodynamics. *Phys. Rev. C*, 88:044916, Oct 2013.

[96] G.P. Kadam and H. Mishra. Bulk and shear viscosities of hot and dense hadron gas. *Nuclear Physics A*, 934:133–147, 2015.

[97] G.I. Taylor and A.E. Green. Mechanism of the production of small eddies from large ones. *Proceedings of the Royal Society of London. Series A - Mathematical and Physical Sciences*, 158(895):499–521, 1937.

[98] J. D. Bjorken. Highly relativistic nucleus-nucleus collisions: The central rapidity region. *Phys. Rev. D*, 27:140–151, Jan 1983.

[99] G.A. Sod. A survey of several finite difference methods for systems of nonlinear hyperbolic conservation laws. *Journal of Computational Physics*, 27(1):1–31, 1978.

[100] K.W. Thompson. The special relativistic shock tube. *Journal of Fluid Mechanics*, 171:365–375, 1986.

[101] H. Culetu. The milne spacetime and the hadronic rindler horizon. *International Journal of Modern Physics D*, 19(08n10):1379–1384, 2010.

[102] S. Plumari, G.L. Guardo, V. Greco, and J.Y. Ollitrault. Viscous corrections to anisotropic flow and transverse momentum spectra from transport theory. *Nuclear Physics A*, 941:87–96, 2015.

[103] S. Plumari, G. L. Guardo, F. Scardina, and V. Greco. Initial-state fluctuations from midperipheral to ultracentral collisions in an event-by-event transport approach. *Phys. Rev. C*, 92:054902, Nov 2015.

[104] S. Plumari. Anisotropic flows and the shear viscosity of the QGP within an event-by-event massive parton transport approach. *The European Physical Journal C*, 79(1), jan 2019.

[105] A. Puglisi, S. Plumari, and V. Greco. Electric conductivity from the solution of the relativistic boltzmann equation. *Phys. Rev. D*, 90:114009, Dec 2014.

[106] M. Ruggieri, F. Scardina, S. Plumari, and V. Greco. Elliptic flow from non-equilibrium initial condition with a saturation scale. *Physics Letters B*, 727(1):177–181, 2013.

[107] M. Ruggieri, F. Scardina, S. Plumari, and V. Greco. Thermalization, isotropization, and elliptic flow from nonequilibrium initial conditions with a saturation scale. *Phys. Rev. C*, 89:054914, May 2014.

[108] F. Scardina, M. Colonna, S. Plumari, and V. Greco. Quark-to-gluon composition of the quark-gluon plasma in relativistic heavy-ion collisions. *Physics Letters B*, 724(4):296–300, 2013.

[109] F. Scardina, S.K. Das, V. Minissale, S. Plumari, and V. Greco. Estimating the charm quark diffusion coefficient and thermalization time from d meson spectra at energies available at the bnl relativistic heavy ion collider and the cern large hadron collider. *Phys. Rev. C*, 96:044905, Oct 2017.

[110] A.H. Taub. Relativistic rankine-hugoniot equations. *Phys. Rev.*, 74:328–334, Aug 1948.

[111] R. Pasechnik and M. Šumbera. Phenomenological review on quark–gluon plasma: Concepts vs. observations. *Universe*, 3(1):7, 2017.

[112] M.F. Borunda, H. Hennig, and Eric J. Heller. Ballistic versus diffusive transport in graphene. *Phys. Rev. B*, 88:125415, Sep 2013.

[113] S. L. Sobolev. *Cubature Formulas on the Sphere Invariant under Finite Groups of Rotations*, pages 461–466. Springer US, Boston, MA, 2006.

[114] Cory Ahrens and Gregory Beylkin. Rotationally invariant quadratures for the sphere. *Proceedings of the Royal Society A: Mathematical, Physical and Engineering Sciences*, 465(2110):3103–3125, 2009.

[115] P. Delsarte, J. M. Goethals, and J. J. Seidel. Spherical codes and designs. *Geometriae Dedicata*, 6(3):363–388, sep 1977.

[116] Robert S. Womersley. *Efficient Spherical Designs with Good Geometric Properties*, pages 1243–1285. Springer International Publishing, Cham, 2018.

[117] J.J. Thomson F.R.S. Xxiv. on the structure of the atom: an investigation of the stability and periods of oscillation of a number of corpuscles arranged at equal intervals around the circumference of a circle; with application of the results to the theory of atomic structure. *The London, Edinburgh, and Dublin Philosophical Magazine and Journal of Science*, 7(39):237–265, 1904.

[118] Event Horizon Telescope Collaboration, K. Akiyama, A. Alberdi, W. Alef, K. Asada, R. Azulay, A.-K. Baczko, D. Ball, M. Baloković, J. Barrett, et al. First M87 Event Horizon Telescope Results. I. The Shadow of the Supermassive Black Hole. *Astrophys. J. Lett.*, 875:L1, apr 2019.

[119] Vasileios Paschalidis. General relativistic simulations of compact binary mergers as engines for short gamma-ray bursts. *Classical and Quantum Gravity*, 34(8):084002, mar 2017.

[120] A. Mezzacappa, M. Liebendörfer, O.E. Bronson Messer, W. Raphael Hix, F.K. Thielemann, and S.W. Bruenn. Simulation of the spherically symmetric stellar core collapse, bounce, and postbounce evolution of a star of 13 solar masses with boltzmann neutrino transport, and its implications for the supernova mechanism. *Phys. Rev. Lett.*, 86:1935–1938, Mar 2001.

[121] O. Just, M. Obergaulinger, and H.-T. Janka. A new multidimensional, energy-dependent two-moment transport code for neutrino-hydrodynamics. *Monthly Notices of the Royal Astronomical Society*, 453(4):3386–3413, 09 2015.

[122] E. O'Connor. An open-source neutrino radiation hydrodynamics code for core-collapse supernovae. *The Astrophysical Journal Supplement Series*, 219(2):24, aug 2015.

[123] Takami Kuroda, Tomoya Takiwaki, and Kei Kotake. A new multy-energy neutrino radiation-hydrodynamics code in full general relativity and its application to the gravitational collapse of massive stars. *The Astrophysical Journal Supplement Series*, 222(2):20, feb 2016.

[124] O. Zanotti, C. Roedig, L. Rezzolla, and L. Del Zanna. General relativistic radiation hydrodynamics of accretion flows – i. bondi–hoyle accretion. *Monthly Notices of the Royal Astronomical Society*, 417(4):2899–2915, 11 2011.

[125] Fragile P.C., Gillespie A., Monahan T., Rodriguez M., and Anninos P. Numerical simulations of optically thick accretion onto a black hole. i. spherical case. *The Astrophysical Journal Supplement Series*, 201(2):9, jun 2012.

[126] C. Roedig, O. Zanotti, and D. Alic. General relativistic radiation hydrodynamics of accretion flows – II. Treating stiff source terms and exploring physical limitations. *Monthly Notices of the Royal Astronomical Society*, 426(2):1613–1631, 10 2012.

[127] A. Sądowski, R. Narayan, A. Tchekhovskoy, and Y. Zhu. Semi-implicit scheme for treating radiation under M1 closure in general relativistic conservative fluid dynamics codes. *Monthly Notices of the Royal Astronomical Society*, 429(4):3533–3550, 01 2013.

[128] Jonathan C. McKinney, Alexander Tchekhovskoy, Aleksander Sadowski, and Ramesh Narayan. Three-dimensional general relativistic radiation magnetohydrodynamical simulation of super-Eddington accretion, using a new code harmrad with M1 closure. *Monthly Notices of the Royal Astronomical Society*, 441(4):3177–3208, 05 2014.

[129] M. Livio, J. R. Buchler, and S. A. Colgate. Rayleigh-taylor driven sn explosions : a two-dimensional numerical study. *Astrophysical Journal*, 238:L139–L143, jun 1980.

[130] E.R. Most, L.J. Papenfort, and L. Rezzolla. Beyond second-order convergence in simulations of magnetized binary neutron stars with realistic microphysics. *Monthly Notices of the Royal Astronomical Society*, 490(3):3588–3600, 10 2019.

[131] S. W. Bruenn. Neutrino interactions and supernovae. In P. G. Bergman, E. J. Fenyves, and L. Motz, editors, *Seventh Texas Symposium on Relativistic Astrophysics*, volume 262 of *Texas Symposium on Relativistic Astrophysics*, pages 80–94, oct 1975.

[132] N Rahman, O Just, and H-T Janka. NADA-FLD: a general relativistic, multidimensional neutrino-hydrodynamics code employing flux-limited diffusion. *Monthly Notices of the Royal Astronomical Society*, 490(3):3545–3572, 10 2019.

[133] Kip S. Thorne. Relativistic radiative transfer: moment formalisms. *Monthly Notices of the Royal Astronomical Society*, 194(2):439–473, 02 1981.

[134] Masaru Shibata, Kenta Kiuchi, Yu-ichiro Sekiguchi, and Yudai Suwa. Truncated Moment Formalism for Radiation Hydrodynamics in Numerical Relativity. *Progress of Theoretical Physics*, 125(6):1255–1287, 06 2011.

[135] Christian Y. Cardall, Eirik Endeve, and Anthony Mezzacappa. Conservative 3+1 general relativistic variable eddington tensor radiation transport equations. *Phys. Rev. D*, 87:103004, May 2013.

[136] F. Foucart. Monte Carlo closure for moment-based transport schemes in general relativistic radiation hydrodynamic simulations. *Monthly Notices of the Royal Astronomical Society*, 475(3):4186–4207, 01 2018.

[137] Jonah M. Miller, Ben. R. Ryan, and Joshua C. Dolence. νbhlight : Radiation GRMHD for Neutrino-driven Accretion Flows. *The Astrophysical Journal Supplement Series*, 241(2):30, apr 2019.

[138] S. Chandrasekhar. *Radiative transfer*. 1960.

[139] O. Porth, H. Olivares, Y. Mizuno, Z. Younsi, L. Rezzolla, M. Moscibrodzka, H. Falcke, and M. Kramer. The black hole accretion code. *Computational Astrophysics and Cosmology*, 4:1, may 2017.

[140] D. Mihalas and L. H. Auer. On laboratory-frame radiation hydrodynamics. *Journal of Quantitative Spectroscopy and Radiative Transfer*, 71(1):61–97, oct 2001.

[141] G. B. Rybicki and A. P. Lightman. *Radiative Processes in Astrophysics*. Wiley-VCH, jun 1986.

[142] J. M. Martí, E. Müller, J. A. Font, J. M. Ibáñez, and A. Marquina. Morphology and dynamics of relativistic jets. *Astrophys. J.*, 479:151, 1997.

[143] Lukas R. Weih, Hector Olivares, and Luciano Rezzolla. Two-moment scheme for general-relativistic radiation hydrodynamics: a systematic description and new applications. *Mon. Not. R. Astron. Soc.*, 495(2):2285–2304, may 2020.

[144] P. C. Fragile, A. Olejar, and P. Anninos. Numerical Simulations of Optically Thick Accretion onto a Black Hole. II. Rotating Flow. *Astrophys. J.*, 796:22, November 2014.

[145] Francois Foucart, Evan O'Connor, Luke Roberts, Matthew D. Duez, Roland Haas, Lawrence E. Kidder, Christian D. Ott, Harald P. Pfeiffer, Mark A. Scheel, and Bela Szilagyi. Post-merger evolution of a neutron star-black hole binary with neutrino transport. *Physical Review D*, 91(12):124021, jun 2015.

[146] J.L. Anderson and H.R. Witting. Relativistic quantum transport coefficients. *Physica*, 74(3):489 – 495, 1974.

[147] L. Luo. Unified theory of lattice boltzmann models for nonideal gases. *Phys. Rev. Lett.*, 81:1618–1621, Aug 1998.

[148] Z. Xu and C. Greiner. Thermalization of gluons in ultrarelativistic heavy ion collisions by including three-body interactions in a parton cascade. *Phys. Rev. C*, 71:064901, Jun 2005.

1/10/22, 3:21 PM   Dichiarazione di conformità — Dottorati di ricerca

**Università
degli Studi
di Ferrara**

Sezioni

Dottorati di ricerca

Dichiarazione di conformità

AL MAGNIFICO RETTORE

**UNIVERSITÀ DEGLI STUDI DI FERRARA
UFFICIO IUSS**
Corso Porta Mare, n. 2 – 44121 Ferrara
e-mail dottorato@unife.it

**ATTENZIONE: il presente modulo è da stampare, firmare e inserire come parte integrante della tesi in
formato cartaceo; va inoltre inviato a dottorato@unife.it, unitamente agli altri documenti, in file formato
pdf.**

Il tuo indirizzo e-mail   Inserisci qui l'e-mail che ti ha fornito l'Università
smndnl1@unife.it
Oggetto: Indicare qui: "Dichiarazione di conformità della tesi di Dottorato"
Dichiarazione di conformità della te:
Io sottoscritto Dott. (Cognome e Nome)
Simeoni Daniele

Nato a: Indicare il Comune di nascita
Roma

Provincia: Scrivere per esteso la provincia di nascita oppure lo Stato (se nato all'estero)
Roma

Il giorno: Trascrivere la data di nascita
1170871990

Avendo frequentato il Dottorato di Ricerca in: Specificare il nome del corso
Fisica

Ciclo di Dottorato   Scrivere in cifre (es. 26)
34

Titolo della tesi: Attenzione: deve essere lo stesso riportato sulla tesi cartacea
Lattice Kinetic Algorithms for *Relativistic Flows; a Unified Treatment*

Titolo della tesi (traduzione): Se la stesura della tesi è autorizzata dal Collegio dei docenti in una lingua diversa
dall'italiano, è obbligatorio compilare il campo secondo queste modalità: - Tesi in inglese: traduzione in lingua
italiana - - Tesi in francese, spagnolo, tedesco etc.: traduzione del titolo sia in italiano che in inglese
Algoritmi cinetici su reticolo per i *Flussi relativistici: un trattamento unificato*

Tutore: Prof. (Cognome e Nome)
Tripiccione Raffaele e Schifano *Sebastiano Fabio*

Settore Scientifico Disciplinare (S.S.D.) Indicare il settore della tesi. Ad esempio, BIO/01
FIS/02

Parole chiave della tesi (max 10):   In Italiano, Inglese ed eventuale terza lingua
lattice relativistic hydrodynamics, lattice boltzmann methods, computational *phisics, computational fluid dynamics*

Consapevole, dichiara   Selezionare con un click

⦿ CONSAPEVOLE: (1) del fatto che in caso di dichiarazioni mendaci, oltre alle sanzioni previste dal codice
penale e dalle Leggi speciali per l'ipotesi di falsità in atti ed uso di atti falsi, decade fin dall'inizio e senza
necessità di alcuna formalità dai benefici conseguenti al provvedimento emanato sulla base di tali dichiarazioni;
(2) dell'obbligo per l'Università di provvedere al deposito di legge delle tesi di dottorato al fine di assicurarne la
conservazione e la consultabilità da parte di terzi; (3) della procedura adottata dall'Università di Ferrara ove si
richiede che la tesi sia consegnata dal dottorando in 2 copie di cui una in formato cartaceo e una in formato pdf
non modificabile su idonei supporti (CD-ROM, DVD) secondo le istruzioni pubblicate sul sito:
http://www.unife.it/studenti/dottorato alla voce ESAME FINALE – disposizioni e modulistica; (4) del fatto che
l'Università, sulla base dei dati forniti, archivierà e renderà consultabile in rete il testo completo della tesi di

dottorato di cui alla presente dichiarazione attraverso l'Archivio istituzionale ad accesso aperto "EPRINTS.unife.it" oltre che attraverso i Cataloghi delle Biblioteche Nazionali Centrali di Roma e Firenze; DICHIARO SOTTO LA MIA RESPONSABILITA': (1) che la copia della tesi depositata presso l'Università di Ferrara in formato cartaceo è del tutto identica a quella presentata in formato elettronico (CD-ROM, DVD), a quelle da inviare ai Commissari di esame finale e alla copia che produrrò in seduta d'esame finale. Di conseguenza va esclusa qualsiasi responsabilità dell'Ateneo stesso per quanto riguarda eventuali errori, imprecisioni o omissioni nei contenuti della tesi; (2) di prendere atto che la tesi in formato cartaceo è l'unica alla quale farà riferimento l'Università per rilasciare, a mia richiesta, la dichiarazione di conformità di eventuali copie; (3) che il contenuto e l'organizzazione della tesi è opera originale da me realizzata e non compromette in alcun modo i diritti di terzi, ivi compresi quelli relativi alla sicurezza dei dati personali; che pertanto l'Università è in ogni caso esente da responsabilità di qualsivoglia natura civile, amministrativa o penale e sarà da me tenuta indenne da qualsiasi richiesta o rivendicazione da parte di terzi; (4) che la tesi di dottorato non è il risultato di attività rientranti nella normativa sulla proprietà industriale, non è stata prodotta nell'ambito di progetti finanziati da soggetti pubblici o privati con vincoli alla divulgazione dei risultati, non è oggetto di eventuali registrazioni di tipo brevettale o di tutela. PER ACCETTAZIONE DI QUANTO SOPRA RIPORTATO
Firma del dottorando

Ferrara, li   10/01/2022 (data)

Firma del Tutore
Visto: Il Tutore
Si approva
Firma del Tutore

Selezionando il tasto "**INVIA**" in fondo alla pagina, la dichiarazione di conformità viene spedita automaticamente alla posta elettronica dell'**Ufficio IUSS**. Per ottenerne una copia in **FORMATO PDF**, fare click sull'icona della stampante del proprio browser (Internet Explorer, Firefox, Google Chrome etc.), quindi selezionare l'opzione Pdf Creator o simili (a seconda del programma in uso).